Physiological Analysis of Structural/Functional Features of Neuronal Calcium Sensor-1

Thesis submitted in accordance with the
requirements of the University of Liverpool
for the degree of Doctor in Philosophy
By

Victoria Marie Martin

September 2013

Contents

Abstract

Calcium (Ca^{2+}) signalling regulates many neuronal functions including neurotransmission, axonal growth and development. Neuronal calcium sensor-1 (NCS-1) has been shown to be involved in many of these processes. On Ca^{2+} binding, NCS-1 changes conformation and exposes a hydrophobic binding pocket. In yeast, NCS-1 binds to a PI4-kinase orthologue required for survival. In mammalian cells, NCS-1 is localised to the Golgi and plasma membranes and has been linked to multiple target proteins that have roles in neuronal signalling. NCS-1 has been shown to regulate the P/Q Ca^{2+} channel subunit $Ca_v2.1$; although no direct binding interaction has been identified between the proteins. The $Ca_v2.1$ C-terminal tail contains two Ca^{2+}-sensor binding regions, the IQ domain and the calmodulin (CaM) binding domain (CBD). The first part of this study investigated NCS-1 or CaM and $Ca_v2.1$ interactions using biochemical and biophysical interactions. Pull-down analysis found that NCS-1 binds to a $Ca_v2.1$ C-terminal peptide in a Ca^{2+}-dependent manner. Use of nuclear magnetic resonance spectroscopy also showed that the IQ domain of $Ca_v2.1$ bound to NCS-1 in the presence of Ca^{2+}, though the NCS-1 region involved in this interaction could not be identified. The second part of this study investigated NCS-1 in the model organism *C. elegans.* In the worm, NCS-1 is expressed predominantly in sensory neurons. An *ncs-1* null mutant worm strain (XA406) was previously shown to be defective in isothermal tracking and this was linked to a requirement for NCS-1 in memory and learning. To ensure this behaviour was not caused by a locomotion or neurotransmission phenotype, these behaviours were quantified and compared to the wild-type strain. No effect of the *ncs-1* null mutation was found in a quantitative body-bend assay or in an assay of aldicarb resistance. The temperature-linked behaviour was further characterised using an acute assay for temperature-dependent locomotion (TDL). In this assay, the rate of locomotion of wild-type worms decreased when the temperature was elevated from $20^{o}C$ to $28^{o}C$. In contrast, the rate of locomotion of the *ncs-1* null worm was significantly increased at the higher temperature. This distinct phenotype was exploited to quantify the rescue of the null strain by expression of wild-type NCS-1 and to identify potential mechanisms involved in NCS-1 function. It was established that NCS-1 regulated TDL when expressed in AIY neurons. Using information from previous studies, key structural elements of NCS-1 were investigated by expressing NCS-1 with specific point mutations or deletions. N-terminal myristoylation of NCS-1 was not functionally required. In contrast, the N- and C-terminal clefts of the hydrophobic pocket of NCS-1 were shown to be physiologically important while the C-terminal tail was not essential for function in the TDL assay. These findings allowed discrimination between two potential modes of interaction of NCS-1 with its target proteins in a physiological context.

Publications

Work presented in this thesis has been published in part in the following paper:

Martin V M, Johnson J R, Haynes L P, Barclay J W and Burgoyne R D (2013). Identification of key structural elements for neuronal calcium sensor-1 function in the regulation of the temperature-dependency of locomotion in *C. elegans*. *Mol Brain* vol 6 issue 1 pp 39

Acknowledgements

First and foremost, I would like to thank my supervisors Prof. Bob Burgoyne and Dr Lee Haynes. I would like to thank Bob for his excellent supervision, guidance and patience throughout my PhD, it has been a privilege to be his student. Thanks Lee for all his help in the lab especially in the early days with protein expression, molecular biology and guidance with protein science. Thanks to Dr Jeff Barclay for putting up with my never ending questions on worms. I owe massive thanks to Dr James Johnson for his microinjecting skills, his countless advice and patience, and to Dr Andy Herbert, I am grateful for his introduction to SPR it was definitely character building. Thank you ALL of Red block past and present including Alan, Matt, Pryank, Sudhanva, Joe, Joanna, Sarah and Helen. And I would like to say a special thank you to Hannah, Ciara, Martin (honorary Red block member), Leanne, Xi, Dayani, Mimi, Marie, Megan, Paul and Michela for their friendship, there have been really fantastic times but also tough times and without your help and encouragement I do not know how I would have got through them. Thank you to those in Lab C and the NMR centre for making me welcome during our collaboration and helping me with chromatography and NMR especially Prof. Lu-Yun Lian, Dr Marie Phelan and Sravan Pandalaneni. I would also like to thank my undergrad lectures at LJMU, without whose excellent teaching I would not have had the confidence and ability to do this in the first place. I would like to thank the Wellcome Trust Studentship Program for funding me and the work in this thesis.

I cannot thank my family enough for their never ending love, support and belief in me. I could not have got through it without you; my Dad, Clare, Gary, Kathy, Bette *et al*, (my friends, the in-laws and out-laws, I love you all, your all amazing). Anthony for being so patient with his student mother and Les for being so understanding at losing his wife to a protein and making me laugh even when all seemed doomed. A special mention must go to my nieces and nephews for the times away from the Lab, pushing all thoughts of my thesis and NCS-1 out of my head, helping me to relax and have fun. Last but not least, I want to thank my mum Pat because although she is no longer with me, I would never have got here without her.

Abbreviations

α1A	Voltage gated P/Q Ca^{2+} channel forming subunit (aka $Ca_v2.1$)
Ach	Acetylcholine
ADF	Amphid dual F
ADL	Amphid dual L
ADP	Adenosine diphosphate
AFD	Amphid finger-like D
AIA	Amphid interneuron A
AIB	Amphid interneuron B
AID	Alpha interacting domain
AIY	Amphid interneuron Y
AIZ	Amphid interneuron Z
ARF 1	ADP ribosylation factor 1
ASE	Amphid single E
ASG	Amphid single G
ASH	Amphid single H
ASI	Amphid single I
ASJ	Amphid single J
ASK	Amphid single K
AVK	Amphid, NR, VC Interneuron K
AWA	Amphid winged A
AWB	Amphid winged B
AWC	Amphid winged C

BAG	Head Sensory Neuron
BSA	Bovine serum albumin
C. elegans	*Caenorhabditis elegans*
$[Ca^{2+}]i$	Intracellular free calcium ion concentration
Ca^{2+}	Calcium ion
CaBPs	Calcium Binding Proteins
CACNA1A	(aka CACNL1A4) Voltage gated P/Q Ca^{2+} channel α1A/Ca_v2.1 subunit gene
CaM	Calmodulin
Ca_v	Voltage gated Ca^{2+} channel (aka VGCC)
Ca_v2.1	Voltage gated P/Q Ca^{2+} channel forming subunit (aka α1A)
CBD	Calmodulin binding domain
CCPNmr	Collaborative Computing Project for NMR
CD	Circular dichroism
CDF	Ca^{2+}-dependent facilitation
CDI	Ca^{2+}-dependent inactivation
CGC	*Caenorhabditis* Genetics Centre
CMD-1	CaM (*C. elegans* orthologue)
D2R	Dopamine receptor 2
DAG	Diacylglycerol
DC	Dorsal cord
DNA	Deoxyribonucleic acid
DTT	Dithiothreitol
DVA	NR, dorsal cord interneuron, tail ganglian

EA-2	Episodic ataxia type-2
ECL	Enhanced chemiluminescence
EDTA	Ethylenediaminetetraacetic acid
EF	EF hand motif
ER	Endoplasmic reticulum
FHM-1	Familial hemiplegic migraine type-1
FLP	Head sensory neuron
Frq-1	Frequenin 1 (Neuronal calcium sensor-1, Budding yeast protein and *Drosophila*)
Frq-2	Frequenin 2 (Neuronal calcium sensor-1 *Drosophila* orthologue*)*
GABA	Gamma-aminobutyric acid
GCAPs	Guanylyl cyclase-activating proteins
GFP	Green fluorescent protein
GRK-2	G-protein-coupled receptor kinase 2
GST	Glutathione *S*-transferase
GTP	Guanosine triphosphate
GTPase	Guanosine triphosphate hydrolysing enzyme
HCLP-1	Hippocalcin-like protein-1
HEPES	Hydroxyethyl piperazineethanesulfonic acid
His-	6X Histidine peptide tag
HPLC	High-performance liquid chromatography
HRP	Horse radish peroxidise
HSQC	Heteronuclear Single Quantum Coherence
IL1RAPL1	Interleukin-receptor 1 accessory protein- like 1

IP_3	Inositol 1,4,5,trisphosphate
IP_3R	inositol 1,4,5,trisphosphate receptors
IPTG	Isopropylthio-β-galactoside
IQ	IQ-like motif
ITC	Isothermal titration calorimetry
KChIPs	Potassium channel interacting proteins
K_v	Potassium channel
MES	Morpholino ethanesulfonic acid
Mg^{2+}	Magnesium ions
MOPS	Morpholino-propanesulfonic acid
Munc-18	Mammalian uncoordinated protein 18
MWCO	Molecular weight cut off
NBRP	National Bioresource Project
NCS	Neuronal calcium sensor family proteins
NCS-1	Neuronal calcium sensor-1 (mammalian and *C. elegans* orthologue)
Ncs-1	Neuronal calcium sensor-1 (Fission yeast orthologue)
NGM	Nematode growth media
NMR	Nuclear magnetic resonance
NR	Nerve ring
OD	Optical density
osm-6	Osmotic avoidance abnormal-6
P/Q	P (Purkinje) or Q-type Calcium channels
PAGE	Polyacrylamide gel electrophoresis

PBS	Phosphate buffered saline
PBST	Phosphate buffered saline tween 20
PCR	Polymerase chain reaction
PDB	Protein database
PEG	Polyethylene glycol
PHA	Phasmid A
PHB	Phasmid B
PHC	Phasmid C (tail neuron possibly in the phasmid)
PI4K IIIβ	Phosphatidylinositol-4-kinase type 3 beta (Mammalian orthologue)
PI4P	Phosphatidylinositol-4-phosphate
Pik-1	Phosphatidylinositol-4-kinase 1 (Budding yeast orthologue)
PKC-2	Protein kinase 2
pm1	Pharyngeal Muscle
PVC	Venteral cord interneuron, tail gangian
Rba-1	Rat brain alpha-1 (Rat $Ca_v2.1$ orthologue)
RIA	Head, NR interneuron
ric-4	Resistance to inhibitors of cholinesterase
RMG	Head Motor/Interneuron G
S.E.M.	Standard error of mean
SDS	Sodium dodecyl sulphate
SNARE	Soluble NSF attachment protein receptor
SPR	Surface plasmon resonance
Src	Sarcoma

SUMO	Small ubiquitin-like modifier
TDL	Temperature-dependent locomotion
TEV	Tobacco etch virus
TFE	2, 2, 2-trifluoroethanol
Tris	Tris-hydroxymethyl-aminomethane
tRNA	Transfer RNA (Ribonucleic acid)
ttx-3	Thermotaxis abnormal-3
ULP-1	Ubiquitin-like protease-1
UNC-18	Uncoordinated protein 18 (Munc-18 *C. elegans* orthologue)
UNC-2	Uncoordinated protein 2 ($Ca_v2.1$ *C. elegans* orthologue)
VC	Ventral nerve cord
VGCC	Voltage gated Ca^{2+} channel (AKA Ca_v)
VILIPs	Visinin-like proteins

Chapter 1: INTRODUCTION

1.1 Calcium Signalling Introduction

Intracellular calcium signalling regulates cell growth, proliferation, cell death and also specialised cell functions (Berridge et al., 2000). In neurons, many specific activities are calcium-dependent including the stimulation of neurotransmission, neuronal development and neuroplasticity (Barclay et al., 2005, Berridge, 1998, Catterall and Few, 2008, Bito et al., 1997). Calcium acts as a messenger via changes in its free ion concentration and location inside the cell. Ca^{2+} is a large positively charged metal ion and transduces intracellular signals by binding to specialised proteins. Ca^{2+} can be neither created or destroyed, so must be regulated by being moved, buffered or sequestered. Resting intracellular free Ca^{2+} concentration ($[Ca^{2+}]i$) is in the range 10–100 nM depending on the cell type and can be increased to 1000 nM or higher when cells are stimulated. Regulation of $[Ca^{2+}]i$ is essential for normal neuronal function. Unregulated $[Ca^{2+}]i$ leads to cell damage and toxicity and it has been suggested that the dysregulation of $[Ca^{2+}]i$ in neurons may be linked to neurodegenerative disorders such as Alzheimer's and Parkinson's disease (Mattson and Magnus, 2006, Berridge, 2010).

Ca^{2+} signalling networks have been divided into four mechanisms (Berridge et al., 2000) (Figure 1.1):

1. Mobilisation of Ca^{2+}. When cells are excited a stimulus allows Ca^{2+} to enter the cell cytoplasm through Ca^{2+} channels by either crossing the plasma membrane or by release from Ca^{2+} storage organelles such as the endoplasmic reticulum (ER).
2. Activation of on-mechanisms. This allows the $[Ca^{2+}]i$ to rise to an active concentration. Ca^{2+} binds to channels, allowing further Ca^{2+} to continue to enter the cytoplasm and remain there.
3. Stimulation of Ca^{2+}-dependent activities. Ca^{2+}-binding proteins control the regulation of these functions.
4. Activation of off-mechanisms. These lower $[Ca^{2+}]i$ to resting levels by the inactivation of Ca^{2+} channels and the action of Ca^{2+} pumps and buffers.

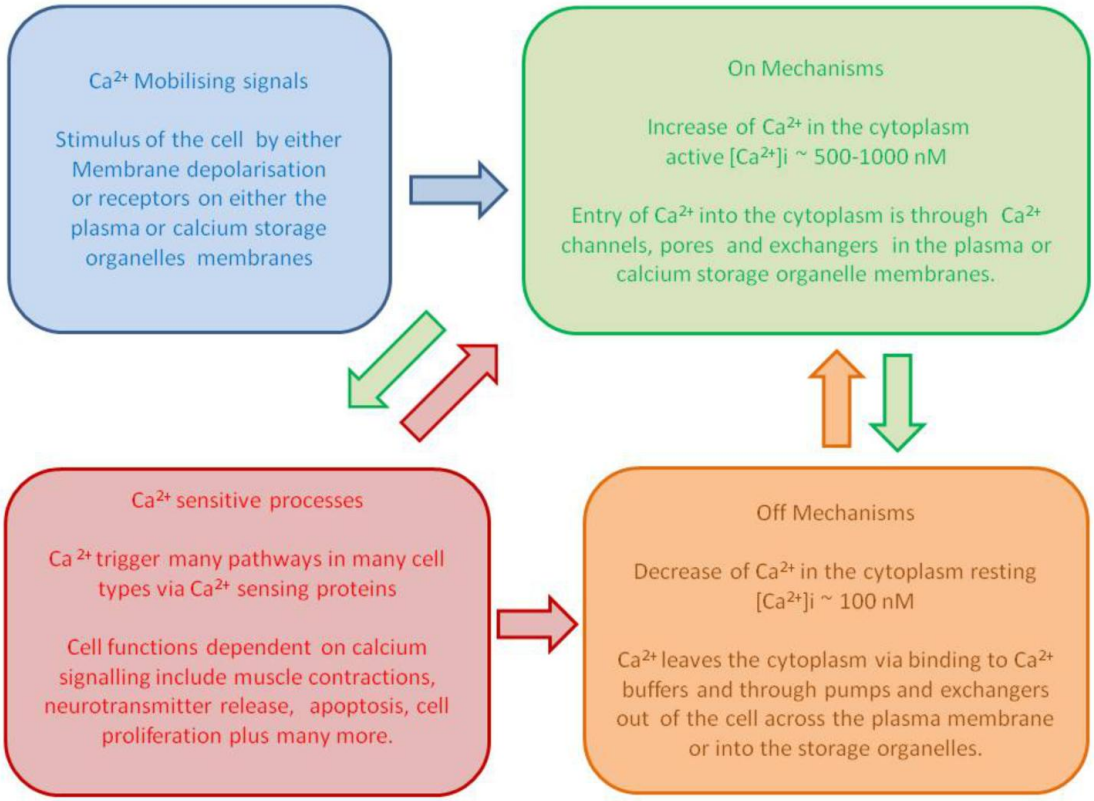

Figure 1.1. Overview of the Ca^{2+} signalling network. A simple schematic showing the relationship between Ca^{2+} signalling mechanisms. Blue shows Ca^{2+} mobillising signals/stimuli. Green shows on-mechanisms which increase Ca^{2+} in the cytoplasm to active levels. Red shows Ca^{2+}-sensitive processes which stimulate Ca^{2+}-dependent function. Orange shows off-mechanisms which decrease the Ca^{2+} to resting levels.

Together these mechanisms regulate changes in $[Ca^{2+}]i$ to allow cell functions to be modified, whilst at the same time, tightly controlling cytoplasm concentrations so that cell damage does not occur. $[Ca^{2+}]i$ is not uniform in the cell and can differ in distinct areas within the cytoplasm. A Ca^{2+} signal has a distinct frequency, duration, amplitude and location. These signal properties determine the function it regulates and form complex Ca^{2+} signalling networks (Berridge et al., 2000, Laude and Simpson, 2009) (Figure 1.1).

1.2 Ca^{2+} Sensor Proteins

Ca^{2+} sensor proteins can have several different roles in Ca^{2+} networks. They have a stimulatory role, regulating effector molecules, to switch Ca^{2+}-sensitive processes on or off. For example, the Ca^{2+} sensor protein synaptotagmin-1 has specific Ca^{2+}-binding domains. This binding to Ca^{2+} causes synaptotagamin-1 to coordinate interactions between soluble NSF attachment protein receptor (SNARE) proteins and membrane lipids involved in vesicle docking and membrane fusion, which is important for the regulation of neurotransmission. Ca^{2+} sensor proteins can have a Ca^{2+} signalling feedback role, modulating other proteins in Ca^{2+} signalling networks. For example, modulation of voltage gated Ca^{2+} channels, involved in both the on and off mechanisms, are regulated by several Ca^{2+} sensor proteins including calmodulin, Ca^{2+} binding protein-1 (CaBP-1) and visinin-like protein -2 (VILIP-2). This can have both a positive feedback effect, allowing Ca^{2+} into the cytoplasm or negative feedback effect by inhibiting the entry of Ca^{2+} into the cytoplasm (Nejatbakhsh and Feng, 2011).

1.2.1 Calmodulin

Calmodulin (CaM) is the most abundant Ca^{2+} sensor protein. CaM is found in all eukaryotic cells and its main role is to pass on Ca^{2+}-dependent signals to target proteins. CaM is a small protein of approximately 150 amino acids long and is highly conserved across diverse species. CaM is dumbbell shaped with distinct N- and C-terminal globular lobes connected by a flexible linker region (Figure 1.2a). Each of these domains contains 2 EF-hand motifs (Sudhakar Babu et al., 1988). EF-hand motifs consist of two alpha helices at right angles to each other, joined by a flexible loop region (Kretsinger and Nockolds, 1973). The 12 amino acid loop motif provides a site for cations, including Ca^{2+}, to bind to proteins. The EF-hand motif contains a conserved amino acid sequence with six amino acids at positions 1, 3, 5, 7, 9 and 12 that coordinate the cation. Atoms on the amino acid back bone and side chains of these particular amino acids provide interactions with the cation.

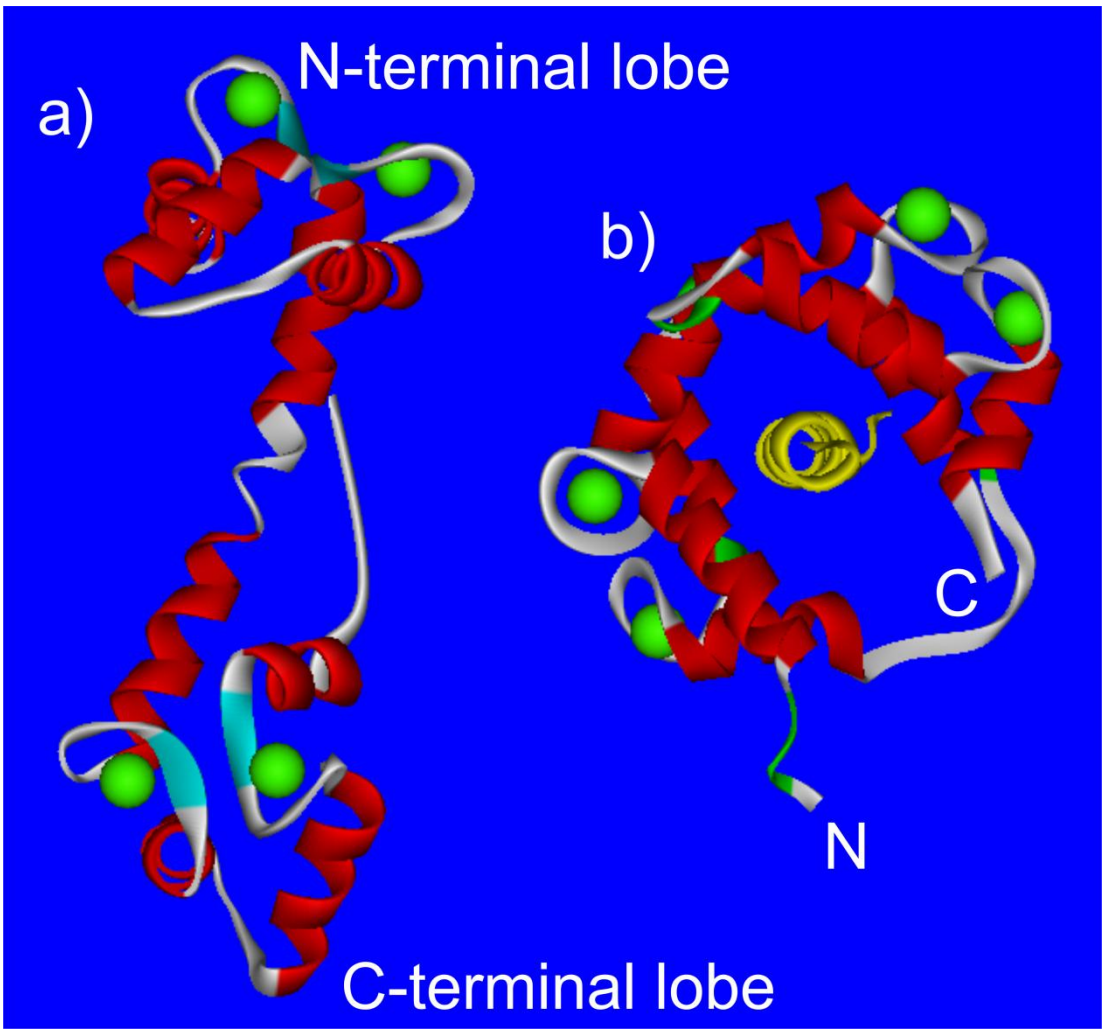

Figure 1.2. The structure of free CaM and a CaM/target peptide complex. Ribbon diagrams showing a) unbound CaM as a dumbbell shaped protein, with two globular lobes at the N- and C-terminals, connected by a flexible helical region. Each domain, containing two EF hands domains, binds Ca^{2+} ions (Green) (PDB, 3CLN), b) CaM bound to Ca^{2+} and a calmodulin target peptide (residues 577-602) of myosin light chain - yellow ribbon) (PDB, 2BBM). The target peptide is enclosed by the hydrophobic pocket formed by the N- and C-lobes of CaM.

Aspartate, found at position 1 and aspartate or glutamate, found most often at position 12 of the motif, provide negatively charged oxygen for the electrostatic interactions between the protein and the cation.

Different EF-hands within CaM and other Ca^{2+} sensor proteins have different affinities for Ca^{2+}, this is thought have a role in the regulation of Ca^{2+} sensor protein function and activity at different physiological [Ca^{2+}]i. When Ca^{2+} binds to CaM, this causes a conformational change exposing a hydrophobic region of the protein that is important for mediating interactions with target proteins (Figure 1.2b) (Zhang et al., 1995).

1.2.2 Ca^{2+} Sensor Proteins in Neurons

Neurons contain a number of CaM related Ca^{2+} sensor proteins. Two families of these proteins are the neuronal Ca^{2+} sensor proteins (NCS) and the Ca^{2+} binding proteins (CaBP), which each contain 4 EF-hands motifs (Table 1.1). The CaBPs show sequence homology to CaM and have been found only in vertebrates (McCue et al., 2010), whilst NCS proteins show approximately 20% homology with CaM and are found in early eukaryotes up to man. This array of Ca^{2+} sensing proteins may allow neurons to have greater versatility in Ca^{2+} signalling.

There are 5 classes of NCS proteins. Class A proteins, which are comprised of NCS-1 orthologs, are found in yeast cells onwards and are the most primitive of the NCS proteins. Class B proteins, which first appeared in nematodes, are comprised of hippocalcin, neurocalcin and visinin-like protein (VILIPs 1-3) and their functions include regulation of cell signalling, apoptosis and receptor trafficking. Both class C and D NCS proteins, which are comprised of recoverin and guanylyl cyclase-activating proteins 1-3 (GCAP1-3) are found in all vertebrate species and are expressed in the retina. Class E proteins first appeared in insects and are comprised of potassium channel interacting proteins 1-4 (KChIPs 1-4) and their functions include regulation of voltage gated potassium channels and repression of transcription.

Table 1.1 Summary of Mammalian NCS-1 and CaBP Protein Families

Calcium Sensor Family Sub-Group	Class/Type	Protein Name
-	-	Calmodulin
NCS	A	NCS-1
	B	VILIP-1
		VILIP-2
		VILIP-3
		Hippocalcin
		Neurocalcin δ
	C	Recoverin
	D	GCAP-1
		GCAP-2
		GCAP-3
	E	KChIP-1
		KChip-2
		KChip-3
		KChip-4
CaBP	Typical CaBPs	CaBP-1
		CaBP-2
		CaBP-3
		CaBP-4
		CaBP-5
		CaBP-5
	Calneurons	CaBP-6
		CaBP-7

NCS proteins are globular shaped and contain a hydrophobic binding domain which is exposed after Ca^{2+} binding (Burgoyne, 2007). Many NCS proteins have a myristoyl or palmitoyl lipid group attached to the N-terminus. The lipid group enables localisation of the protein to plasma or organelle membranes. In some myristoylated NCS proteins the lipid group is only exposed when bound to Ca^{2+}. This is known as the Ca^{2+}-myristoyl switch and has a role in the regulation of membrane localisation of these NCS proteins (O'Callaghan et al., 2002). Other NCS proteins have a lipid group which is thought to be always exposed, allowing the protein to be constitutively associated with the membrane, even in the absence of Ca^{2+} binding.

The Ca^{2+}-myristoyl switch mechanism allows Ca^{2+}-dependent localisation of several NCS proteins. When not bound to Ca^{2+}, the myristoyl group is located within the hydrophobic core of the protein, allowing the NCS protein to be free in the cytoplasm. When the protein is Ca^{2+} bound, its conformation changes, this exposes the myristoyl group and tethers the protein to organelles or the plasma membrane. How the NCS proteins, are localised to specific membranes is not yet known but the specific membrane localisation of NCS proteins could allow them to have different regulatory roles in neurons and other cell types.

1.3 Neuronal Ca^{2+} Sensor Protein 1

Neuronal Ca^{2+} sensing protein 1 (NCS-1) is found in all eukaryotes, from yeast through to higher organisms including man. NCS-1 was first identified as frequenin in *Drosophila melanogaster* (Pongs et al., 1993). In mammals it has been shown to have a role in synaptic transmission, neuronal outgrowth and memory and learning (Saab et al., 2009, Génin et al., 2001, Pongs et al., 1993). It is found in neuronal and neuroendocrine mammalian cells (Weiss and Burgoyne, 2001) and has been observed to be localised to presynaptic terminals in both hippocampal and cerebral neurons (Jinno et al., 2002). Conservation of the NCS-1 sequence has been retained throughout the species. Fission yeast Ncs-1 and budding yeast Frq-1 orthologues have 60% similarity to mammalian NCS-1 (Lim et al., 2011). Like CaM, NCS-1 has been shown to regulate a large array of proteins (Burgoyne, 2007, Haynes et al., 2006).

NCS-1 has been shown to interact with more than 20 potential target proteins (Burgoyne and Haynes, 2012). Many of these interactions are known, however, only from yeast 2-hybrid or pull-down experiments and have not been validated by other approaches or investigated in functional experiments. A smaller number of target proteins have been well characterised. The budding yeast orthologue of NCS-1 (Frq1) binds to phosphatidylinositol-4-kinase 1 (Pik-1) (Hendricks et al., 1999). In mammals NCS-1 has been shown to interact with and activate the Pik-1 orthologue,

PI4K IIIβ in a Ca^{2+}-dependent manner (Zhao et al., 2001, Haynes et al., 2005). This enzyme is important in cell signaling as it regulates phosphoinositide levels. PI4K IIIβ produces phosphatidylinositol 4-phosphate (PI4P) which is involved in the localisation of specific cytosolic proteins to the Golgi membrane (Downes et al., 2005). NCS-1 and ADP ribosylation factor 1 (ARF 1), a GTPase, have both been shown to co-localise with PI4K IIIβ in mammalian cells and are both involved in PI4K IIIβ regulation and membrane traffic from the Golgi complex to the plasma membrane (Haynes et al., 2007, Haynes et al., 2005).

NCS-1 also interacts with interleukin-receptor 1 accessory protein- like 1 (IL1RAPL1) (Bahi et al., 2003). IL1RAPL is a plasma membrane protein, found in the brain and like NCS-1 it has been linked to neuronal development and exocytosis. During a genetic study of families who have autistic spectrum disorders, a NCS-1 (R102Q) mutation was found in an individual and mutations of IL1RAPL were found in a number of subjects (Piton et al., 2008). Structural studies have shown this mutation in NCS-1 does not prevent IL1RAPL1 binding but does have structural and functional effects on NCS-1 (Handley et al., 2010). NCS-1 has also been shown to associate with dopamine receptor 2 (D2R) and blocks the phosphorylation of the receptor by G-protein-coupled receptor kinase 2 (GRK-2) (Kabbani et al., 2002). This prevents the receptor being internalised and has been shown to promote memory and learning in mice (Saab et al., 2009).

NCS-1 regulates inositol 1,4,5,trisphosphate receptors (IP_3R), which are Ca^{2+} channels situated mainly on the ER and release Ca^{2+} to the cytoplasm. NCS-1 has been shown to bind directly to the IP_3R and to enhance channel opening in the presence of IP_3 (Schlecker et al., 2006). NCS-1 and IP_3R interactions are thought to increase the frequency of Ca^{2+} oscillations in cardiac cells (Zhang et al., 2010, Nakamura et al., 2011). There has been no evidence to show that NCS-1 regulates the IP_3R in neurons.

1.3.1 NCS-1 Structure and Localisation

NCS-1 is a small globular protein of 190 amino acids and a molecular mass of approximately 22 kDa. It contains a core hydrophobic pocket which is exposed on binding to Ca^{2+} and forms a binding site for target proteins. Two tryptophan residues (W30 and W130 in human NCS-1) have been shown to move out of the core of the protein in the presence of Ca^{2+} (Aravind et al., 2008) and these may be essential amino acids for target protein interactions.

NCS-1, like CaM, contains 4 EF-hands; however, only EF-hands 2, 3 and 4 bind Ca^{2+}. The Ca^{2+} affinity of EF-hand 2 is 10.0 μM and for EF-hand 3 and 4 is 0.4 μM (Ames et al., 2000). It has been shown that EF-hands 2 and 3 bind Mg^{2+} at resting $[Ca^{2+}]i$ (Aravind et al., 2008). NMR has revealed the structure of NCS-1 in the Mg^{2+} bound form has a different conformation than in the Apo-NCS-1 form, with the hydrophobic pocket tightly closed in the core. Mg^{2+} lowers the affinity of NCS-1 for Ca^{2+} and is thought to have a role in NCS-1 regulation, reducing non-specific binding of NCS-1 at resting Ca^{2+} levels (Aravind et al., 2008). The effects of Mg^{2+} on NCS-1 and its interactions with target proteins are beginning to be investigated. Mg^{2+} may stabilise NCS-1 structure by binding to EF-hand 3. Mg^{2+} may also compete with Ca^{2+} for EF-hand 2 binding which may disrupt target protein binding and inactivate NCS-1 at resting $[Ca^{2+}]i$ (Woll MP, 2011).

NCS-1 is N-terminally myristoylated and is localised to the Golgi complex and the plasma membrane (O'Callaghan et al., 2002). It was thought that all NCS-1 proteins have a constitutively exposed myristoyl tail and are always localised to membranes. In contrast, a recent study looking at Ncs-1 in S*. pombe*, discovered that this orthologue has a Ca^{2+} dependent-myristoyl switch, as seen in other classes of NCS proteins such as recoverin, suggesting this NCS-1 orthologue is not always tethered to the membrane (Lim et al., 2011).

To date the only fully characterised NCS-1 target protein complex structures are of yeast Frq1 and Ncs-1 with a Pik-1 peptide fragment (residues 121–174) (Figure 1.3). One region of Pik-1 binds to the N-terminal cleft of the binding pocket of Frq-1

while the second region binds to the C-terminal cleft, showing 1:1 stoichiometric ratio (Strahl et al., 2007, Lim et al., 2011). This binding is thought to change the conformation of the Pik-1 protein activating its catalytic site (Lim et al., 2011).

Based on indirect data it has been suggested that NCS-1 forms a homodimer when in complex with the D2R in either a 1D2R:2NCS-1 or 2D2R:2NCS-1 stoichiometric ratio (Woll MP, 2011, Lian et al., 2011). The interaction of NCS-1 and a C-terminal D2R peptide has, however, also been examined using NMR (Figure 1.3). It was suggested from these data that a single NCS-1 protein binds to two identical alpha helix regions, each of which are provided by two separate D2R (Lian et al., 2011). The receptors could form a homodimer on binding to NCS-1 in 2D2R:1NCS-1 stoichiometry.

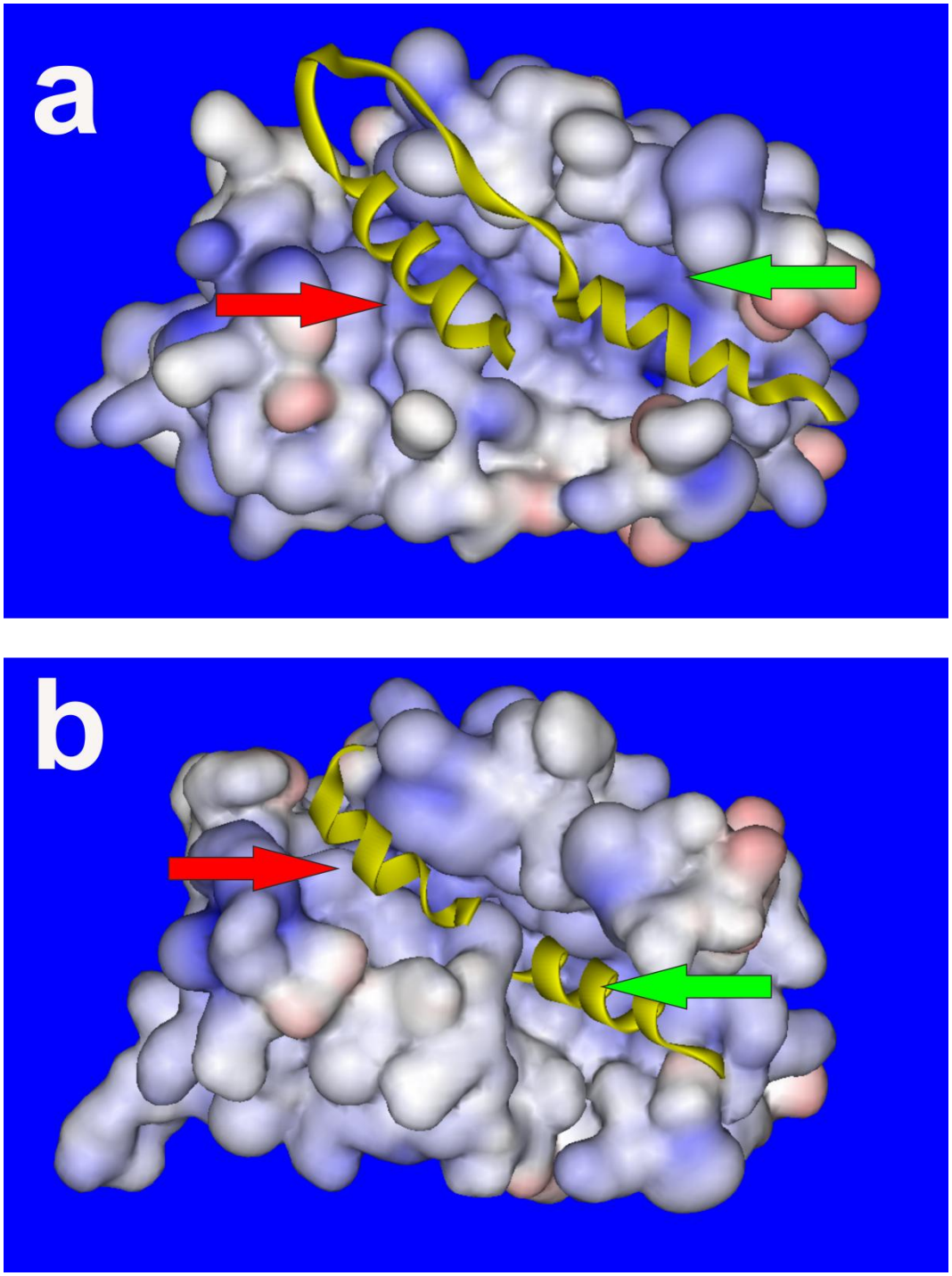

Figure 1.3. NMR derived structures for Frq1 and NCS-1 in target peptide complexes. Surface models of NCS-1 orthologues bound to Pik-1/D2R peptides, a) *S. cerevisiae* Frq-1 in complex with Pik-1 (yellow helix) (residues 121-175) (PDB, 2JU0) and b) Mammalian NCS-1 in complex with two identical peptides of D2R (yellow helix), NCS-1 structure derived from (PBD, 1G8I). Helical regions of the target peptide (yellow helix) bind to two distinct regions of the hydrophobic binding pocket, the N-terminal cleft (red arrows) and C-terminal cleft (green arrows). Red and blue shading represents positive and negative electrostatic regions of the protein surface respectively. Figures taken from Burgoyne and Haynes 2012 and adapted.

1.4 Voltage Gated Ca^{2+}Channels

Voltage gated Ca^{2+} channels (VGCC or Ca_v) are present in excitable cells. In neurons they are localised at the presynaptic terminals close to the SNARE complex machinery (Augustine et al., 2003). The Ca_v channels are the link between membrane depolarisation and neurotransmission. They open as the axon potential reaches the synapse and the membrane depolarises. Ca^{2+} enters the cell through the open channel increasing the $[Ca^{2+}]i$ (Catterall, 2000, Augustine et al., 2003).

Ca_v channels are heteromeric proteins consisting of 4-5 subunits, which are $\alpha1$, β, $\alpha2$, δ and sometimes an additional γ subunit. The $\alpha1$ subunit of the Ca_v channel consists of four transmembrane domains, I-IV, each consisting of six alpha helices. The domains span the plasma membrane and form the Ca^{2+} channel pore (Catterall, 2000). Cytoplasmic loop regions between the four domains and a C-terminal tail provide sites for interaction with regulatory molecules and other channel subunits. There are 10 known genes for $\alpha1$ channel subunits. These genes may have different isoforms and splice variants, expressed in different cell types (Catterall, 2000). The type of $\alpha1$ subunit the channel determines which group it belongs to. The 5 major groups of Ca_v channels were originally determined by the type of Ca^{2+} current they carried. L-type (Ca_v1s) channels, carry long lasting Ca^{2+} currents, P/Q-type, N-type and R-type (Ca_v2s) channels carry non-long lasting currents and T-type (Ca_v3s) channels carry transient currents (Catterall and Few, 2008).

The auxiliary β subunit of the channel is an intracellular globular protein that regulates the channel function. The $\alpha1$ I-II loop contains a motif called the α interacting domain (AID), which binds to the β subunit (Pragnell et al., 1994). This interaction is involved in voltage dependent inactivation of the channel. The $\alpha2\delta$ heterodimer consists of the transmembrane $\alpha2$ subunit and the extracellular δ subunit that are attached by disulphide bonds. This subunit also has a regulatory role. The function of a fifth γ subunit, which is associated with some Ca_v channels, is not fully understood.

1.4.1 Ca_v 2.1 subunit of the P/Q channel

The Ca_v 2.1 (aka α1A) is the α1 subunit of the P/Q-type Ca^{2+} channel and is found mainly in the central nervous system in mammals. It is located on the presynaptic terminal membrane in nanodomains that contain the exocytosis machinery essential for neurotransmission (Westenbroek et al., 1995, Taverna et al., 2004). The α1 subunit has orthologues in different organisms which include cacophony in *D. melanogaster* and UNC-2 in *C. elegans.* The protein was first identified as a 2262 amino acid protein. A further 4 isoforms have been identified in humans rangeing from approximately 2200 to 2500 amino acids. The gene for the protein, CACNA1A (aka CACNL1A4) is located at chromosome 19p13 (Ophoff et al., 1996).

Mutations of CACNA1A have been linked to decreased Ca^{2+}-dependent facilitation of channels in neurons (Adams et al., 2010) and have also been linked to disease. Mutations of the gene change Ca_v2.1 expression or function (Nejatbakhsh and Feng, 2011). Familial hemiplegic migraine type 1 (FHM-1, OMIM 141500) is a condition which causes classic migraines. Recently a stroke patient with FHM-1 was shown to carry a CACNA1A mutation and treatment with a Ca^{2+} channel inhibitor prevented further signs of stroke (Knierim et al., 2011). There are at least also 30 mutations of the CACNA1A4 isoform which are linked to Episodic ataxia type 2 (EA-2, OMIM 108500) (Ophoff et al., 1996). Severe uncoordinated movement is the primary symptom of this disorder and has been linked to epilepsy and migraine. Mutation R1820Stop, codes for a complete pore-forming region but does not have the C-terminal cytoplasmic tail and has been linked both to EA-2 and epilepsy (Jouvenceau et al., 2001). Cells expressing this mutated gene do not display a voltage-dependent current. It is possible that the channel is expressed without the C-terminal region which is important in channel regulation. Alternatively the stop mutation may prevent the channel being expressed by the cell. Other mutations in CACNA1A are responsible for spinocerebellar ataxia 6 (SCA6, OMIM 183086) (Zhuchenko et al., 1997). This is a progressive degenerative disorder with symptoms including ataxia, involuntary eye movement and motor speech disorder. Many mutations cause abnormal splicing of the channel. The CACNA1A mutations include CAG repeats of varying length which have been shown to create abnormal splice

sites near the C-terminus. Modulation of the Cav2.1 subunit of the P/Q channel by Ca^{2+} sensor proteins will be discussed and investigated in Chapter 3.

1.5 *Caenorhabditis elegans* as a Model Organism

In nature, *Caenorhabditis elegans* (*C. elegans*) is a non-pathogenic nematode worm found in decaying vegetation in soil in temperate regions of the world, (Kiontke and Sudhaus, 2006). It was established as a model organism by Sidney Brenner and used to study the genetic basis of behaviour (Brenner, 1974). It was the first multi-cellular organism to have its whole genome sequenced (CSC, 1998). Many genes of interest from other species including humans have homologues in *C. elegans* leading to many laboratories using the worm to study biological functions and diseases (Kaletta and Hengartner, 2006). In 2002, Brenner, Sulston and Horvitz won the Nobel Prize "*for their discoveries concerning genetic regulation of organ development and programmed cell death*'" which included work using the *C. elegans* model organism (Nobelprize.org., 2002, Sulston and Horvitz, 1977, Brenner, 1974, Ellis and Horvitz, 1986). Other prominent discoveries that have been made using *C. elegans* include, the work of Fire and Mello who won a Nobel prize for the use of RNA interference in the worm to knockdown genes of interest (Nobelprize.org., 2006, Fire et al., 1998). Martin Chalfie won a Nobel prize for his part in " *the discovery and development of the green fluorescent protein, GFP*" whereby he expressed GFP in specific cells within living *C. elegans* (Nobelprize.org., 2008, Chalfie et al., 1994).

The worm is small (approximately 1 mm long), low cost, easy to manipulate, maintain and store long term. It is a multi-cellular organism which does not have the ethical and moral issues of using vertebrate organisms and provides a whole animal model to discover and test physiological mechanisms. *C. elegans* are transparent which enables live imaging of their internal structures. *C. elegans* has two sexes, hermaphrodites (XX) which give rise to genetically identical progeny and males (XO) which mate with the hermaphrodite and can be used to introduce

mutations into strains. The lineage of all 959 cells of the adult hermaphrodite worm have all been identified (Sulston and Horvitz, 1977).

C. elegans lacks the major complex organs found in humans, but they share similar molecular mechanisms which can be exploited to understand human physiology and diseases. For example, despite having no organs comparable to the kidney, *C. elegans* have been used to investigate kidney function, development and polycystic kidney disease because genes and molecular pathways which are involved in male mating behaviour in the worm are homologous to those of the human kidney (Barr and Sternberg, 1999, Barr, 2005).

C. elegans have a short reproduction and developmental cycle, giving rise to hundreds of adults in a few days. The complete life cycle of *C. elegans* from fertilisation to death is approximately 20-30 days (Olsen et al., 2006) making *C. elegans* ideal for high-throughput studies of not only developmental control mechanisms, which can take months in other models (Sulston et al., 1983), but also molecular pathways, disease models and drug targets. (Kaletta and Hengartner, 2006).

1.6 *C. elegans* Nervous Systems

Hermaphrodite *C. elegans* have a simple nervous system which consists of 302 neurons compared to the complex nervous system in humans which contains billions of neurons (White et al., 1986). The function of the *C. elegans* nervous system is to detect its environment, process information and adapt behaviour allowing the worm to find food and amiable habitat and to an avoid harmful conditions. A wiring diagram for chemical synaptic connections for every neuron in hermaphrodite worm has been created (White et al., 1986, Varshney et al., 2011). No wiring diagram exists for the gap junctions, which allow electrical signalling between the neurons or modulation of neurons by neuropeptides released from contains sensory, interneurons and motor neurons like the human nervous system (Figure 1.4)

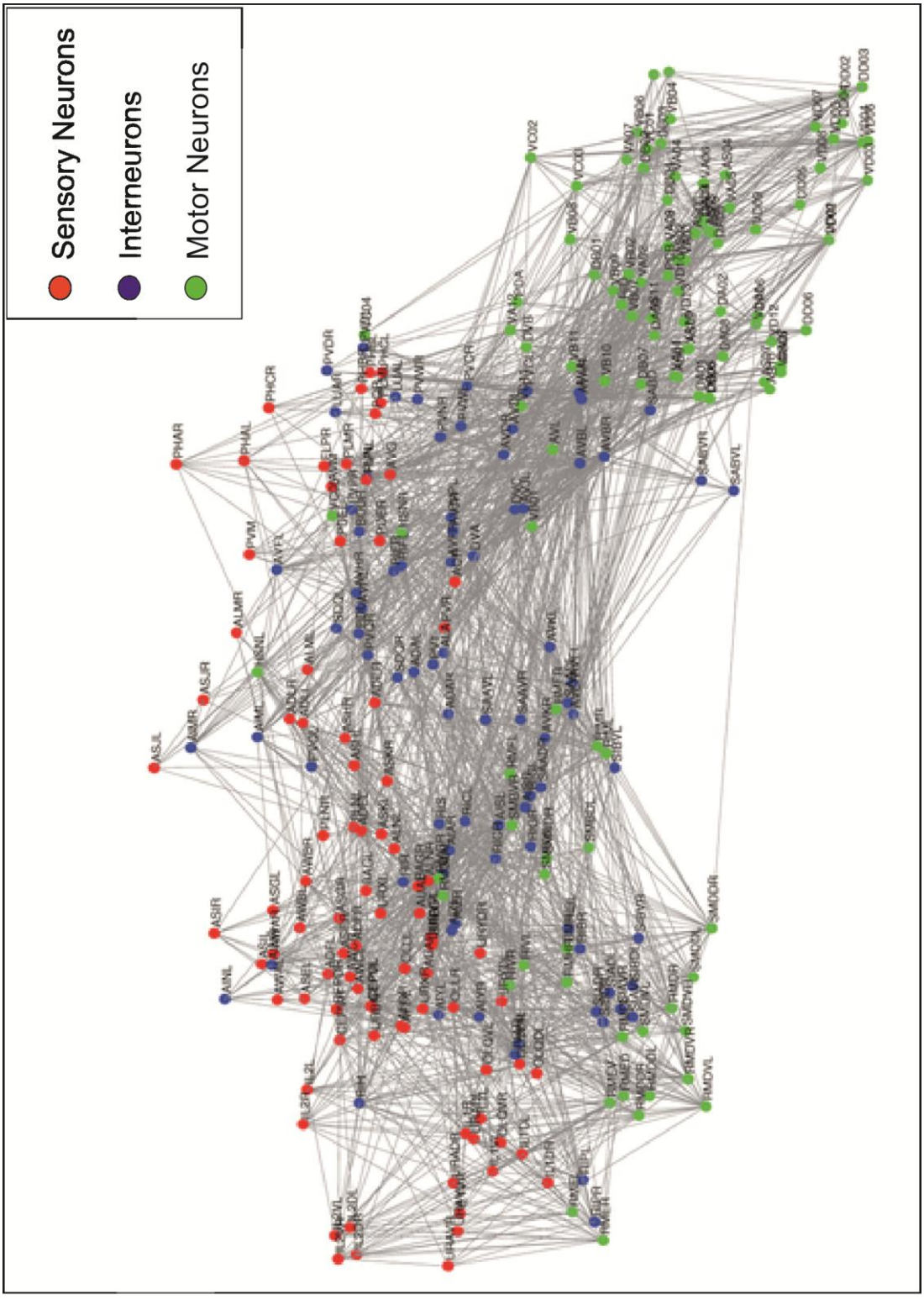

Figure 1.4 *C. elegans* Neuronal Conectome. The current complete *C. elegans* wiring diagram, which has common features to the human neuronal system. Chemical synapses have been shown as connections between neurons. The signal flow direction is mainly from left top of the diagram to the bottom right, traveling from the sensory neurons (red), to the interneurons (blue) to the motor neurons (Diagram reprinted from (Varshney et al., 2011).

The nervous system of *C. elegans* contains genetic and molecular pathways similar to those in mammals and has been used to study many of the shared mechanisms including the SNARE complex machinery involved in neurotransmission (Barclay et al., 2012). For example, UNC-18 is a protein which has a role in SNARE complex formation. Mouse Munc-18 (the murine orthologue of UNC-18) has been expressed in the worm *unc-18* null mutant where it completely rescued the defective neurotransmission function in the mutant (Gengyo-Ando et al., 1996). *C. elegans* has also been used as a model for neurodegenerative diseases to screen for novel neuronal drug targets (Leung et al., 2008, Chen and Burgoyne, 2012, Johnson et al., 2010).

The worm nervous system is divided into two separate systems, the general nervous system which consists of 282 neurons and the pharyngeal nervous system which consists of 20 neurons and functions as a neuromuscular pump for feeding. (Altun et al., 2002-2012). The two nervous systems operate almost independently communicating via the RIP interneuron pair (Altun et al., 2002-2012).

The general nervous system is made up of four types of neuron, sensory neurons, interneurons, motor neurons and polygonal neurons which perform the functions of more than one type of neuron (Figure 1.4). It consists of four major structures. The nerve ring (NR) in the head, the ventral nerve cord (VC), the dorsal cord (DC) and the tail nerve structures (Figure 1.5). There are approximately 200 neuronal processes from sensory neurons and interneurons which create the nerve ring around the pharynx in the head of the worm. Here the processes form synaptic connections with other neurons to transmit signals. The head and the tail of the worm contain sensory structures and ganglia consisting of neural cell bodies. The VC is made up of cell bodies and processes of motor neurons and interneurons (Figure 1.5). The DC runs parallel to the VC on the opposite side of the body. It is made mainly of motor neuron processes which extend from VC by lateral nerve tracts and a small number of interneuron processes from the nerve ring (Figure 1.5).

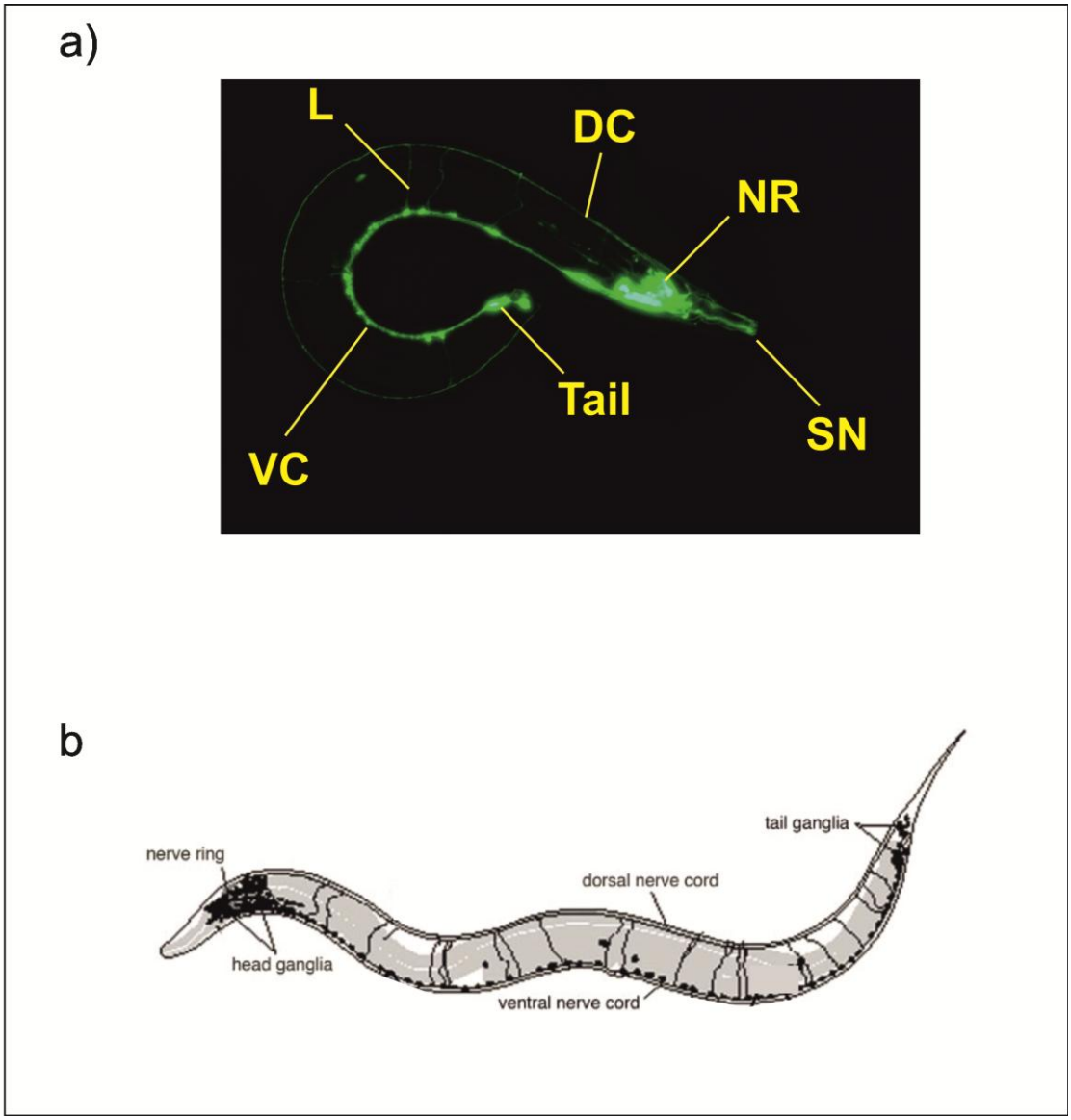

Figure 1.5 Overview of the Hermaphrodite C*. elegans'* General Nervous System. a) The Nerve ring (NR) is the major neuronal structure and runs around the pharynx. Sensory neurons (SN) in the head extend dendrites from the cell body to the nose tip. The two major nerves of the worm are the ventral cord (VC) and dorsal cord (DC), which run parallel to each other on opposite sides of the body from the head to the tail. Lateral nerves (L) form connections between the major nerves. The tail tip contains sensory structures and tail ganglia. All neurons of the nervous system labelled with GFP driven by the pan-neuronal *rab3* promoter. b) Simplified anatomy of the hermaphrodite nervous system (Diagram reprinted from (Von Stetina et al., 2007)

1.6.1 Motor Neurons

Motor neurons control the motility of the alimentary canal and locomotion of the organism. After receiving a signal from the interneurons, three types of motor neurons in the VC and DC regulate the dorsal and ventral muscle wall cell function. Type A and B motor neurons are excitatory cholinergic neurons, which cause the muscle wall cell to contract (White et al., 1986). Type A neurons regulate backward motion and type B regulate forward motion (Chalfie et al., 1985). Type D motor neurons are inhibitory dorsal cord neurons which cause the muscle wall cells to relax (White et al., 1986) The characteristic rhythmic wave of *C. elegans* locomotion is regulated by the coordinated relaxation and contraction of muscle wall cells at opposite sides of the worm (McIntire et al., 1993). Motor neurons can change locomotion by modulating the body wall muscle in response to a stimulus upstream in the neuronal circuit, which can include touch or other sensory stimulus. Changes in locomotion can include forward or backward movement, acceleration or turns (Chalfie et al., 1985).

1.6.2 Interneurons

In humans interneurons are located predominately in the central nervous system. *C. elegans* interneurons are located predominately in the nerve ring and VC (Altun et al., 2002-2012) and perform a similar role to those of humans, forming connections in the neuronal network; they also receive input from sensory neurons, process the signal, modulate a decision and relay an output to the motor neurons.

1.6.3 Sensory Neurons

There are approximately 40 classes of sensory neurons, many of which are ciliated (Altun et al., 2002-2012, Hope, 1999) and can form sensory structures called sensillia. Those within the head include the amphids, anterior deirids, the inner and outer labials and the cephalics and those in the tail include the phasmids and the posterior deirids. Isolated sensory neurons may also be located in the body, head or

tail tip. The cell bodies of sensory neurons of sensory structures, such as the amphids, may form ganglions in the head and tail. Dendrites project from the cell body of the neuron and extend to the tip of the nose or tail surface (Figure 1.5). In the head, the axons of sensory neurons project from the cell body and can enter the nerve ring where they communicate with other neurons and pass on the sensory input (Sasakura and Mori, 2012).

1.6.4 Ciliated Sensory Neurons

Cilia are organelles which form projections from the cell surfaces, and contain microtubules as their major component. There are two groups of cilia; motile cilia which are required for movement or flow and primary cilia (non-motile) which are present on most types of mammalian cells and appear to have a role in cell signalling regulating homeostasis and development (Lee and Gleeson, 2010). Some specialised sensory neurons in humans are ciliated, these include photoreceptors in the eye, cochlear hair cells in the inner ear and olfactory sensory neurons in the nose, which detect external signals of light, sound or smell from the outside world via the cilia to the nervous system (Lee and Gleeson, 2010, Jenkins et al., 2009).

As with other types of sensory neurons, the majority of ciliated sensory neurons in *C. elegans* are in the head. The amphid contains three groups of ciliated neurons: - single or dual rod cilia, winged cilia and finger-like of which there is one class (Table 1.2.). The tail of the worm also contains rod ciliated sensory neurons, in a sensory structure called the phasmid (Table 1.2). The cilia of the rod ciliated sensory neurons in the amphid and phasmid are exposed to the external environment, while the winged and finger-like ciliated neurons are surrounded by a stealth cell (Figure 1.6) (Perkins et al., 1986). Several amphid and phasmid ciliated neuronal pairs have been shown to express NCS-1 (Gomez et al., 2001). Other types of ciliated sensory neurons in the head also terminate at the tip of the head while the posterior deirids terminate at the surface of the tail near the anus.

Table 1.2 Amphid and Phasmid Ciliated Sensory Neurons

Name	Cilia Type	External exposed	Sensory Role (From Wormatlas, Individual Neuron Database http://www.wormatlas.org)
ASE	Single rod cilia	Y	Gustatory-chemosensory
ASG	Single rod cilia	Y	Gustatory-chemosensory
ASH	Single rod cilia	Y	Nociceptive osmo-, mechano- and odour
ASI	Single rod cilia	Y	Gustatory-chemosensory, thermosensory
ASJ	Single rod cilia	Y	Sensory
ASK	Single rod cilia	Y	Gustatory-chemosensory and pheromone sensory
ADF	Dual rod cilia	Y	Chemosensory and oxygen sensory
ADL	Dual rod cilia	Y	Chemosensory, odour sensory, pheromone sensory and nociceptive
AWA	Winged Cilia	N	Odour sensory
AWB	Winged Cilia	N	Odour sensory
AWC	Winged Cilia	N	Odour sensory and thermosensory
AFD	Finger-like	N	Thermo (thermal nociception and thermotaxis) $C0_2$ sensory
PHA	Single rod cilia	Y	Chemosensory
PHB	Single rod cilia	Y	Chemosensory

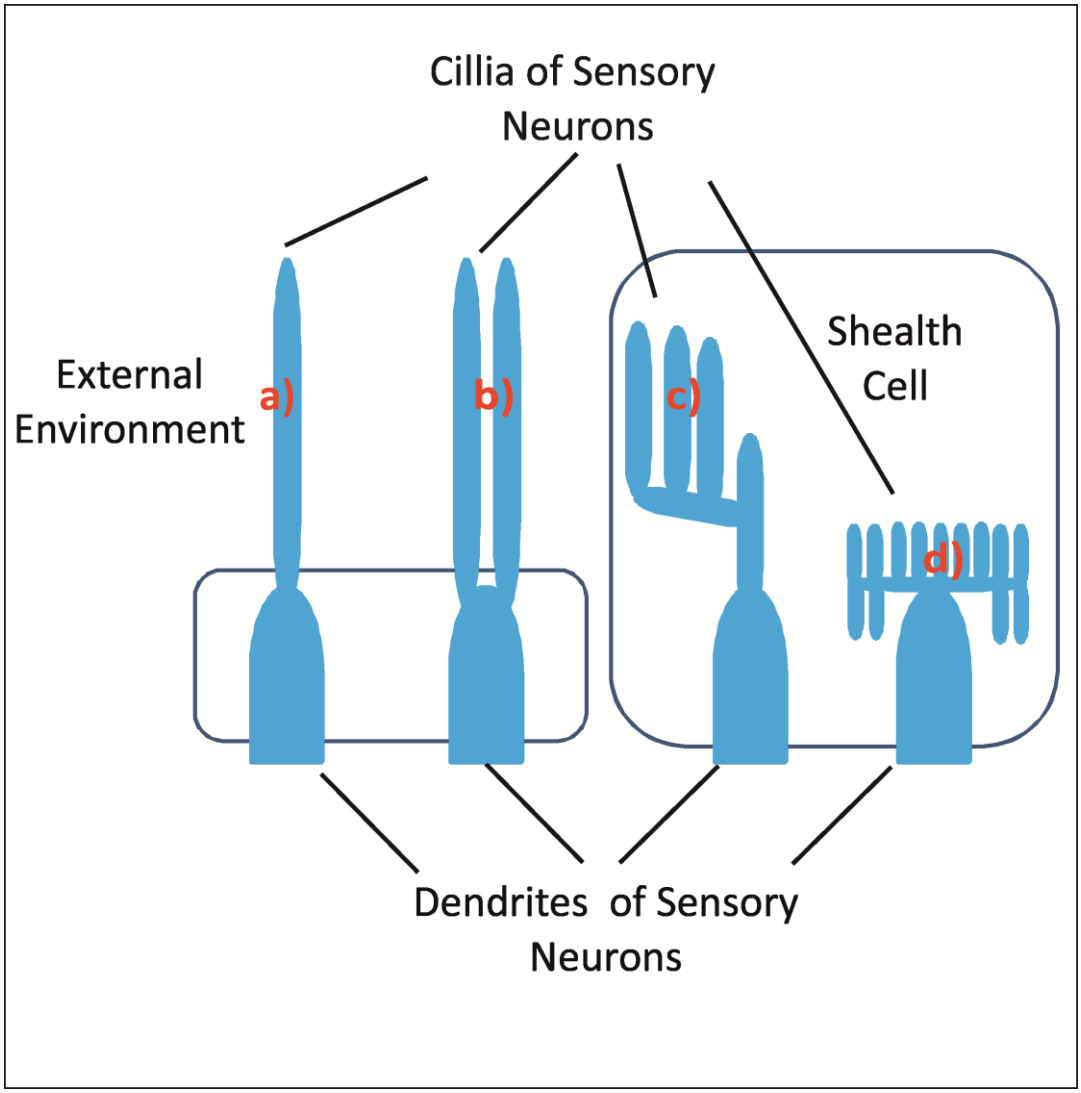

Figure 1.6 Ciliated Sensory Neurons of the Amphid and Phasmid at *C. elegans* Head and Tail. Illustration of ciliated neurons (adapted from images shown in (Perkins et al., 1986) a) single and b) dual rod ciliated neurons are exposed to the external environment but c) winged and d) finger-like ciliated sensory neurons are embedded in sheath cells.

1.7 Thermosensation and Regulation

In the wild, *C. elegans* live in moderate soil temperatures between 16°C -26°C. The worm has the ability to detect changes in temperature (Schafer, 2012). Thermotaxis and thermoavoidance (Schafer, 2012, Wittenburg and Baumeister, 1999, Hedgecock and Russell, 1975) are the two distinct types of thermosensation in *C. elegans* that have been studied. These behaviours are necessary for the worm to regulate its temperature for homeostasis, to seek food and favourable conditions

and to avoid noxious conditions i.e. extreme high or low temperatures. Three reviews give a complete picture of the complexity and controversy surrounding the thermosensation field including neuronal circuits and signalling pathways involved in isothermal tracking and memory (Sasakura and Mori, 2012), on the negative temperature bias (Ma and Shen, 2012) and on thermoavoidance (Liu et al., 2012). This section of the introduction will give a brief summary on these behaviours.

1.7.1 Thermotaxis

Thermotaxis behaviour of *C. elegans* was identified in 1975. During thermotaxis, the worm migrates towards its cultivation temperature (Hedgecock and Russell, 1975). Thermotaxis, along with other sensory-regulated locomotion behaviours such as chemotaxis, is regulated by two strategies:- the gradual steering strategy and the biased random walk strategy (Sengupta and Samuel, 2009). The biased random walk strategy navigates the worm towards the favourable conditions it has detected which it does by increasing the length of its forward runs. If it encounters unfavourable conditions it will shorten a forward run by turning, thereby increasing the frequency of the turns until conditions are more favourable (Sengupta and Samuel, 2009). The gradual steering strategy works in tandem with the biased random walk and it enables the worm to travel up gradients and remain within favourable conditions (Sengupta and Samuel, 2009).

Thermotaxis was assayed initially using two methods. Firstly, populations of worms were placed on a linear temperature gradient and the worms were allowed to migrate to their preferential temperature and the accumulations of worms at specific temperatures were recorded. The second assay measured isothermal tracking which is an example of the gradual steering strategy (Sengupta and Samuel, 2009). Isothermal tracking is the ability of the worm to identify, locate to and remain on track, within a specific temperature with a variation of approximately 3^{o}C. To assay this behaviour, individual worms were placed on NGM agar plates which had a radial thermal gradient and the radial tracks left by the worm were recorded (Mori and Ohshima, 1995, Hedgecock and Russell, 1975).

In the wild-type *C. elegans* the thermotaxis behaviour was shown to be modified by the cultivation temperature the worm had previously experienced, suggesting a function of memory and learning (Hedgecock and Russell, 1975). The worms display behavioural plasticity and are able to associate temperature with the availability of food. When cultivated at the standard temperature of 20^{o}C, worms migrated towards 20^{o}C and displayed isothermal tracking behaviour. When cultivated at a lower temperature of 16^{o}C they migrated and tracked to 16^{o}C and had the same response when cultivated at the higher temperature of 25^{o}C. *C. elegans* can also use this memory to avoid temperatures that it predicts it will not find food, hence displaying learning behaviours. Thermotaxis behaviour has been further characterised by video tracking which analysed run duration time, turn frequency and run speed and swimming locomotion (Ryu and Samuel, 2002, Tsalik and Hobert, 2003, Sasakura and Mori, 2012).

Mutant worms display several thermotactic phenotypes. Thermophilic mutants that migrated towards higher temperatures retained the ability to be modulated by cultivation temperatures, and cryophilic mutants migrated to colder temperatures suggesting that positive thermotaxis (movement towards warmer than cultivation temperatures) and negative thermotaxis (movement towards colder than cultivation temperatures) are both required for wild-type thermotaxis. Cryophilic mutants were not affected by alterations of the cultivation temperatures nor were they able to perform isothermal tracking suggesting that positive thermotaxis, memory and isothermal tracking are linked (Hedgecock and Russell, 1975). Recent studies showed that the AIY interneuron signalling drove positive thermotaxis and was involved in memory but not negative thermotaxis, while AIZ interneurons was responsible for negative thermotaxis and not positive thermotaxis (Mori and Ohshima, 1995, Mori et al., 2007). Other mutants and neuronal ablations show athermotaxis and do not favour a specific temperature (Hedgecock and Russell, 1975, Mori and Ohshima, 1995, Sasakura and Mori, 2012).

1.7.2 Thermotaxis Neuronal Circuits

Three pairs of sensory neurons are involved in the thermotaxis circuit, the AFD neurons are the major thermotaxis sensory neurons, the AWC neurons have been shown to be involved in signalling during temperature change (Figure 1,7) (Biron et al., 2008, Kuhara et al., 2008) and the ASI neurons have also been shown to be involved in negative thermotaxis (Beverly et al., 2011). Using thermotaxis behavioural assays and neuronal Ca^{2+} imaging in sensory neuronal ablated animals, different combinations of these thermosensing neurons pairs appear to have single or combined responses under specific temperature conditions, such as cultivation temperature and gradient temperature, which enables the worm have normal thermotaxis bias (Beverly et al., 2011).

The molecular pathways in AWC, AFD, AIY, AIZ and RIA neurons have also been shown to be involved in isothermal tracking and memory (Sasakura and Mori, 2012, Mori et al., 2007, Kimata et al., 2012) (Figure 1.7).

A recent review hypothesised that the ASI sends thermosensory signals to the AIA and AIB interneurons (Figure 1.8) (Ma and Shen, 2012). ASI, AIA or AIB are not thought to be involved in isothermal tracking and memory as ablating the AIB neuron was shown to not affect isothermal tracking, while ablation of the AIY or the AIZ neurons did affect this behaviour (Mori and Ohshima, 1995, Ma and Shen, 2012).

AFD, AWC and ASI neurons are three different types of amphid sensory (finger-like, winged and single rod) ciliated neurons and also have been shown to have a role in other sensory responses. The AFD neurons sense CO_2; the AWC neurons sense odour and the ASI neurons are gustatory chemosensory neurons (Bargmann and Horvitz, 1991) and together with AWC neurons are involved in the regulation of sexual attraction (White and Jorgensen, 2012).

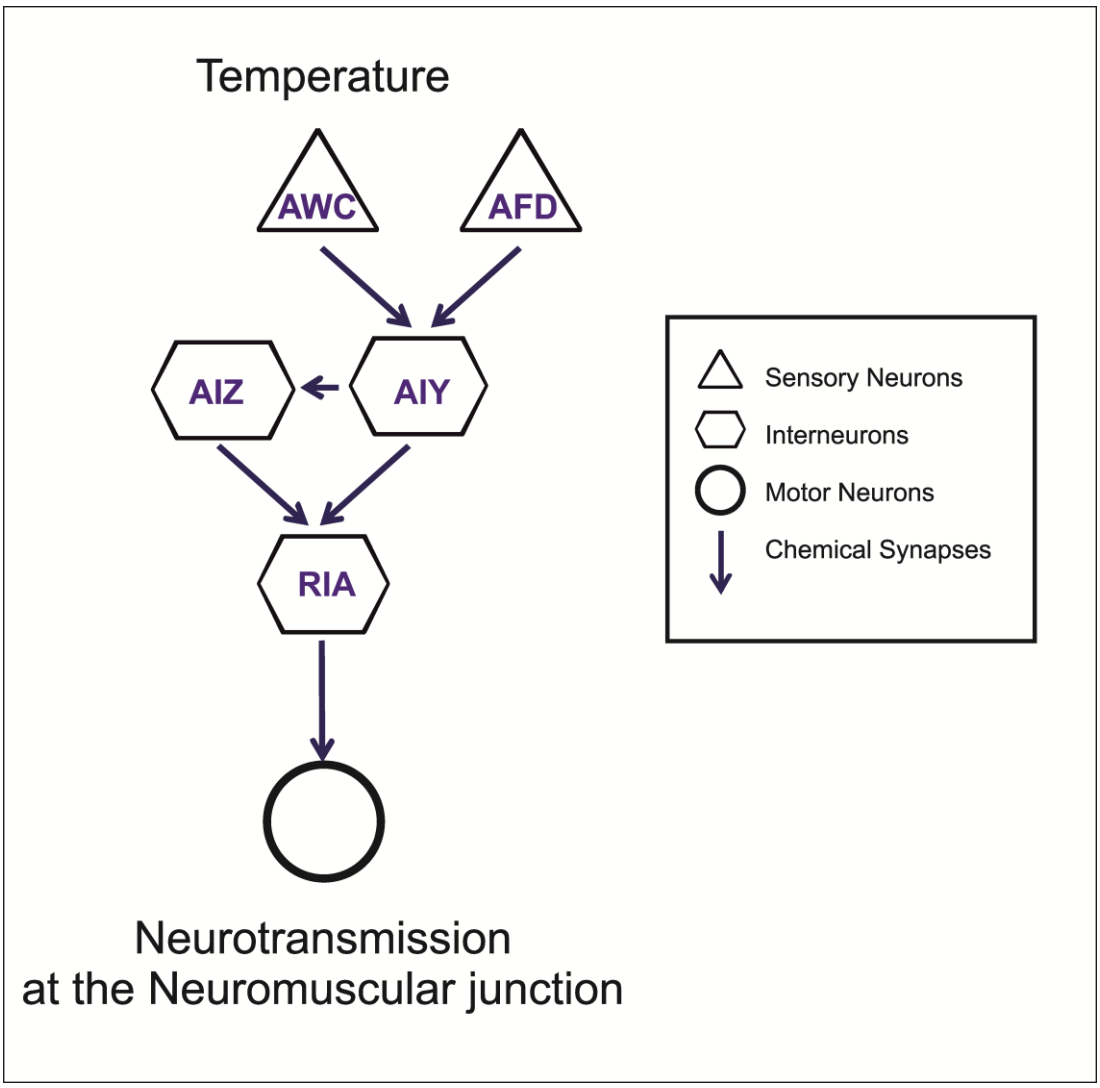

Figure 1.7 Isothermal tracking and Memory Neuronal Circuit. The current wiring diagram of neurons involved in thermotaxis, isothermal tracking and memory (adapted from (Sasakura and Mori, 2012). Pathways in all of the sensory and interneurons in this circuit have shown behavioural plasticity. AWC and AFD sensory neurons detect temperature and store information. Signals are transmitted to the AIY (thermophilic drive) and AIZ (cryophilic drive) interneurons which signal to the RIA interneuron and regulate locomotion in response to temperature.

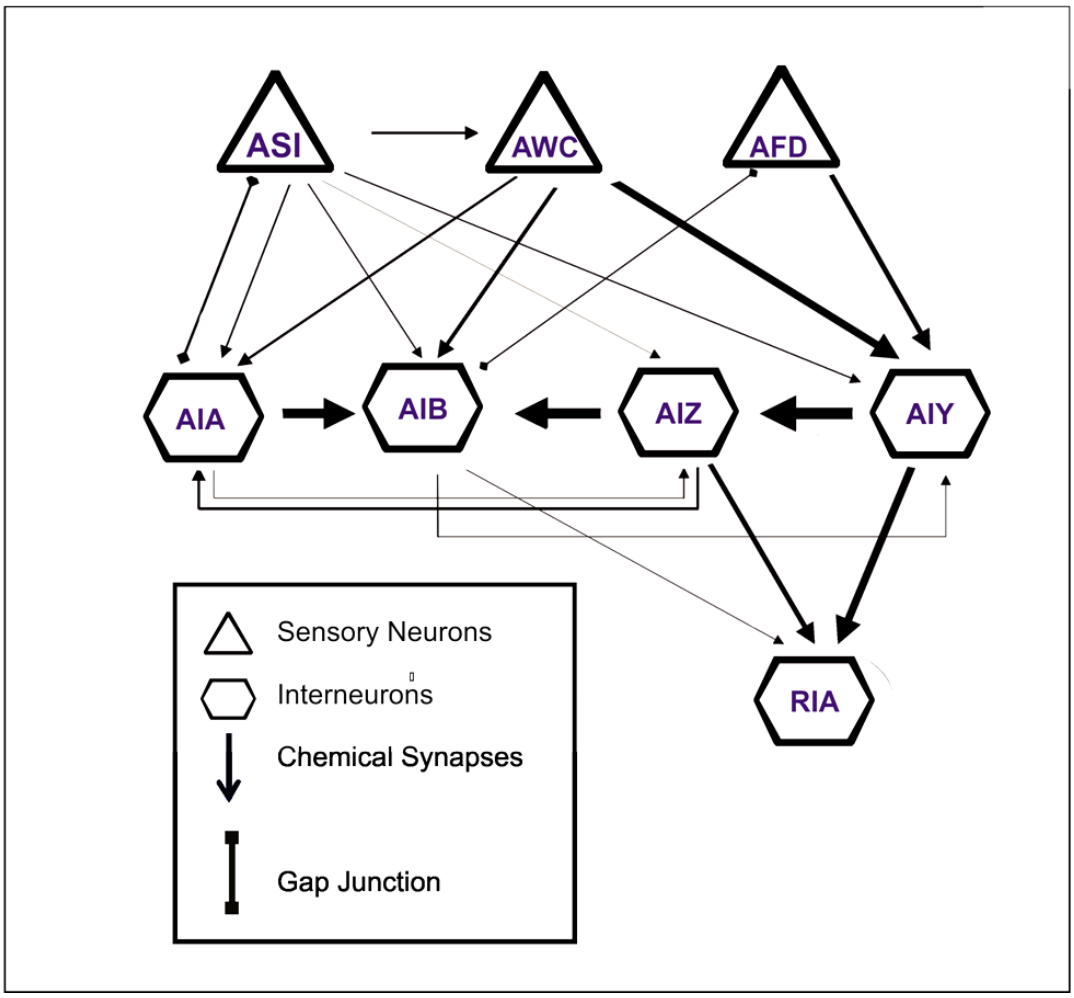

Figure 1.8 The Hypothesised Negative Thermotaxis Neuronal Circuit. A wiring diagram showing proposed synaptic and gap junction neuronal conections. The diagram shows the excepted thermotaxis circuitry sensory and interneurons neurons AFD, AWC , AIY, AIZ and RIA. The ASI sensory neuron recently linked to negative thermotaxis and AIA and AIB hypothesized to also be involved. (Figure taken from (Ma and Shen, 2012)

1.7.3 Thermoavoidance

Thermoavoidance is the detection and escape behaviour in response to harmful extreme high or low temperatures. The first neurons identified as being responsible for thermal nociception were the FLP neurons, phasmid PHC neurons and the PVC interneurons in the VC (Wittenburg and Baumeister, 1999) (Figure 1.9). Recently the amphid AFD neurons have also been recognised to detect noxious temperatures (Liu et al., 2012). During thermal nociception the AFD sends a signal to the AIB interneuron through a gap junction rather than to the AIY interneuron

which is signalled in thermotaxis by synaptic neurotransmission (Kimura et al., 2004) (Figure 1.9). Thermoavoidance behaviour is not effected by altering cultivation temperature and shows no memory adaption (Wittenburg and Baumeister, 1999).

1.7.4 Temperature-Dependent Locomotion

Recently our group employed a temperature-dependent locomotion (TDL) assay for *C. elegans* to study the diacylglycerol (DAG) signalling pathway in SNARE complex formation and synaptic function. The assay is based on the hypothesis that the AFD sensory neuron can signal to downstream neurons via synaptic neurotransmission (Mori and Ohshima, 1995, Edwards et al., 2012). Rather than using the established thermotaxis methods such as isothermal tracking, linear gradients or neuronal Ca^{2+} imaging, this method involved comparing locomotion rates in a liquid medium at a standard cultivation temperature ($20^{o}C$) and after elevation to a higher temperature of $28^{o}C$. Wild-type worms showed an approximate reduction of 70% of their locomotion rate at $28^{o}C$ compared to $20^{o}C$. Various exocytosis mutants and rescue worms were also assayed. The results suggested that on detecting heat protein kinase C- 2 (PKC-2) is activated by DAG signalling and phosphorylates UNC-18 at residue S322. The TDL assay proved to be a useful method for analysing the regulation of neurotransmission and its role in thermosensation. Data from previous studies on the AFD neuron and its role in thermosensation suggest it signals to the AIY neurons, the interneuron involved in thermophilic signaling, via neurotransmission. The AFD neuron is unlikely to be signalling to the AIZ interneurons in this TDL assay as this connection is involved in cryophilic signalling at lower than cultivation temperatures. So far no studies have examined memory and adaption to cultivation temperature for this behaviour.

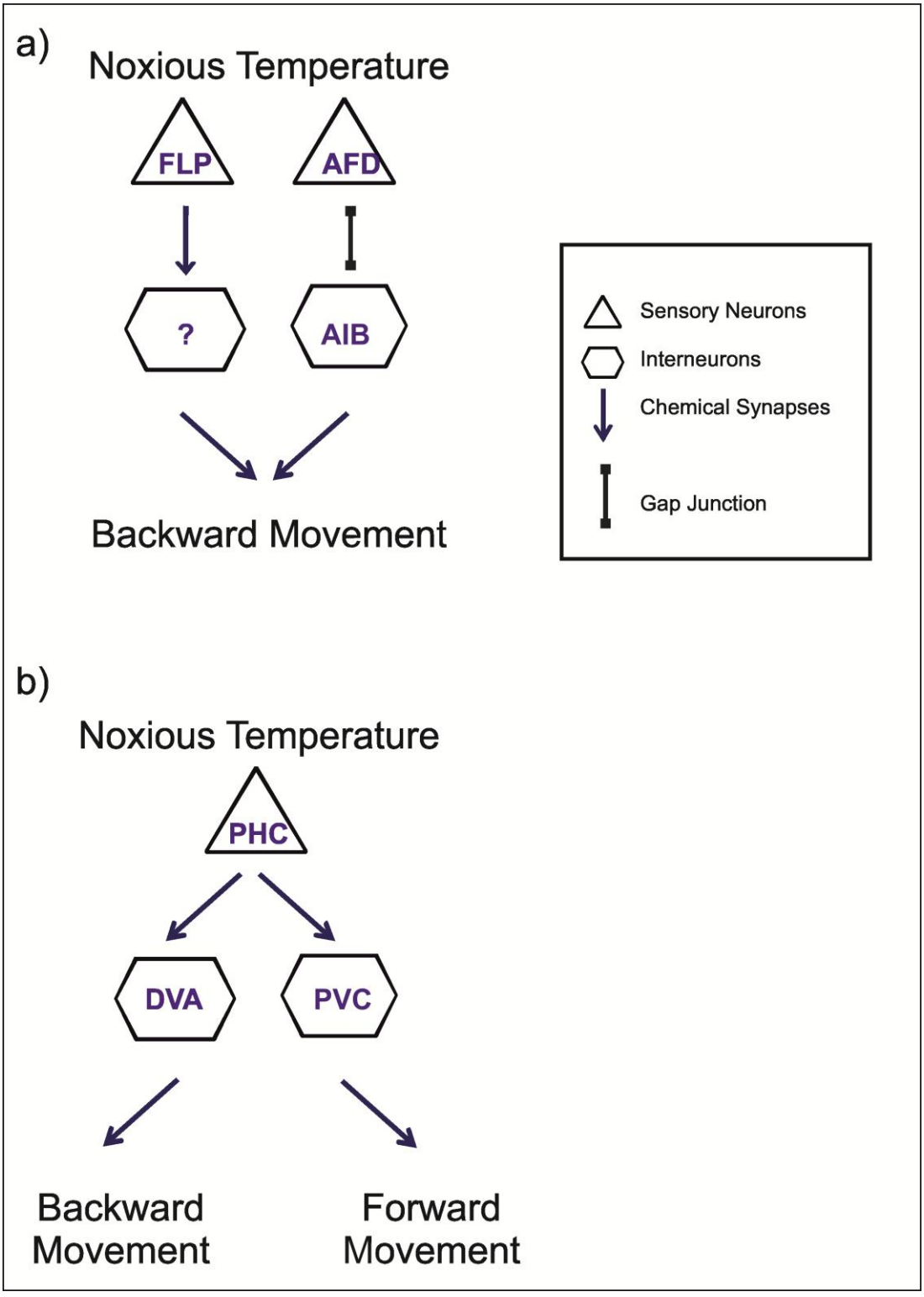

Figure 1.9 Thermoavoidance Neuronal Circuit. The current wiring diagram of head and tail neurons involved in thermoavoidance (adapted from (Liu et al., 2012). a) Detection of a noxious temperature in the head causes the worm to display backwards thermal avoidance locomotion. AFD sensory neuron sends information to the AIB interneuron via gap junction signalling. FLP sensory neuron signals to an unidentified interneuron. b) Detection of a noxious temperature in the tail causes the worm to display either forward or backward thermal avoidance movement. PHC sensory neuron signals to the DVA (driving backwards movement) or PVC (driving forwards movement), which regulates thermoavoidance behaviour.

1.8 *C. elegans* and Ca^{2+} Binding Proteins

C. elegans have a large number of proteins involved in Ca^{2+} signalling. Computational analysis performed on the *C. elegans* genome predicted Ca^{2+} binding properties for 209 proteins of which 170 posses EF hand motif proteins including calmodulin, NCS and proteins which have other functions such as forming ion channels which also contain the EF hand motif. The other 39 proteins contained different Ca^{2+} binding motifs such as the C2 domain (Kumar et al., 2012). *C. elegans* have more than 100 candidate neuronal Ca^{2+} binding proteins, of which 65 contain EF hand motifs and no other functional domains (Hobert, 2013). They include the worm CaM orthologue (CMD-1) and eight other CaM related genes (Hobert, 2013). Previously three NCS proteins in the worm were identified NCS-1,2 and 3 (Decastro et al., 1995, Rajaram et al., 2000). Recent reanalysis of the *C. elegans* genome has identified four additional potential NCS proteins (NCS-4 to NCS-7) (Hobert, 2013). The nomenclature of the *C. elegans* NCS proteins suggests they are all NCS-1 Class A orthologues of mammalian NCS-1, however, only NCS-1 and NCS-3 genes have orthologues with NCS-1 showing the highest sequence identity of 75% to human NCS-1 (Table 1.3).

Table 1.3 *C. elegans* NCS Proteins

Orthologue and % Sequence Identity of Ce- NCS to Human NCS were calculated using NCBI.BLASTp. *Functional EF hand motifs were predicted using Interpro.EMBL sequence functional analysis software using the SMART.EMBL database.

Ce NCS	Human NCS #	Sequence Identity Ce NCS to Human NCS #	Class	Position number of predicted functional EF hand motifs *
NCS-1	NCS-1	75%	A	2,3,4
NCS-2	HCLP-1	51%	B	2,3,4
NCS-3	NCS-1	67%	A	2,3,4
NCS-4	KChIP1, 2, 3, 4?	~35%?	E	2, 4
NCS-5	-	-	-	4
NCS-6	-	-	-	0
NCS-7	KChIP1,2,3,4	~40%?	E	2,3,4

A blast search of NCS-2 shows its closest human orthologue is NCS class B hippocalcin-like protein 1 (HCLP-1) showing 51% sequence identity. NCS-4 and NCS-7 share sequence identity with the human class E proteins KChIPs 1-4 (approximately 35% and 40% respectively). NCS-5 and NCS-6 do not appear to be orthologues of any class of human NCS proteins, although, they show a higher sequence identity to human KChIP2 than to any other human protein. As discussed early in this chapter, NCS proteins contain an inactive EF hand (motif 1), which is unable to bind Ca^{2+} and three functional EF hand motifs 2, 3, and 4. Analysis of all *C. elegans* NCS sequences (wormbase) using functional analysis software (Interpro.EMBL) predicted that only NCS-1, 2, 3 and 7 proteins contain all three functional Ca^{2+} binding sites. Therefore it is questionable whether NCS-4, 5, 6 are functional NCS proteins. It could be that these proteins form a different subclass of NCS protein with divergent structures and functions; however considerable work will be needed to establish this.

Analysis of the worm *ncs-3* null strain showed no obvious phenotype. It was only assessed, however, for a kinked motion behaviour and other behaviours have not been characterized (Rajaram et al., 2000). It was surmised that *ncs-3* null showed no phenotype–because there is redundancy with other NCS proteins, in particular NCS-1 to which it shows 80% homology (Rajaram et al., 2000). In worm Alzheimer's disease model, in which amyloid aggregates build up in muscle cells and cause paralysis, knockdown of *ncs-3* was shown to suppress the toxicity (Lopez, 2010). This not only suggests that NCS-3 is expressed in muscle cells but also that NCS proteins might have a role in control of amyloid plaque formation in Alzheimer's disease and other amyloid pathologies (Lopez, 2010). Although localisation and function of NCS-2 have not been established, it appears to have an essential role in the worm, as knockout is lethal. The location of expression and functions of the other NCS proteins is yet to be determined.

NCS-1 has been shown to be expressed in *C. elegans* in 10 pairs of sensory neurons, two pairs of interneurons, one polymodal interneuron/motorneuron pair and a one

muscle cell type by GFP reporter gene and validated by immunostaining (Table 1.4) (De Castro, 1997, Gomez et al., 2001).

Table 1.4. *C. elegans* Cell Types Expressing NCS-1

Cell (De Castro, 1997, Gomez et al., 2001)	Cell Type Taken from (Altun et al., 2002-2012)	Function Taken from (Altun et al., 2002-2012)
ASE L/R	Amphid Sensory Neuron	Gustatory-chemosensory
ASG L/R	Amphid Sensory Neuron	Gustatory-chemosensory
ADF L/R	Amphid Sensory Neuron	Chemosensory and oxygen sensory
AWA L/R	Amphid Sensory Neuron	Odour sensory
AWB L/R	Amphid Sensory Neuron	Odour sensory
AWC L/R	Amphid Sensory Neuron	Odour sensory and thermosensory-(thermotaxis)
AFD L/R	Amphid Sensory Neuron	Thermosensory- (thermal nociception and thermotaxis) and $C0_2$ sensory
BAG L/R	Head Ciliated Sensory Neuron (Not part of amphid)	Nociception, $C0_2$ and oxygen sensory
PHA L/R	Phasmid Sensory Neuron	Chemosensory
PHB L/R	Phasmid Sensory Neuron	Chemosensory
AVK L/R	Interneuron NR/VC	Little known
AIY L/R	Interneuron Head	Amphid interneuron receives and processes output from amphid neurons, involved in regulating gustatory and olfactory behaviour, thermotaxis, memory, lifespan and stress responses.
RMG L/R	Polymodal Interneuron/Motorneuron Head	Receives and processes signals from sensory neurons, modules chemosensory responses. Involved in Pheromone and social behaviour.
pm1	Pharyngeal Muscle Cell	1st layer of pharynx muscle

Over-expression of NCS-1 driven by its endogenous promoter on a wild-type background showed improved memory compared to the wild-type worm based on the ability to associate the presence of food with a specific temperature, whereas the *ncs-1* null (qa406) worm showed impaired memory formation (Gomez et al., 2001). The regulation of memory by NCS-1 was shown to be Ca^{2+} dependent, as expression of the NCS-1 loss of function protein, in which all 3 functional EF hands motifs (EF 2,3, and 4) are muted and unable to bind Ca^{2+}, failed to rescue memory in the null worm (Gomez et al., 2001).

Using neuron-specific promoters to drive NCS-1 expression, the AIY neuron was shown to be the site where NCS-1 regulates memory and isothermal tracking (Gomez et al., 2001). Expression of NCS-1 in the AFD neuron failed to rescue this behaviour, suggesting that NCS-1 has an alternative role in this neuron (Gomez et al., 2001). AWC was not identified as being involved in temperature sensation at the time of this study; as a consequence the role of NCS-1 in this neuron was not investigated.

The *ncs-1* null strain showed no thermoavoidance or chemosensory phenotype even though NCS-1 is expressed in neurons involved in these behaviours suggesting NCS-1 has no role in these phenotypes (Gomez et al., 2001, Ghosh et al., 2012). To identify the full role of NCS-1 in every cell type in which it is expressed, further research is required, including phenotyping other behaviours regulated by the expressing cells. NCS-1 may share its function with other NCS proteins especially NCS-3 as it shows the highest sequence identity. It may be necessary to knockdown both proteins to establish and rescue NCS-1 in specific neurons to establish its role in all cell types to prevent interference due to the presence of NCS-3. A recent study has identified a new phenotype for the *ncs-1* null strain. It was shown to have impaired alkalinity sensing and live Ca^{2+} imaging showed impaired Ca^{2+} signaling in the ASE sensory neurons suggesting that NCS-1 has a role in the regulation of $[Ca^{2+}]i$ in this neuron (Murayama et al., 2013).

In chapter 4 the *ncs-1* null worm is used as a tool to characterise key features of NCS-1 structure identified in previous structural studies and relate them to the function of NCS-1 in *C. elegans*.

1.9 Aims and Objectives

Up until now no direct interaction between P/Q channels and NCS-1 has been described. During the first part of this PhD study biochemical and biophysical techniques were used to address the following aims.

- To identify whether the P/Q channel interacts directly with NCS-1

- To identify which domains of the P/Q channel interact with NCS-1

To characterise the interaction using surface plasmon resonance and nuclear magnetic resonance, to identify which amino acids of the NCS-1 binding pocket are important for this interaction.

Using *C. elegans* as a model organism, the objective of the second part of this study was to take the known structural and binding information for NCS-1 and apply it to a physiological system in order to address the following aims.

- To investigate the behaviour of *ncs-1* null strains expressing mutated NCS-1 and evaluate the molecular significance for function of key characteristics of the NCS-1 protein identified in structural studies

- To determine in which neurons NCS-1 functions in relation to the neuronal circuit for temperature-dependent locomotion.

- To determine the identity of the NCS-1 target proteins in the temperature-dependent locomotion pathway.

Chapter 2: METHODS

2.1 Materials and Methods for Characterisation of NCS-1 Protein and Analysis Target Peptide Binding

2.1.1 Reagents

All P/Q Ca_v 2.1 subunit fragments were derived from rat Rba-1 (NP037050.2) and other constructs from human CaM (CAA36839) or rat NCS-1 (NP077342.1).

The pEYFPN1-NCS-1 plasmid encoding NCS-1 (O'Callaghan et al., 2002), pGex-6P1 plasmid encoding GST-NCS-1 (Haynes et al., 2004) and pET-m11 plasmid encoding His tagged NCS-1 (Handley et al., 2010) were described previously. pGex-6P1 plasmids (GE Healthcare) encoding a GST fusion tag containing human CaM or rat P/Q-L inserts and pE-SUMOpro plasmids (LifeSensors) with a His-SUMO protein fusion tag encoding P/Q-XL and P/Q-CBD were a gift from Dr Haynes, University of Liverpool. The pOPINS plasmid with a His-SUMO tag encoding P/Q-L and a modified pET15b plasmid encoding rat CaM gene insert and a deletion to remove the His-tag coding region were a gift from Sravan Pandalaneni, University of Liverpool. The rat P/Q-IQ peptide defined in previous structural studies to contain the IQ domain (Kim et al., 2008), was synthesised and purified by HPLC (GenicBio Limited).

All primers were synthesised by Sigma-Aldrich. Plasmid sequencing was performed by DNA Sequencing & Services (MRCPPU, College of Life Sciences, University of Dundee, Scotland, www.dnaseq.co.uk) using Applied Biosystems Big-Dye Ver 3.1 chemistry on an Applied Biosystems model 3730 automated capillary DNA sequencer. PCR products were cleaned up using spin column PCR purification kits (NBS Biologicals Ltd). All DNA fragments were run on a 1 % Agarose gel with Sybersafe DNA gel stain (Invitrogen) and Hyperladder I (Bioline) DNA molecular weight marker. Extracted DNA bands were purified using a spin column DNA gel extraction kit (NBS Biologicals Ltd). All plasmids were amplified using a spin column DNA plasmid miniprep kits (NBS Biologicals Ltd) following the manufacturer's instructions. The PCR polymerase enzymes used were Phusion High Fidelity Polymerase (Finnzymes) or Pfu Turbo DNA polymerase (Stratagene). The restriction enzymes used were DpnI (Promega) and XbaI, BsmBI and XhoI (New England

Laboratories) and the ligase enzyme used was T4 DNA ligase (New England Laboratories).

All recombinant proteins and peptides where analysed using SDS-PAGE electrophoresis using 15% polyacrylmide (v/v) gel and See Blue Plus 2 molecular mass markers (Invitrogen), all gels were stained with Coomassie blue to visualise the protein.

2.1.2 Preparation of Plasmids for Protein Expression

2.1.2.1 pE-SUMOpro-NCS-1

To clone NCS-1 into the pE-SUMOpro plasmid, the NCS-1 sequence was amplified from pEYFPN1-NCS-1 (O'Callaghan et al., 2002). PCR was performed using Phusion High Fidelity Polymerase (Finnzymes) for amplification of rat cDNA and following the manufactures protocol. Briefly, 0.5 μg of each Primer (forward 5'-ATATCGTCTCAAGGTATGGGGAAATCCAACAGC-3 and reverse 5'-ATATCTCGAGTCATACCAGCCCGTCGTAGAG-3') and 0.5 μg of template DNA was required for PCR. The annealing temperature used was 69^{o}C and extension time was 15 seconds. The NCS-1 PCR product was purified and digested with the restriction enzymes BsmBI and XhoI (NEB). pE-SUMOPro was digested with BsaI (which has a complementry overhang to BsmBI) and XhoI (NEB). The digested DNA was run on a gel and DNA bands were extracted. pE-SUMOPro and the NCS-1 insert were ligated using a 1:3 ratio, at room temperature for 20 minutes.

2.1.2.2 His-SUMO-P/Q-N and His-SUMO-P/Q-N2

To clone His-SUMO-P/Q-N and His-SUMO-P/Q-N2, the Stratagene QuikChange® Site-Directed Mutagenesis protocol was followed. The constructs were created by inserting a stop codon at the appropriate point in the longer His-SUMO-P/Q-XL template plasmid. Briefly, 0.5 μg of template plasmid and 125 ng of primers, for His-SUMO-P/Q-N (forward 5'-GGTCTCAAGGTAAGTCCACGGACCTGACATGGG-3' and reverse 5'- CCCATGTCAGGTCCGTGGACTTACCTTGAGACC-3') and for His-SUMO-P/Q-N2 (forward 5'-GCCAAAACGCCCTAATCCACTCAGCTGGACCC-3' and reverse

5'- GGGTCCAGCTGAGTGGTTAGGGAAGGGCGTTTGGC-3) were used for PCR, using Pfu Turbo DNA polymerase (Stratagene). An annealing temperature used was 55^{o}C; with an extension time of 13 minutes (double recommended time) was used. 16 cycles of PCR were required to insert the single stop codon by site directed mutagenesis. To remove the template plasmid, the sample was incubated with DpnI (Promega) restriction enzyme.

All cloned His-SUMO plasmids, were amplified using standard transformation protocols, into BIOBlue *E. coli* cells (Bioline) and grown in LB media (1 % w/v Tryptone, 0.5 % w/v yeast exact, 5.6 mM NaCl, pH 7.2), containing 30 μg/ml of kanamycin. To ensure the insertion of the NCS-1 sequence into pE-SUMOpro, the amplified plasmid was digested with XbaI and XhoI (NEB). BsmBI could not be used as a diagnostic restriction enzyme as this site is removed from the pE-SUMOPro plasmid during cloning. The digested sample was analysed by DNA electrophoresis. All plasmids were amplified and purified using miniprep kits (NBS biologicals Ltd). All three newly cloned constructs were sent for DNA sequence verification (The sequencing service, Dundee). The resulting DNA sequences were translated to their amino acid sequence using ensembl software and aligned to the relevant protein sequences using Clustal W2 software (EMBL-EBI).

2.1.3. Protein Expression and Purification of Unlabeled NCS-1, GST-CaM and P/Q peptides

Standard transformation protocols were used to produce colonies of bacteria containing the relevant plasmid. Plasmids encoding for GST-CaM, GST-P/Q-L, His-SUMO-NCS-1, His-SUMO-P/Q-XL, His-SUMO-P/Q-N and His-SUMO-P/Q-L were transformed into BL21 (DE3) *E. coli* cells (Bioline). The plasmid encoding for P/Q-CBD was transformed into both BL21 (DE3) and Rosetta 2 (DE3) pLysS *E. coli* cells (Novogen). Colonies were selected and grown in super media (1.5% w/v tryptone, 2.5% w/v yeast extract, 2.8 mM NaCl, pH 7.2) overnight at 37^{o}C, 220rpm.

BL21 cells transformed with pGEX-6P1 plasmids were grown media containing 100 μg/ml ampicillian. BL21 cells transformed with pOPINS or pE-SUMO plasmids were grown in media containing 30 μg/ml kanamycin. Rosetta 2 (DE3) pLysS cells transfected with pE-SUMO plasmid was grown in media containing 30 μg/ml kanamycin and 34 μg/ml chloramphenicol.

After overnight incubation, the starting culture was used to inoculate the growth media so that the starting optical density at wavelength of 600 nm (OD_{600}) was less than 0.1. Protein expression was induced when the OD_{600} reached 0.6-0.8 by adding 1mM IPTG (Merck) then incubated at 37^{o}C, 220 rpm for 3 hours.

2.1.4. Protein Purification

Bacterial culture samples were centrifuged at 2500 x g for 15 minutes at 4^{o}C. The pellets were resuspended in breaking buffer containing Complete Mini, cocktail protease inhibitor tablet (Roche). Cell expressing GST proteins were suspended in GST buffer (20 mM Tris.HCL, 50 mM NaCl, pH 7.4). Cells expressing His-SUMO-P/Q-L was suspended in Talon buffer (50 mM Na_2HPO_4, 300 mM NaCl, pH 7). Cells expressing all other His-SUMO proteins were suspended in Histrap buffer (50 mM HEPES, 150 mM NaCl pH 7.5). All resuspended pellets were frozen at -80^{o}C overnight. Pellets were defrosted quickly and the cells lysed using a Cell Disrupter One Shot (Constant systems Ltd) at 27 kPsi. 250 μg of DNaseI (Sigma) was added to the Rosetta 2 (DE3) pLysS cell lysate and incubated for 15 minutes on ice. All protein preparations were ultracentrifuged at 100K x g for 1 hour at 4^{o}C.

GST fused recombinant proteins and peptides were purified by binding to pre-washed glutathione cellulose resin (Bioline). Supernatant was incubated with the resin on a rotor for 1 hour at 4^{o}C. The protein bound resin was then further washed with buffer. Protein was eluted using Glutathione elution buffer (50 mM Tris.HCl, 10 mM reduced Glutathione, pH 8).

His-SUMO-P/Q-L was purified on cobalt affinity Talon resin (Clontech). The supernatant was incubated on the prewashed resin on a rotor for 1 hour at 4^{o}C. The resin was then washed with Talon buffer and the recombinant protein eluted with Talon buffer containing 200 mM, 400 mM and 800 mM imidazole concentrations respectively.

GST-NCS-1 and GST-CaM protein were dialysed overnight in buffer (50 mM Tris.HCl, 150 mM NaCl, 1 mM EDTA and 1 mM DTT, pH 7). The protein was then bound to the glutathione cellulose resin. Precision protease, a gift from Dr Hannah McCue (University of Liverpool), was added to the resin and the sample incubated overnight at 4^{o}C. The resin was centrifuged at 3000 xg for 5 minutes and the supernatant was retained as it contained the untagged recombinant protein. The cleaved GST remained on the resin along with the GST-tagged PreScission protease.

His-SUMO-P/Q-XL, His-SUMO-P/Q-CBD, His-SUMO-NCS-1 and His-SUMO required for SPR were purified using an ATKA (GE Healthcare) chromatography system. The first purification step used a nickel affinity, Histrap FF 5ml column (GE Healthcare). After the supernatant was loaded on to the column, it was washed with 2 column volumes of Histrap running buffer. The recombinant protein was eluted from the column using Histrap elution buffer (0.5 M Imidazole, 50 mM HEPES, 150 mM NaCl, pH 7.4), with a 0-100% elution gradient over 20 column volumes, the flow rate was 5 ml/min and fraction size was 5ml.

To remove the His-SUMO tag from His-SUMO-NCS-1, His-SUMO-P/Q-CBD, His-SUMO-P/Q-XL and His-SUMO-P/Q-N samples were incubated with His-SUMO protease, ubiquitin-like protease-1 (ULP-1), a gift from Dr Herbert, University of Liverpool. The protein was simultaneously dialysed (Snakeskin molecular weight cut off (MWCO) 3 kDa) with Histrap buffer at 4^{o}C to remove imidazole from the sample while cleavage was taking place. The untagged protein was manually run through a Histrap column using a syringe to remove the free His-SUMO tag and any uncleaved protein. The flow through containing the untagged peptide or protein was collected and retained. The tag was removed from the column using Histrap elution buffer.

Untagged NCS-1, untagged P/Q-CBD, His-SUMO-P/Q-XL and His-SUMO-P/Q-CBD samples were concentrated using Vivaspin 20 columns (GE Healthcare) with a MWCO 3 or 10 kDa as appropriate. The samples were then diluted 1 in 6 with Mono Q buffer (20 mM HEPES, pH 7.0) to lower the concentration of salt from previous steps. The sample was then further concentrated to 2.5 ml. Untagged and tagged proteins where further purified using ion exchange chromatography. The sample was injected on to a Mono Q 5/5 1 ml column (GE Healthcare) at a flow rate of 1 ml/min. Elution buffer (20 mM Hepes, 1 M NaCl, pH 7.0) was run through the column at 0-100% gradient over 25 column volumes. His-SUMO-P/Q-CBD was concentrated and underwent a third purification step by Gel filtration. After concentrating, using a Vivaspin 20 (MWCO of 10 kDa), the sample was loaded on a to a HiLoad 26/60 Superdex 75 column 26/60 (GE Healthcare) for size exclusion chromatography. Running buffer (10 mM HEPES 150 mM NaCl, pH 7.4) was run though the column at a flow rate of 2ml/min and fractions were eluted at 5 ml volumes.

2.1.5 Expression of Unlabeled CaM, ^{15}N Labelled NCS-1 and CaM.

pET-15b CaM or pET-m11 His-NCS-1 plasmids were transformed into BL21 (DE3) using standard protocols. Media for CaM expression contained 100 μg/ml ampicillian and for NCS-1 expression contained 30 μg/ml kanamycin. An LB starting culture of 5 ml was grown for 5 hours at 37 ^{o}C, with agitation at 220 rpm, then transferred to a starter culture of 2M9 minimal media (20 mM ^{15}N labelled ammonium chloride, 20 mM glucose, 55 mM KH_2PO_4, 88 mM Na_2HPO_4, 1 mM $MgSO_4$, 136 μM $CaCl_2$ 30 μM) and incubated overnight at 37^{o}C, 220 rpm. After overnight incubation, the starter culture was used to inoculate 2M9 minimal growth media then protein expression was induced as described above, the media for CaM was supplemented with 0.1 M Biotin to increase the expression. The cultures were incubated overnight at 18^{o}C, 190 rpm. The cells were harvested and resuspended in buffer (50 mM Tris.HCl, 500 mM NaCl, 5 mM $CaCl_2$ pH 7.5 and

Complete Mini EDTA free Protease inhibitor tablets (Roche)) and frozen at -20^{o}C overnight. The cells were lysed using a cell disrupter as above and 250 μg DNaseI (Sigma) added. The lysate was centrifuged at 50,000 xg for 30 minutes at 4^{o}C. The CaM preparations underwent an additional purification step, the supernatant was removed and it was heated to 65^{o}C for 3 minutes. This heat step denatures protein impurities in the sample, centrifugation was repeated at 50,000 x g for 30 minutes at 4^{o}C, and supernatant retained.

2.1.6 Purification by Hydrophobic Interaction and Size Exclusion Gel Chromatography

Supernatants for both CaM and His-NCS-1 were filtered (0.2 μm acrodisc). The samples were loaded on a HiPrep 16/10 Phenyl FF High Sub column (GE Healthcare), using a flow rate of 2 ml/min. Then loading buffer (50 mM Tris.HCl, 500 mM NaCl, 5 mM CaCl, pH 7.5) was run over the column to saturate the column with the recombinant protein and remove unbound proteins. Saturation was indicated by decline of the load peak on the chromatogram. Wash buffer (50 mM Tris.HCl, 0.5 mM CaCl, pH 7.5) was ran over the column until the chromatogram UV units reached ~ 50 mUV to remove impurities. Elution buffer (50 mM Tris.HCl, 10 mM EDTA, pH 7.5) was used to remove CaM from the column and distilled water was used to remove NCS-1 from the column. A flow rate of 2 ml/min was used and protein fractions were eluted at 5ml volumes.

His-NCS-1 fractions were concentrated as above and buffer exchanged using a PD10 column (GE Heathcare) into TEV cleavage buffer (50 mM Tris.HCl, 500 mM NaCl, and pH 7.4). The sample was then incubated with TEV protease, a gift from Sravan Pandalaneni, (University of Liverpool), overnight at 4^{o}C to cleave the His tag from the protein. The untagged protein was manually run through a Histrap column using a syringe, as described above, to remove the His tag and any uncleaved protein. The flow through containing the untagged NCS-1 was collected and retained. After hydrophobic chromatography CaM fractions were buffer exchanged using a PD10 column (GE Heathcare) into gel filtration buffer (20 mM MES, 150 mM

NaCl, 5 mM $CaCl_2$,pH 6.5). CaM and untagged NCS-1 samples were injected on to HiLoad 26/60 Superdex 75 column 26/60 (GE Healthcare) using the gel filtration buffer and conditions used above. Aliquots of fractions were flash frozen using liquid nitrogen and stored at – 80 ^{o}C.

2.1.7 Mass spectrometry

For identification, the untagged P/Q-CBD peptide band was extracted from an SDS PAGE gel stained with Coomassie blue. In-gel, tryptic digestion and mass spectrometry were performed by Mark Wilkinson and Mark Prescott, University of Liverpool as follows. Gel slices from SDS-PAGE were washed with 50% acetonitrile, 0.2 M ammonium bicarbonate pH 8.9 and then dried in a rotary evaporator. The slices were re-swollen in 0.2 M ammonium bicarbonate pH 7.8 containing trypsin and incubated at 25ºC overnight. Peptides were extracted from the gel slices with 60% acetonitrile, 0.1% TFA and then de-salted for MS using C18 ZipTips. MS analysis was performed on a MALDI-Tof instrument (Waters-Micromass). Peptides were mixed 1:1 with a saturated solution of alpha-cyano-4 hydroxycinnaminic acid in 50% acetonitrile/0.1% trifluoroacetic acid and analysed in the mass range 800 – 4000 Da

2.1.8 Analysis of the P/Q-IQ peptide

2.1.8.1 Helical Prediction

The helical prediction software AGADIR was used to calculate the helical content of the 27 residue P/Q-IQ peptide from its amino acid sequence TVGKIYAAMMIMEYYRQSKAKKLQAMR.

2.1.8.2 Circular Dichroism

For Circular Dichroism (CD) spectroscopy the P/Q-IQ peptide was diluted to a concentration of 250 μM in distilled water/2, 2, 2-trifluoroethanol (TFE), the TFE titrations were 0%, 15%, 30% and 50%. A Jasco-J810 spectrophotometer was used for CD measurements in the far-UV region from 190 to 260 nm for each titration. A rectangular cell with a path length of 0.1 cm was used and assays were run at

25^{o}C. Seven scans were performed for the peptide at each TFE titration. The CD signal was averaged and corrected for the buffer.

Measured ellipticity θ (CD mdeg) at 222 nm was converted to mean residue molar ellipticity [θ_{222}], using the following equation:-

$[\theta_{222}]= (100 x\theta) /Cnl$,

Where C is the protein concentration, *n* is the number of residues in the peptide and *l* is the path length in cm.

Percentage helicity was calculated using the following formula

$([\theta_{222}]/[^{max}\theta_{222}])$ x100=% helicity

$[^{max}\theta_{222}]= -40,000 [1 - (2.5/n)]$,

Where -40,000 is the constant for infinite helicity at 0^{o}C, 1 - (2.5/n) corrects for peptide length, *n* = number of amino acids in peptide.

2.1.9 Pull-down Assay The analysis of the Ca^{2+}-dependency of binding of GST-P/Q-L -NCS-1

2.1.9.1 Binding Assay

The concentrations of GST-P/Q-L and untagged NCS-1 was determined using densitometry by comparing the bands of recombinant protein to known BSA standards with Image J software. Samples were prepared in 25 mM Tris.HCl, 50 mM KCl, 5 mM EGTA, 5 mM NTA, 1 mM DDT, 2 mM Free Mg^{2+} pH 7.4. A titration of Ca^{2+} concentrations was performed adding $CaCl_2$ to give 0, 0.1, 0.3, 0.6, 1, 3, 6 mM free Ca^{2+} in the buffers. Free $Ca^{2+}$and Mg^{2+}concentrations were calculated using the Chelate DOS program. Washed glutathione resin was placed in a microcentrifuge

tube and each of the following buffer conditions was run in duplicate. GST-P/Q-L was added to a final concentration of 1 μM to tubes containing the appropriate Ca^{2+} buffer 0-6 mM. The tubes were incubated on a rocker on ice for 30 minutes. NCS-1 was added to a final concentration of 1 μM and incubated for 1 hour. The resins were washed three times with the appropriate Ca^{2+} buffer. The tubes were centrifuged to remove excess wash buffer and boiled with 30 μl SDS loading buffer for 5 minutes. The resin was centrifuged again and the SDS loading buffer was analysed using SDS-PAGE and Western blotting.

2.1.9.2 Western Blot of Pull-Down Assay

For Western blot analysis, protein bands were transferred from the gel to a nitrocellulose membrane using electroblotting. The membrane was then blocked using 3% (w/v) milk in PBS to prevent non-specific binding of antibodies. The membrane was then incubated with 1:1000 rabbit polyclonal anti-human NCS-1 antibody (McFerran et al., 1998) in 3% (w/v) milk PBS, overnight on a rocker at $4^{o}C$ (McFerran et al., 1998) . After washing three times with PBS and 0.05% (v/v) tween 20 (PBST) and rinsed, the membrane was then incubated with 1:400 dilution HRP conjugated goat anti-rabbit secondary antibody (Sigma) in 3 % (w/v) milk PBS, for 1 hour. The membrane was further washed and incubated with equal volumes of ECL reagents. The blot was visualised using the ChemiDoc System (Bio-Rad), using Chemi-Hi sensitivity setting. The image was further analysed by measuring the density of the bands using ImageJ software. The density was plotted against Ca^{2+} concentration and fitted against a hyperbolic model using Origin8 software.

2.1.10 Gel Filtration analysis

The mixture of NCS-1 and P/Q-IQ peptide, at concentrations of 100 μM and 350 μM respectively, containing a putative complex was suspended in a buffer (20 mM MES, 100 mM NaCl, and 5 mM $CaCl_2$ buffer pH6.5), and analysed by size exclusion gel filtration. A volume of 500 μl was injected on to an analytical Superdex 75 HR 10/300 mm column. Separation buffer (50 mM Tris.HCl, 150 mM NaCl, pH 7.4) was

run through the column at a flow rate of 0.75 ml/ min and 0.5 ml eluted fractions were collected

To calculate the partition coefficient (K_{av}) of the peak the following equation was used:-

$K_{av}= V_e-V_0/V_c-V_{0,}$

Where V_e is elution volume, V_0 is void volume, V_c is the column volume.

2.1.11 NMR Spectroscopy

All NMR spectra were of samples with volumes of 500 μl in Shigemi microtubes (Sigma) and were recorded on Bruker DRX 800 and 600 MHz spectrometers equipped with CryoProbes. The number of scans used to acquire data was 32 unless otherwise stated and the number of dummy scans performed before data collection was 8. To process the data a time domain size of 1024 data points was used. Data were collected and processed using the Bruker Software TopSpin version 2.1 and analysed using the Collaborative Computing Project for NMR (CCPNmr) analysis software version 2.1.5 (Vranken et al., 2005). All experimental spectra were acquired at 308K. To increase the number of chemical shift peaks the NMR experiments were performed at pH 6.5 to minimise the rate of exchange of amine protons with the solvent.

2.1.11.1 CaM and P/Q-IQ interactions

Labeled ^{15}N CaM (500 μM) was prepared in buffer (20 mM MES, 100 mM NaCl, and 5 mM $CaCl_2$, pH 6.5). NMR spectra were collected with temperature titrations of 298K, 300K, 305K and 308K. Using previously assigned $^{1}H^{15}N$ HSQC spectra for CaM (Lian et al., 2007), assignments were transferred to peaks on spectra acquired at 298K. These assignments were then transferred to the resonances of the temperature titrations. The transfer of assigned residues was performed manually

viewing overlaid spectra using topspin. Synthetic P/Q-IQ peptide was prepared using the buffer above and was added at concentrations of 100 - 2000 μM by titrating aliquots into the sample. For each P/Q-IQ titration, $^{1}H^{15}N$ HSQC spectra were collected at 308K. Using data collected by NMR in a previous study (Lian et al., 2007), the P/Q-IQ titration spectra were analysed using CCPNmr analysis software to characterise the interaction of the CaM binding domain to the P/Q-IQ peptide.

2.1.11.2 NCS-1 and P/Q-IQ interactions

Labelled ^{15}N NCS-1 (100 μM) was prepared in the MES buffer described above. $^{1}H^{15}N$ HSQC spectra were acquired at increasing temperatures; 298K, 303K, 305K and 308K. Using CCPN software, the assignments of NCS-1 $^{1}H^{15}N$ HSQC spectrum were transferred from that previously reported NCS-1 spectrum (Handley et al., 2010) and assigned to each spectrum in the temperature titration series. $^{1}H^{15}N$ HSQC spectra were acquired for P/Q-IQ over the concentration range 0-350 μM in a similar manner to those above. Spectra for final NCS-1 (100 μM) and P/Q-IQ (350 μM) spectra were performed using 32, 64 and 544 scans to reduce background noise.

2.2 Materials and Methods –For analysis of NCS-1 function in *C. elegans*

2.2.1 Reagents

2.2.1.1 C. *elegans* Strains

C. elegans strains used in this project were wild-type or contained various mutations and were obtained from several suppliers listed in Table 2.1

Table 2.1 *C. elegans* Strains

Strain	Gene	Allele	Mutation Type	Source
N2	wild-type			*Caenorhabditis* Genetics Centre (CGC) (University of Minnesota, USA).
XA406	*ncs-1*	qa406	Homozygous null allele and was created by transposon insertion and deletion of 2149 bp which contained exons 1- 5 and the ATG start codon of the *C. elegans ncs-1* gene.	CGC
TM437	*ncs-1*	tm437	Homozygous for the allele which contains a 618 bp deletion of bases 2994- 3611, inclusive, located in intron 1 of the *C. elegans ncs-1* gene created by UV/TMP knockout.	National Bioresource Project for the Experimental Animal (NBRP) (Tokyo Women's Medical University, Japan)
RM956	*ric-4*	md1088	Contains the *ric-4* gene with a deletion, size and location of the deletion site is yet to be identified; mutagenesis technique used to create this strain was not recorded on wormbase or CGC database.	CGC
FX2328	*pifk-1* (F35H12.4)	tm2348	Homozygous for the null allele created by UV/TMP knockout. The allele contains a deletion of 502 bp and insertion of 4 bp 11095/11096-TAAA-11595/11596	Mori lab, Nagoya University, Japan Originally from NBRP
OH161	*ttx-3*	ot22	Homozygous null allele created by EMS, premature stop codons inserted in place of amino acids Q275 and Q303	CGC

2.2.1.2 Plasmids and *C. elegans* Sequences

The plasmid pPD117.01 [$P_{mec\text{-}7::GFP}$] was obtained from the Fire Lab via Addgene and contains the GFP reporter protein gene driven by the *C. elegans mec-7* promoter. Marker plasmid pRAB100 [$P_{rab\text{-}3::GFP}$] was obtained from the Nonet Lab (Washington University of St Louis, USA) and., marker plasmid pG[$P_{osm\text{-}6}$::GFP] was obtained from James Johnson, University of Liverpool. Both marker plasmids contained the GFP reporter protein gene which was driven by either the *C. elegans rab-3* pan-neuronal or *osm-6* pan-sensory neuronal promoter respectively. pBlueScript (Stratagene) is an empty cloning plasmid. The PAIY::MCS plasmid was a gift from Hobert Lab (Columbia University Medical Center, N.Y.) and contains the promoter to drive the expression of transgenic proteins in the AIY neuron only. This promoter is situated within the introns and exons of the ttx-3 gene on chromosome X of the worm genome.

The *C. elegans ncs-1* genomic gene sequence, was derived from the *C. elegans ncs-1* gene (Wormbase gene sequence C44C1.3, Accession number CCD63971). The *C. elegans ncs-1 gene* promoter sequence was defined as 3.5 kbp before the start sequence of the *C. elegans ncs-1* gene as previously reported (Gomez et al., 2001). The WRM063AD10 fosmid was obtained from *C. elegans* Reverse Genetics Core Facility, Canada via Addgene. The fosmid contains a region of genomic X chromosome DNA and includes the unspliced wild-type sequence of the *C. elegans ncs-1* gene and its promoter. Plasmids containing synthetic spliced wild-type and spliced mutated *C. elegans ncs-1* genes, all without introns, were purchased from Geneart (Life technologies) (Table 2.2).

Table 2.2. Synthetic Spliced *C. elegans ncs-1* Wild-Type and Mutated Gene Inserts

Synthetic gene/variant	Description
ncs-1 wt	Wild-type
ncs-1 G2A	Single amino acid mutation
ncs-1 W30A	Single amino acid mutation
ncs-1 L89A	Single amino acid mutation
ncs-1 W103A	Single amino acid mutation
ncs-1 V125A	Single amino acid mutation
ncs-1 W30A L89A	Double amino acid mutation
ncs-1 W30A W103A	Double amino acid mutation
ncs-1 W103A V125	Double amino acid mutation
ncs-1 Δ177-191	C terminal truncation
ncs-1 Δ174-191	C terminal truncation
ncs-1 Δ169-191	C terminal truncation

2.2.1.3 Enzymes

AscI, BamHI, and XhoI restriction enzymes and T4 DNA ligase were obtained from Promega. Phusion High Fidelity Polymerase was purchased from New England Biolabs. Gateway BP and LR Clonase II enzyme mix kits were obtained from Life Technologies.

2.2.2 *C. elegans* Husbandry

C. elegans were grown and maintained on nematode growth media (NGM) (50 mM NaCl, 1 mM $CaCl_2$, 1 mM $MgSO_4$, 25 mM KH_2PO_4, 5 μg/ml cholesterol, 0.25% w/v peptone, 2 % w/v agar) on 60 mm petri plates, following standard protocol as described previously (Brenner, 1974) and kept at 20°C. The plates were seed with *E. coli* OP50 strain as the single food source. To maintain well-fed healthy adult strains, 5-10 young hermaphrodite worms were manually transferred using a sterile tungsten pick (World Precision Instruments), from old overgrown, but not starved plates to fresh seeded NMG plates, every generation. Worms were observed using a PZMIV dissecting binocular stereomicroscope (World Precision Instruments) and illuminated with either a halogen cold light source or for strains

expressing transgenic GFP an epifluorescent UV light, when either transferring worms or for visual assessment of behaviour.

To age synchronise *C. elegans* strains 5-10 young healthy hermaphrodite adult worms were transferred as above to seeded plates, left for ~ 16 hour to lay eggs, then removed and the eggs and larva were incubated for ~36 hours, ~ 60 hours or ~84 hours for progeny to hatch and mature to approximately stage 4 larval/Day 0, Day 1 or Day 2 adults respectively.

2.2.3 Preparation of Plasmids for Microinjection.

2.2.3.1 PCR and Restriction Digestion

Plasmids containing *C. elegans ncs-1* genes where created by molecular cloning techniques, those created by standard cloning techniques in this section are illustrated in Figure 2.1. To create plasmids containing [$P_{ncs\text{-}1::ncs\text{-}1\ unspliced}$] and [$P_{ncs\text{-}1::}$] PCR was performed using Phusion High Fidelity Polymerase for amplification of *C. elegans* chromosomal cDNA. Briefly, 0.5 μg of each fwd and Rev Primer and 0.5 μg of template DNA was required for PCR specific conditions are indicated in Table 2.3).

Table 2.3. PCR Conditions for Amplification of *ncs-1* Promoter or Gene Inserts

Insert Name	Amplified From Construct	Primer Sequences	Annealing Temprature (^{o}C)	Extension Time (Seconds)
ncs-1::ncs-1 (unspliced)	WRM063AD10 fosmid	P*ncs-1* forward 5'-TCAAGGCGCGCCCTCTGAGTT CTTGCAATGCTTGG-3 *ncs-1* reverse 5'-TTGAGGATCCTCAAGAGAGA GACCCTCATACAATG-3'	70	180
P_{ncs-1}	WRM063AD10 fosmid	P*ncs-1* forward 5'-TCAAGGCGCGCCCTCTGAGTT CTTGCAATGCTTGG -3' *ncs-1* reverse 5'-TTGAGGATCCTCAAGAGGAG AGACCCTCATACAATG-3'	70	105
ncs-1 (unspliced)	WRM063AD10 fosmid	*ncs-1* forward 5'- TTGTGGATCCGAAATGGGCA AAGGGAACAGCAAG-3' *ncs-1* reverse 5'-TTGAGGATCCTCAAGAGGA GAGACCCTCATACAATG-3'	63	90
PAIY	PAIY::MCS	PAIY forward 5'-ATATGGCGCGCCAAGCTT TTTTGAAACGATCTTTG-3' PAIY reverse 5'-ATATGGATCCCATTTGACACC GAAGACAATTATTATG-3'	65	15

The PCR products were purified and digested along with pPD117.01 plasmid using the restriction enzymes AscI and BamHI (NEB). The digested DNA was run on an agarose gel and DNA bands were extracted using a gel extraction kit (NBS Biologicals Ltd). pPD117.01 and the inserts were ligated using a 1:3 ratio, at room temperature for 20 minutes using T4 DNA ligase (Promega).

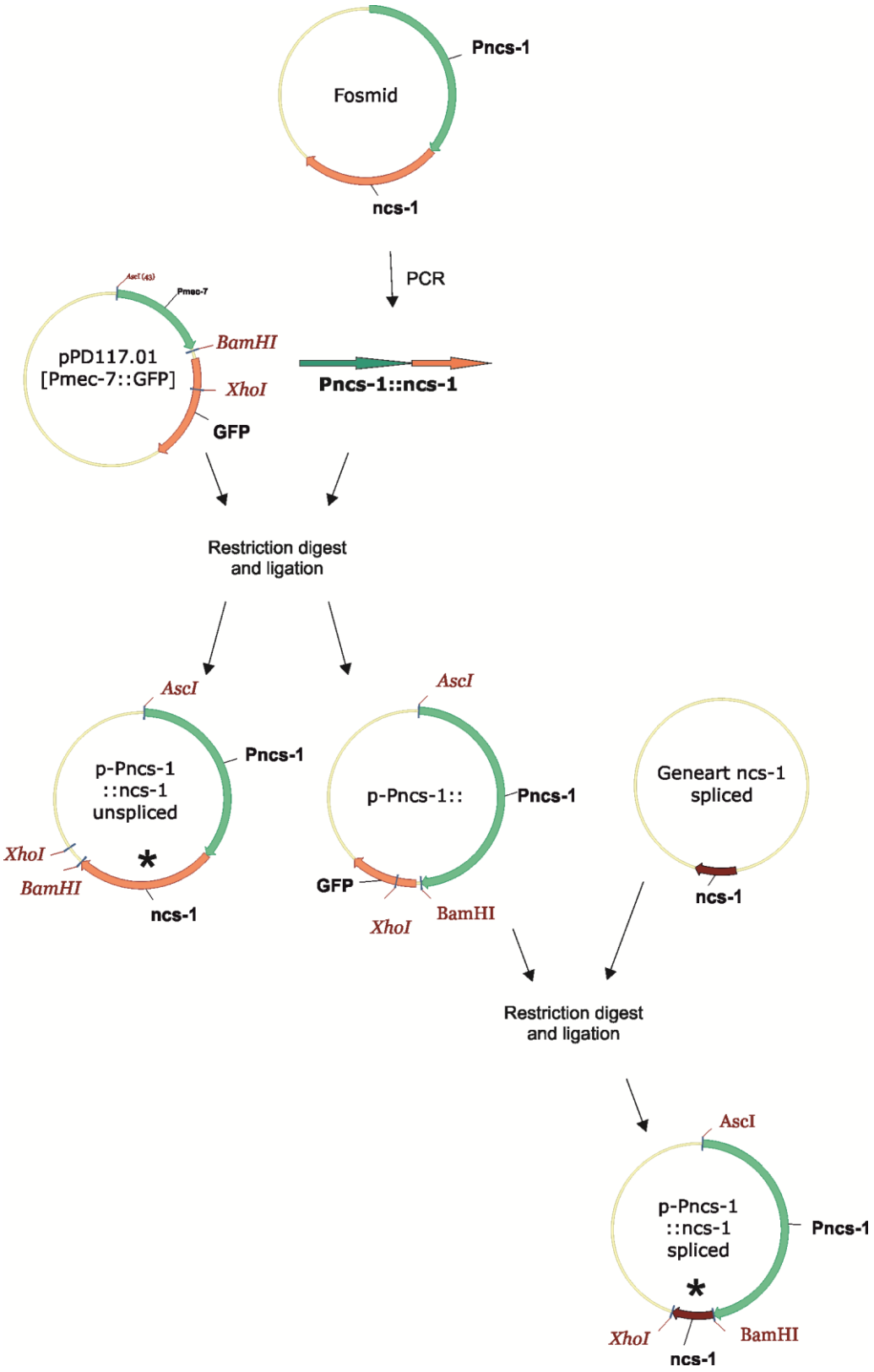

Figure 2.1 Creation of p[$P_{ncs\text{-}1}$::$_{ncs\text{-}1\ unspliced}$] and p[$_{Pncs\text{-}1::ncs\text{-}1\ spliced}$] Plasmids. Standard PCR and restriction digest cloning techniques were used to replace the promoter and genes in the pPD117.01[$_{Pmec\text{-}7::GFP}$] with the genomic *ncs-1* and genomic unspliced or synthetic spliced *ncs-1* genes and create * p[$P_{ncs\text{-}1::ncs\text{-}1\ unspliced}$] and wild-type or mutant p[$_{Pncs\text{-}1::ncs\text{-}1\ spliced}$] plasmids (* Indicates plasmids used for microinjection).

Geneart plasmids containing the synthetic spliced *ncs-1* wild-type or mutant variants inserts were amplified in Bioblue *E. coli* cells using standard protocols and grown on LB/AMP plates overnight. A colony for each construct was selected for miniprep cultivation and purification following the manufactures instructions (NBS Biologicals Ltd). To create [$P_{ncs\text{-}1::ncs\text{-}1\ spliced}$] plasmids containing either *ncs-1* wild-type or mutant variants, the Synthetic gene plasmid and the destination plasmid [$P_{ncs\text{-}1::}$] were digested using BamHI and XhoI (Table 2.2). The digested DNA was run on an agarose gel and the relevant bands extracted and ligation was performed using T4 ligase (Promega), as above.

2.2.3.2. Gateway Cassette Cloning

Both plasmids created using the Gateway cloning system are illustrated in Figure 2.2. To create a plasmid pG[$P_{osm\text{-}6::ncs\text{-}1(unspliced)}$], expressing unspliced *ncs-1* under the pan sensory neuron *osm-6* promoter, the genomic *ncs-1* gene sequence was amplified from the WRM063AD10 fosmid. PCR amplification was performed as described above (see Table 2.3) specific conditions). The PCR product contained the gene and attB recombinase flanking sequences and was separated on an agarose gel, the band was extracted and the gene inserted into the Gateway donor plasmid pDONR221, containing the attP recombinase flanking sequences and cassette, using BP Clonase II recombinase following the manufacturer's instructions.

The pDONR221 plasmid was amplified in Bioblue *E. coli* and purified using the standard miniprep protocol as above. The donor vector also contained the attL flanking sequences which allowed the gene to be inserted into the destination plasmid pG[$P_{osm\text{-}6::attR}$], using LR Clonase II following the manufacturer's instructions. The destination plasmid contained the gateway cassette and the attR sequences and was formed from the original pPD117.01 plasmid by James Johnson using standard recombinant cloning techniques.

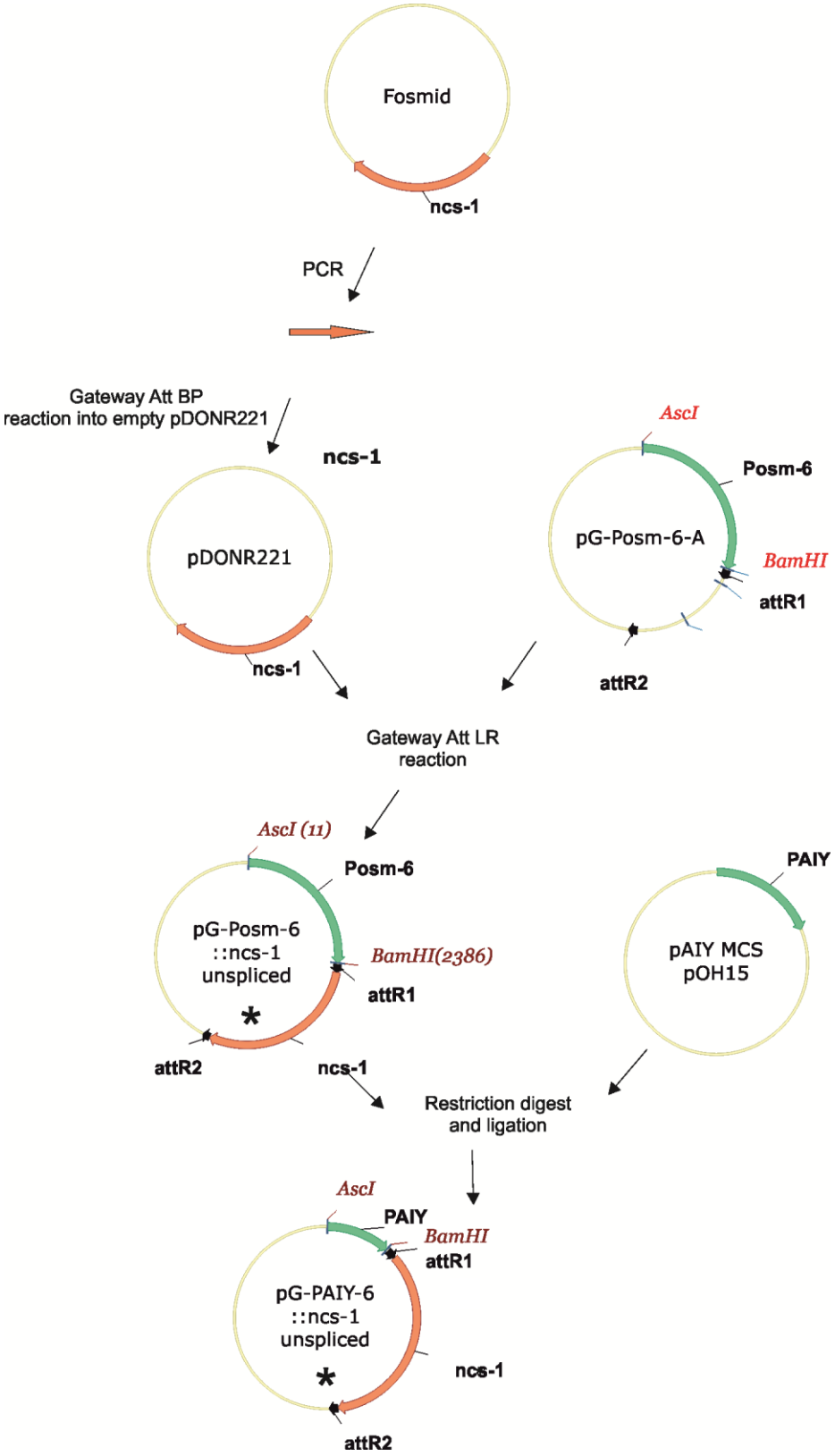

Figure 2.2 Creation of pG[$P_{osm\text{-}6::ncs\text{-}1\ unspliced}$] and p[$PAIY_{::ncs\text{-}1\ spliced}$] Plasmids. Gateway, standard PCR and restriction digest techniques were used to replace the promoter and genes in the pG[$_{Posm\text{-}6A}$] with the genomic *osm-6* or AIY neuron promoters and the genomic unspliced *ncs-1* gene and create pG[$P_{osm\text{-}6::ncs\text{-}1\ unspliced}$] and pG[$PAIY_{::ncs\text{-}1\ unspliced}$] plasmids (* Indicates plasmids used for microinjection).

Restriction cloning techniques were used to create plasmid pG[$P_{AIY::ncs\text{-}1(unspliced)}$]. The sequence of the AIY neuron promoter was amplified by PCR using Phusion DNA polymerase from the PAIY::MCS plasmid, using techniques described previously (for specific details see Table 2.3). The PAIY PCR product and plasmid pG[$P_{osm\text{-}6::ncs\text{-}1(unspliced)}$] were cut with AscI and BamHI restriction enzymes and ligation was carried out as before.

2.2.4 Microinjection

The transgenic lines created can be seen in Table 2.4.Larval stage 4 to Day 1 adult N2 or XA406 *ncs-1* null worms were injected with extra-chromosomal genes into the germline cells of the dorsal, gonad. Using a micropipette needle the injection mixtures contained DNA concentrations of 100 ng/μl DNA consisting of 10 ng/μl *ncs-1* expressing plasmid, 40 ng/μl of GFP marker plasmid and 50 ng/μl of empty pBluescript plasmid in injection buffer (20 mM KPO_4, 3 mM Citrate, 2 % PEG 6000). Worms were immobilised on a 2% agarose pad on a glass coverslip and coated with halocarbon oil. The worms were visualised for injection using Nikon Eclipse Ti-S inverted microscope at 40x and a Eppendorf micromanipulator was used to position the needle. After injection the worms were rehydrated with M9 buffer and moved to a seed NGM plate. Injected plates were observed for GFP expression in progeny. F1 generation worms were isolated on to individual plates. Expression of GFP in the F2 generation confirmed incorporation of the extra chromosomal plasmids in the worm. Three separate lines for each plasmid injection were generated and their phenotypes assessed.

Table 2.4. Transgenic Strains Created by Microinjection

(* Injections performed by Dr James Johnson, University of Liverpool)

Strain Injected	Plasmid Containing *ncs-1* Gene	Neuronal Expression of Gene of Interest	Plasmid Containing GFP Marker Gene	Neuronal Expression of Marker GFP
N2	-	-	p[$P_{rab\text{-}3::GFP}$]	All neurons
N2*	p[$P_{ncs\text{-}1::ncs\text{-}1\ unspliced}$]	All NCS-1 expressing neurons	p[$P_{rab\text{-}3::GFP}$]	All neurons
XA406	p[$P_{ncs\text{-}1::ncs\text{-}1\ unspliced}$]	All NCS-1 expressing neurons	p[$P_{rab\text{-}3::GFP}$]	All neurons
XA406	p[$P_{ncs\text{-}1::ncs\text{-}1\ spliced}$]	All NCS-1 expressing neurons	p[$P_{rab\text{-}3::GFP}$]	All neurons
XA406*	p[$P_{ncs\text{-}1::ncs\text{-}1\ G2A\ spliced}$]	All NCS-1 expressing neurons	p[$P_{rab\text{-}3::GFP}$]	All neurons
XA406*	p[$P_{ncs\text{-}1::ncs\text{-}1\ \Delta 177\text{-}191\ spliced}$]	All NCS-1 expressing neurons	p[$P_{rab\text{-}3::GFP}$]	All neurons
XA406*	p[$P_{ncs\text{-}1::ncs\text{-}1\ \Delta 174\text{-}191\ spliced}$]	All NCS-1 expressing neurons	p[$P_{rab\text{-}3::GFP}$]	All neurons
XA406*	p[$P_{ncs\text{-}1::ncs\text{-}1\ \Delta 169\text{-}191\ spliced}$]	All NCS-1 expressing neurons	p[$P_{osm\text{-}6::GFP}$]	All ciliated sensory neurons
XA406	p[$P_{ncs\text{-}1::ncs\text{-}1\ W30A\ spliced}$]	All NCS-1 expressing neurons	p[$P_{rab\text{-}3::GFP}$]	All neurons
XA406*	p[$P_{ncs\text{-}1::ncs\text{-}1\ L89A\ spliced}$]	All NCS-1 expressing neurons	p[$P_{rab\text{-}3::GFP}$]	All neurons
XA406*	p[$P_{ncs\text{-}1::ncs\text{-}1\ W30A\ L89A\ spliced}$]	All NCS-1 expressing neurons	p[$P_{rab\text{-}3::GFP}$]	All neurons
XA406*	p[$P_{ncs\text{-}1::ncs\text{-}1\ W103A\ spliced}$]	All NCS-1 expressing neurons	p[$P_{rab\text{-}3::GFP}$]	All neurons
XA406*	p[$P_{ncs\text{-}1::ncs\text{-}1\ V125A\ spliced}$]	All NCS-1 expressing neurons	p[$P_{rab\text{-}3::GFP}$]	All neurons
XA406*	p[$P_{ncs\text{-}1::ncs\text{-}1\ W103A\ V125A\ spliced}$]	All NCS-1 expressing neurons	p[$P_{rab\text{-}3::GFP}$]	All neurons
XA406*	pG[$P_{osm\text{-}6::ncs\text{-}1\ unspliced}$]	All ciliated sensory neurons	p[$P_{osm\text{-}6::GFP}$]	All ciliated sensory neurons
XA406*	pG[$PAIY_{::ncs\text{-}1\ unspliced}$]	Left and Right AIY interneurons	p[$P_{osm\text{-}6::GFP}$]	All ciliated sensory neurons

2.2.5 Imaging

Day 1 wild-type, null or transgenic worms were immobilised on a microscope slide in a droplet of mounting media (20% w/v PEG, 20% w/v glycerol PBS) and a coverslip placed on top. The worms were imaged using Nikon Eclipse Ti-S inverted microscope with x200 magnification lens. Images were obtained using either differential interference contrast (DIC) or fluorescence illumination for the comparison of anatomy or for verification of expression of extra-chromosomal GFP marker genes by the transgenic animals, respectively.

2.2.6 *C. elegans* Protein Extraction and Western Blotting.

Recombinant *C. elegans* NCS-1 was separated by SDS page electrophoresis on a 4-12% Bis-Tris polyacrylamide gel, run using MOPS SDS running buffer (50 mM MOPS, 50 mM Tris.Base, 0.1% SDS, 1 mM EDTA, pH 7.7) at 200 volts for 50 minutes. The protein bands were transferred to a nitrocellulose membrane by electroblotting. The membrane was then blocked using 3% milk in PBS to prevent non-specific binding of antibodies. The membrane was then blocked and incubated with 1:1000 polyclonal rabbit anti-NCS-1 antibody (McFerran et al., 1998) or 1:1000 monoclonal mouse anti-NCS-1 (Sigma) in 3% milk PBS, overnight on a rocker at 4^{o}C. After washing, the membrane was incubated with 1:400 dilution HRP conjugated goat anti-rabbit secondary antibody (Sigma) in 3 % milk PBS, for 1 hour. After 0.05% tween PBS and 0.5 M NaCl PBS washes, the membrane was further was incubated with equal volumes of ECL reagents for imaging.

To determine if the polyclonal anti-NCS-1 antibody was efficient at detecting recombinant *C. elegans* NCS-1, serial dilutions of recombinant mammalian and *C. elegans* NCS-1 of equal concentrations were run gels and probed by Western blotting as above using 1:1000 rabbit polyclonal anti-NCS-1 antibody.

To extract proteins from the worms, thirty five whole animals were placed in 25 μl 4% SDS loading buffer for each strain and frozen at – 80 ^{o}C overnight, the sample

was heated to 100^{o}C for 20 minutes. SDS page and Western blot analysis was performed as above using the polyclonal antibody.

2.2.7 Behavioural Assays

2.2.7.1 Crawling locomotion Assays

Locomotion is an indicator of neuronal function and so crawling locomotion of the wild-type and NCS-1 null strain was assessed. To correct for environmental variations, the worms were measured alternating between control, mutant and transgenic strains, age synchronised worms were used at adult day 1 or day 2. To correct for behaviour variations caused by transferring the worm from its growth plate, individual worms were left for 10 minutes on the unseeded experimental NGM plates before crawling locomotion assessment at 20 ^{o}C. Quantification for the body bend assay was performed by counting each complete sinusoidal movement. For each assay n=20 of each strain was used. All results were expressed as means ± S.E.M.

2.2.7.2. Neurotransmission (Aldicarb Resistance) Assay

To establish if NCS-1 had effect on neurotransmission the rate of acetylcholine (ACh) released at the release neuromuscular junction was indirectly assessed. Worms were treated with 1 mM Aldicarb, an ACh esterase inhibitor. Wild-type and mutant worms (n=40) were transferred to unseeded 1mM Aldicarb (Sigma) NGM plates at -5 minutes. Paralysis of worms was assessed by prodding the head and tail of each animal gently with a tungsten wire, at 10 minute intervals from 0 to 90 minutes and the rate of paralysis recorded. All data were expressed as means ± S.E.M.

2.2.7.3 Temperature-Dependent Locomotion Assay

The temperature-dependent locomotion (TDL) rate was assessed by measuring the swimming rate of the worms at 20 ^{o}C and 28 ^{o}C for wild-type and mutant strains. A Petri dish was placed on the centre of a Peltier effect thermoelectric plate and 200 µl of Dent's solution (140 mM NaCl, 6 mM KCl, 1 mM $CaCl_2$, 1 mM $MgCl_2$, 5 mM HEPES, pH 7.4 with bovine serum albumin at 0.1 mg/ml) was put in it. The temperature of the Dent's solution was monitored by a thermocouple and the temperature was recorded in real time. A day 1 or day 2 adult worm was removed from a NGM plate and immersed in the Dent's solution at 20^{o}C ±0.3. The worm was left to acclimatise for 10 minutes then the thrashes per minute were counted. A single thrash was defined as a complete change direction of bending of the mid body then back again to the original position.

The droplet of Dent's solution was then heated up to 28^{o}C ±0.3, the worm was left for a further 10 minutes to acclimatise and the thrashing rate was recorded at the higher temperature. 15-100 worms were assayed were recorded for each of the strains. Where indicated, temperature-dependent locomotion rates from two or three separate lines were pooled. All data were expressed as means ± S.E.M. Where indicated, the data was pooled and normalised to thrashes per minute against wild-type strain N2 at 20^{o}C and significance to locomotion rates at 20^{o}C and 28^{o}C was measured using the Mann–Whitney *U* test and for multiple comparisons, the error rate was controlled using the Bonferroni correction.

2.2. 8 Predicted Models of *C. elegans* NCS-1 Protein Structure

Based on the published solution NMR structure of human NCS-1 (PDB entry 2LCP) (Heidarsson et al., 2012) or the crystal structure (PDB entry 1B8I) (Bourne et al., 2001), the structures were predicted from the *C. elegans* NCS-1 amino acid sequence using the SWISS-MODEL server (Arnold et al., 2006). The three-dimensional predicted models of the structures were rendered in PyMol (Delano Scientific).

Chapter 3: RESULTS
Characterisation of NCS-1 and Calmodulin Interactions with the P/Q-type ($Ca_v2.1$) Calcium Channel

3.1 Introduction Modulation of $Ca_v2.1$ by Ca^{2+} Sensor Proteins

Many mechanisms regulate $Ca_v2.1$; but here I will focus on regulation by activity-dependent feedback. This feedback allows the channel to respond to changes in $[Ca^{2+}]i$ via two Ca^{2+}-dependent regulatory pathways. These are Ca^{2+}-dependent facilitation (CDF) and Ca^{2+}-dependent inactivation (CDI) (Findeisen and Minor Jr, 2010). CDF enables the channel to remain open as $[Ca^{2+}]i$ rises, whereas, CDI accelerates inactivation of the channel in response to high $[Ca^{2+}]i$ (Figure 3.1). These modulations are caused by interactions between $Ca_v2.1$ C-terminal domains and Ca^{2+} sensor proteins. The exact mechanisms leading to CDF and CDI of the channel are not fully understood.

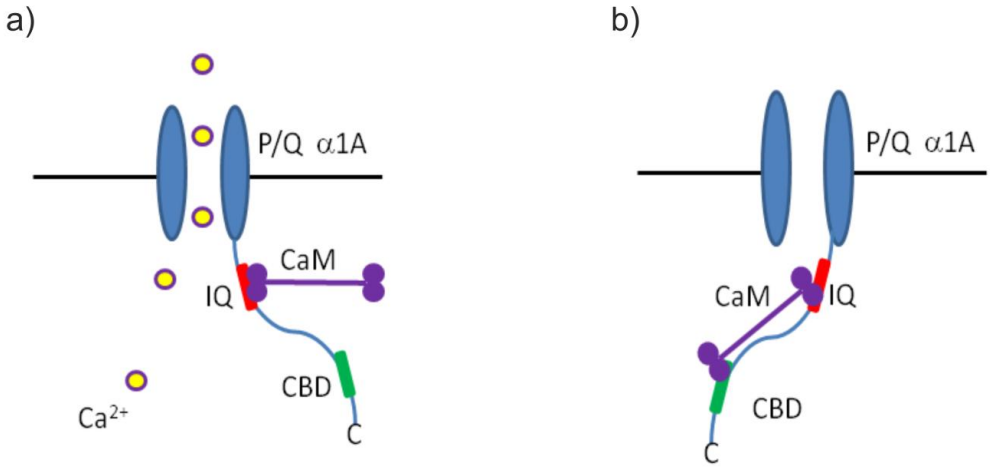

Figure 3.1. A model for the modulation of the P/Q channel. The diagram shows P/Q modulation during a) CDF and b) CDI. At low Ca^{2+} levels, a) the N-terminal lobe of CaM was shown to interact with the IQ domain and facilitate the channel opening. As the Ca^{2+} levels inside the neuron rise, b) the C-terminal lobe of CaM interacts with the CaM binding domain (CBD) to inactivate the channel.

3.1.1. Introduction- Modulation of the P/Q channel by CaM

Activity dependent modulation of $Ca_v2.1$ by CaM has a role in short-term synaptic plasticity (Mochida et al., 2008). Two distinct regions of the P/Q channel have been identified in CaM modulation. Voltage gated channels have an alpha helical domain which contains a conserved IQ motif. Confusingly, in $Ca_v2.1$ this motif contains IM rather than IQ residues (Demaria et al., 2001). Here it will be referred to, nevertheless, as the IQ domain. Further towards the C-terminal of the protein is a CaM binding domain (CBD) (Lee et al., 1999). CaM was first discovered to bind to the CBD of $Ca_v2.1$, in a Ca^{2+}-dependent manner and cause CDI (Lee et al., 1999). Further study also showed the IM residues of the IQ domain are involved in CDF (Demaria et al., 2001).

CaM binds to the $Ca_v2.1$ IQ domain when the channel is open (Figure 3. 4a) (Lee et al., 2003, Demaria et al., 2001). During this step the $[Ca^{2+}]i$ is relatively low and only the high Ca^{2+} affinity EF-hands in the C-lobe of CaM are Ca^{2+} bound. As the channel remains open the $[Ca^{2+}]i$ increases causing the lower affinity N-lobe EF-hands of CaM also bind to Ca^{2+}. The N-lobe of CaM interacts with the CBD of $Ca_v2.1$ and is involved in CDI (Demaria et al., 2001, Lee et al., 1999) (Figure 3. 4b). Mutations of the C-terminal lobe of CaM prevents facilitation of the channel (Lee et al., 2002, Demaria et al., 2001), while mutations at the N-terminal lobe prevent inactivation (Lee et al., 2003).

Further studies have shown the modulation of the P/Q channel is more complicated than first proposed. The C-terminus of CaM binds to the IQ domain and is involved in CDF but there is also Ca^{2+}-independent binding by the N-lobe of CaM to stabilise this interaction (Lee et al., 2003). Also the CaM N-terminal lobe binding to the CBD is involved in CDF as well as CDI (Lee et al., 2003). It has been predicted that CaM is bound to the C-terminal tail of $Ca_v2.1$, at resting $[Ca^{2+}]i$, at a pre-IQ domain (Lee et al., 2003, Demaria et al., 2001). The β subunit also has a role in activity dependent regulation and P/Q channels containing the β_{2a} subunit have an increased response to CaM mediated CDF and CDI than those containing other β subunit isoforms (Lee et al., 2000).

Crystal structures showed that both N- and C-lobes of CaM interact with peptides derived from the IQ domain of $Ca_v2.1$ (Kim et al., 2008, Mori et al., 2008). Two studies have shown that CaM, wraps around the alpha helix of the target peptide. The structures derived from these two studies contradict each other due to differences in the observed orientation of the IQ domain in the CaM binding pocket (Figure 3.2). These studies also identified different IQ domain amino acids which interact with CaM (Figure 3.2), although, both studies agree that residues I (-6), M (-2) and S (+8) in the IQ domain bind to CaM (Figure 3.2). Mutations of IQ domain amino acids I (-6) and M (-2) caused a decrease in CDF but it is not clear whether the N- or C- terminal lobe of CaM is important for this (Kim et al., 2008). To date there has been no structure published of the CaM/Ca_v 2.1 CBD complex.

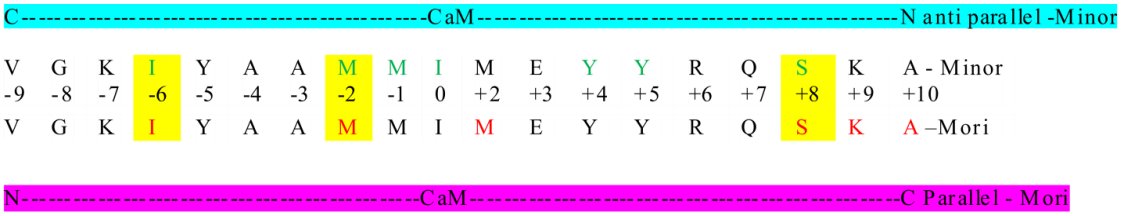

Figure 3.2 Characterisation of $C_{av}2.1$ subunit IQ domain and CaM interactions. A diagram showing differences and similarities of two structural studies in which the interactions between CaM and IQ domain (VGKIYAAMMIMEYYRQSKA) were characterised. Kim *et al* (2008) proposed an antiparallel complex between CaM (blue) and the IQ domain. Mori *et al* (2008) proposed a parallel complex conformation between CaM (Pink) and the IQ domain. The $C_{av}2.1$ subunit IQ residues proposed to be involved in CaM interactions by Kim *et al* (2008) are in coloured in green, while those proposed by the Mori *et al* (2008) group are coloured in red. Residues which both groups propose to be involved in complex formation are highlighted in yellow.

Other Ca^{2+} sensor proteins are involved in regulation of the P/Q channel and add greater complexity to activity dependent modulation of the $Ca_v2.1$ subunit. CaBP-1 binds to the CBD in a Ca^{2+}-independent manner and causes faster CDI than CaM (Lee et al., 2002). No evidence has been found that CaBP-1 interacts with the IQ domain of $Ca_v2.1$ (Lee et al., 2002). CaBP-1 also interacts with the L-type channel $Ca_v1.2$ subunit. CaBP-1 interacts with the IQ domain of $Ca_v1.2$ which inhibits CDI

and enhances CDF (Findeisen and Minor Jr, 2010). VILIP-2 modulates the P/Q channel in a Ca^{2+}-dependent manner and this effect is greater in channels containing the β_{2a} subunit (Lautermilch et al., 2005) . It is thought to bind to the CBD preventing CaM binding and slowing CDI. VILIP-2 also binds to the IQ domain and enhances CDF similarly to CaM (Lautermilch et al., 2005).

NCS-1 has been shown to regulate P/Q channels in a voltage-independent manner (Weiss and Burgoyne, 2001). Cells expressing the NCS-1 EF-hand 3 mutant (E120Q), which is unable to bind Ca^{2+}, were not able to display P/Q channel facilitation via a voltage-independent Src kinase pathway whereas cells expressing the wild-type protein were able to display facilitation. The Src kinase pathway facilitates Ca^{2+} channels rapidly, independently of the membrane potential (Diversé-Pierluissi et al., 1997). NCS-1 has also been shown to be involved in activity dependent facilitation of P/Q channels in nerve terminals (Tsujimoto et al., 2002). In addition, NCS-1 expression has been linked to decreased $Ca_v2.1$ Ca^{2+} currents with the effect dependent on specific β subunit interactions (Lautermilch et al., 2005).

Both P/Q channels and NCS-1 cluster in presynaptic microdomains, although these microdomains appear to occupy different locations on the synaptic membrane (Taverna et al., 2007). A recent study using a knockout of both NCS-1 orthologues (Frq1 and Frq2) in *Drosophila*, showed that the frequenins are involved in neurotransmitter regulation and nerve terminal growth (Dason et al., 2009). Cacophony (the *Drosophila* orthologue of $Ca_v2.1$) was shown to be essential for frequenin dependent nerve growth in larva (Dason et al., 2009). Genetic studies also indicated that frequenins interacts with the cacophony (P/Q channel orthologue) C-terminal region and regulates neurotransmission (Mori et al., 2008).

3.2 Results

3.2.1 Recombinant protein expression and purification

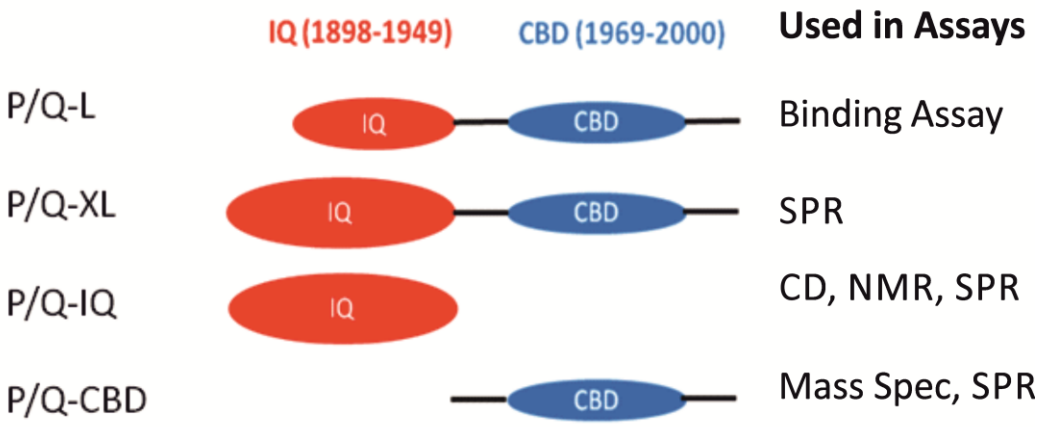

Figure 3.3. P/Q peptide fragments utilised in this study. Schematic of peptide fragments which contain either IQ, CaM binding domain (CBD) or both domains of $C_{av}2.1$ subunit of the P/Q channel used in this study. All P/Q fragments are recombinant peptides with the exception of the synthetic P/Q-IQ fragment

The initial part of the study was aimed at expressing various constructs based on the C-terminus of the $Ca_v2.1$ subunit of the P/Q channel for use in subsequent biochemical and biophysical investigations. Figure 3.3 shows w the P/Q fragments used in this study contain either the IQ, the CBD or both domains. Figure 3.4 shows all of amino acid sequences of the different P/Q fragments utilised in this study.

The recombinant proteins, GST, GST-NCS-1, GST-CaM and GST-P/Q-L in the pGex-6P1 plasmid and His-SUMO-P/Q-L in the pOPINS plasmid, were successfully expressed in BL21 (DE3) *E. coli.*

The molecular mass of GST is ~26 kDa and was expressed with relatively little contaminating proteins. GST-P/Q-L is a ~ 40.5 kDa product and it migrated as the top band on the gel (Figure 3.5a).

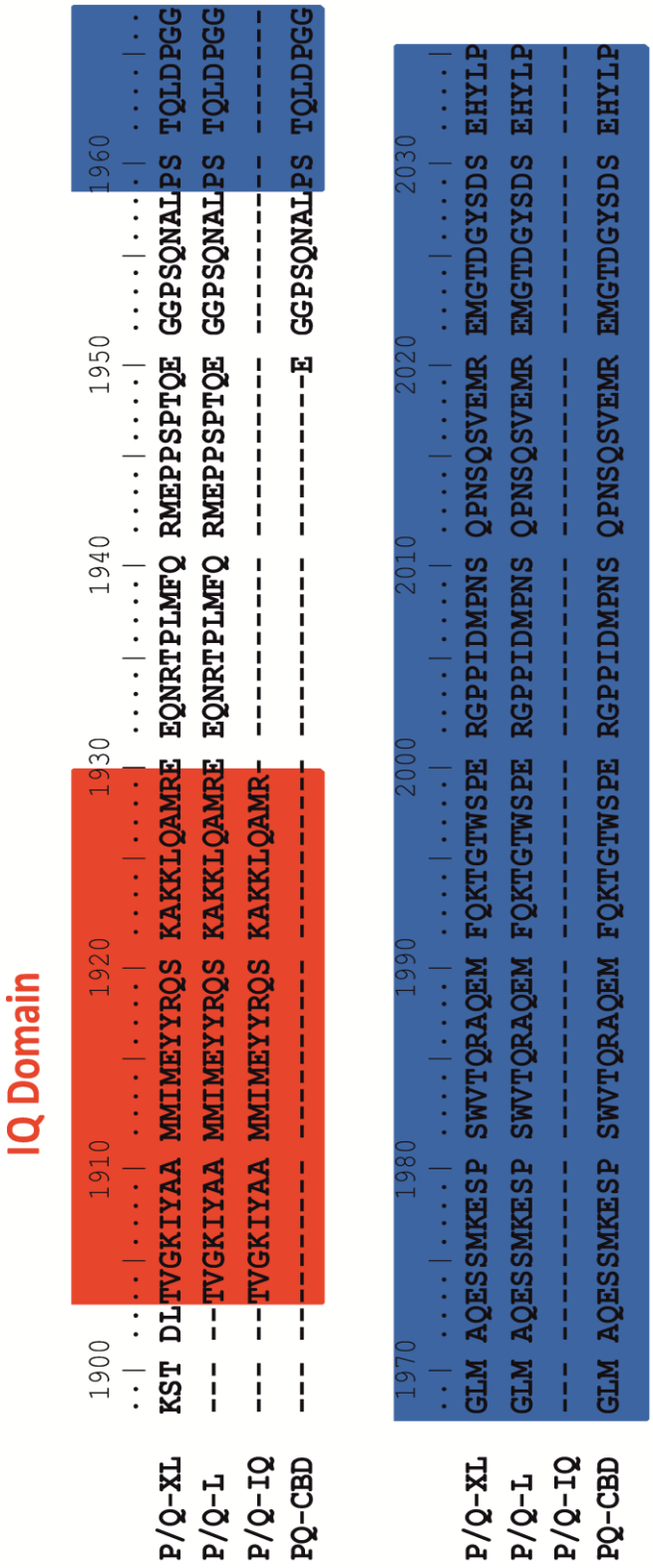

Figure 3.4 The amino acid sequences of the P/Q channel peptide fragments of the $C_{av}2.1$ subunit. IQ domain=Red, CDB=Blue.

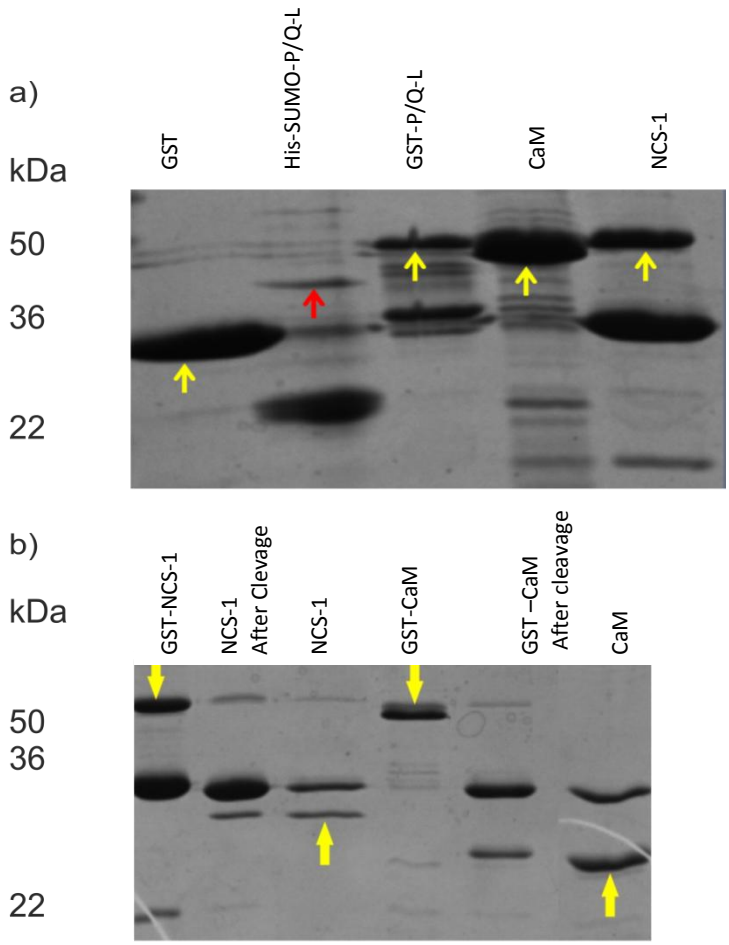

Figure 3.5. Preparation of recombinant GST Proteins and His-SUMO-P/Q-L. SDS PAGE gel recombinant proteins expressed are indicated with arrows.

A high level of GST-CaM was expressed(Figure 3.5a) and ran at the expected position on the gel for its molecular mass of ~43 kDa. The molecular mass of GST-NCS-1 is ~ 48 kDa and it ran at the expected size (Figure 3.5a). In the lanes for GST-NCS-1 and GST-P/Q-L there are contaminating proteins bands which ran at the same molecular mass as the free GST tag. All the GST fusion proteins preparations contained varying levels of contaminating proteins, which were not removed during purification.

The molecular mass of His-SUMO-P/Q-L is ~26.5 kDa. The purified protein ran at ~36 kDa (Figure 3.5a) and the sample also contained several contaminating proteins including a major band which ran at ~20 kDa. The GST-NCS-1 (Figure 3.5b) and GST-CaM (Figure 3.5b) proteins, before cleavage to remove GST, ran at the expected molecular masses. After cleavage with PreScission Protease (GE Healthcare) and purification on glutathione resin, the unbound supernatants contained untagged NCS-1 (~22 kDa) (Figure 3.5b) and untagged CaM (~17 kDa) (Figure 3.5b) at the expected molecular masses as well as contaminating GST which had not been removed by the glutathione resin.

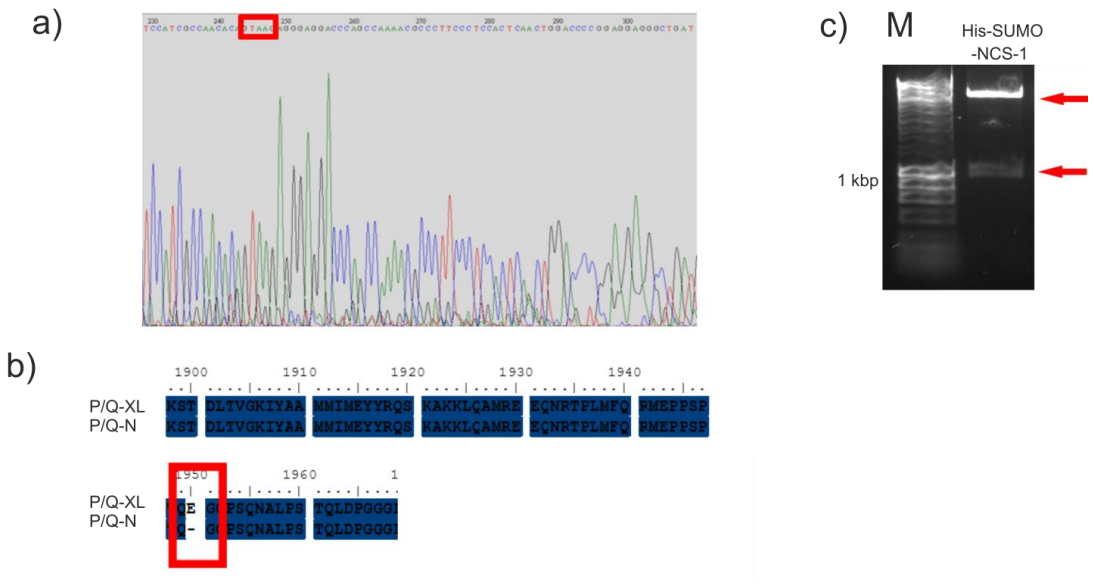

Figure 3.6 pE-SUMOpro Cloning a) A DNA chromatogram of the mutated His-SUMO-P/Q-XL plasmid. The red box shows that the stop codon (TAA) has been inserted to create the His-SUMO-P/Q-N plasmid. Sequencing and chromatography was performed by The Sequencing Service, University of Dundee. b) Alignment of part of the amino acid sequence His-SUMO-P/Q-XL fragment (P/Q-XL) and His-SUMO-P/Q-N (P/Q-N). The red box shows that the stop codon has been inserted at position 1950. The DNA sequence was translated into an amino acid sequence using ensembl and the alignment of the amino acid sequences was generated using Clustal W2. c) An agarose gel showing a restriction enzyme digest of His-SUMO-NCS-1 using BamHI and XbaI. The top arrow indicates the larger pE-SUMOpro plasmid backbone fragment and the bottom arrow indicates a smaller fragment containing the NCS-1 insert and a small region of plasmid backbone.

The pE-His-SUMO-P/Q-N plasmid was created by inserting a stop codon at the desired location in the pE-His-SUMO-P/Q-XL plasmid (Figure 3.6a and b). The translated amino acid sequence of His-SUMO-P/Q-N was aligned with His-SUMO-P/Q-XL and showed that the stop codon has been inserted after the 1949 amino acid codon of the His-SUMO-P/Q-XL plasmid to produce His-SUMO-P/Q-N. Similarly for preparation of pE-SUMO-P/Q-N2, the stop codon was inserted after the 1959 amino acid codon in the pE-SUMO-P/Q-XL plasmid. The pE-SUMO-NCS-1 plasmid was digested into two fragments, using XbaI and XhoI (Figure 3.6c). The higher band consists of the pE-SUMOPro pro backbone and which runs at ~5 kbp on the gel. The lower fragment runs at ~ 900 bp and consists of the NCS-1 insert (573 bp) and part of the plasmid backbone (~350 bp). This indicates successful preparation of the pE-His-SUMO-NCS-1 plasmid.

Expression of His-SUMO-NCS-1 in BL21 cells was very low compared to His-SUMO-P/Q-XL and His-SUMO-P/Q-CBD. No attempt was made to transfect the pE-SUMO-P/Q-N2 plasmid in to recombinant protein expressing bacteria in this study, so the expression of His-SUMO-P/Q-N2 protein was not assessed in this system. When expressed in BL21 (DE3), the His-SUMO-P/Q-CBD band was a minor component of this sample (Fractions 24-30) (Figure 3.7a). A ladder of smaller molecular mass proteins, which could potentially be truncated P/Q-CBD peptides, was also seen. When His-SUMO-P/Q-CBD was expressed in Rosetta 2 (DE3) pLysS cells, it was produced at a higher concentration and was the major component of the sample (fractions 26-30) (Figure 3.7b). The lower molecular mass fragments were a smaller component of this sample in comparison to the full-length His-SUMO-P/Q-CBD product.

After His-SUMO protease cleavage, the P/Q-CBD sample was cloudy showing precipitation of the peptide. On an SDS-PAGE gel, untagged P/Q-CBD, which is predicted to be ~9.5 kDa, migrated to ~18 kDa (Figure 3. 7d). The P/Q-CBD sample was concentrated and after a second nickel affinity purification the untagged P/Q-CBD peptide sample contained no contaminating protein bands (Figure 3.7d). The molecular mass of free SUMO should be ~12 kDa but it ran on the gel at ~ 20 kDa.

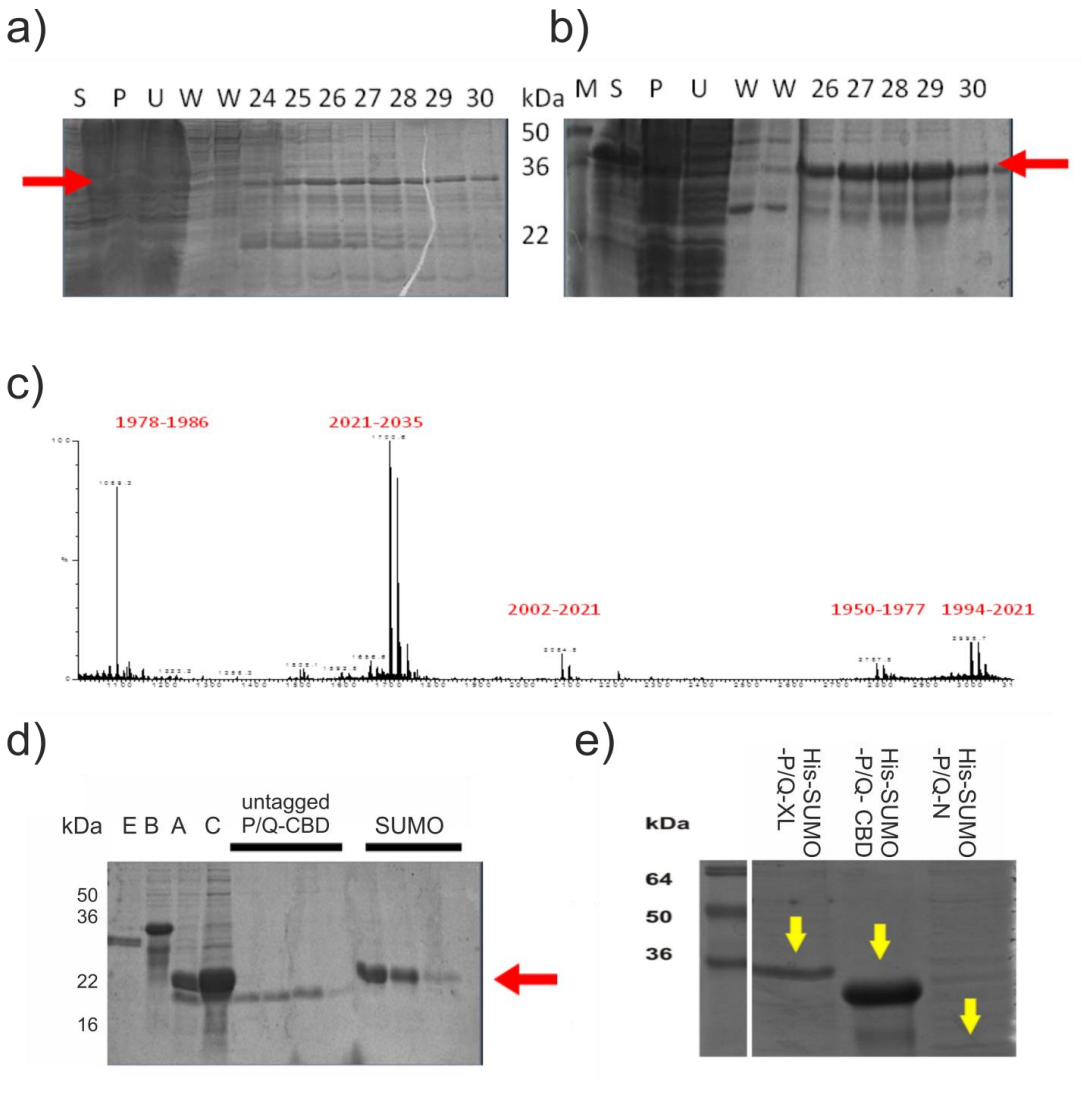

Figure 3.7 Preparation of recombinant P/Q fragments SDS-PAGE gels showing His-SUMO-P/Q-CBD purified using affinity chromatography using Histrap FF columns, a) produced in BL21 (DE3) E. coli and b) produced in Rosetta 2 (DE3) pLysS E. coli. The red arrows (a and b) indicate the His-SUMO-P/Q-CBD proteins. a and b) Lane S represents the soluble proteins in the supernatant which was loaded on to the column, lane P represents insoluble protein in the pellet after ultracentrifugation, lane W represents column washes, a) lanes 24-30 and b) lanes 26-30 column fractions containing His-SUMO-P/Q-CBD. c) A mass spectrogram of untagged P/Q-CBD peptide after In-Gel tryptic digestion. Peaks represent digested peptide fragments. Double peaks represent digested fragments and are 16 Daltons apart. Tryptic digest and mass spectrometry performed by Dr Mark Wilson and Mark Prescott (University of Liverpool). d) SDS-PAGE gel showing cleavage of His-SUMO-P/Q by His-SUMO Protease ULP1. Lane E contains SUMO Protease, lane B contains uncleaved His-SUMO-P/Q-CBD. Lane A contains a mixture of untagged P/Q-CBD and His-SUMO. Lane C is concentrated untagged P/Q-CBD and His-SUMO. Lanes labelled untagged-CBD contain the protein after His trap purification. Lanes labelled SUMO indicates 3 lanes containing His-SUMO and His tagged SUMO protease, eluted from the Histrap column. e) SDS-PAGE gel showing recombinant His-SUMO tagged P/Q peptides purified by affinity chromatography using a Histrap FF column.

The untagged P/Q-CBD peptide was sent for analysis by mass spectrometry. A good coverage of the tryptic digested fragments of P/Q-CBD peptide was obtained, with all digested fragments, except 1987-1993, were identified (Figure 3.7c). This confirms that the full-length peptide was expressed. All fragment peaks, with the exception of fragment 1979-1986, appeared on the spectrogram as double peaks 16 kDa apart. These double peaks are characteristic of oxidation of methionine residues in digested fragments.

His-SUMO protease cleavage was also performed for His-SUMO-NCS-1 and cleavage was successful, however, cleavage was unsuccessful for His-SUMO-P/Q-XL (results not shown). His-SUMO tag cleavage was successful for the poorly expressed His-SUMO-P/Q-N protein, but all of the untagged peptide precipitated out of solution (results not shown).

All of the expressed His-SUMO tagged P/Q peptides were analysed by SDS-PAGE and ran higher than their predicted molecular masses. His-SUMO-P/Q-CBD predicted molecular mass is 21 kDa and its band ran below the 36 kDa marker (Figure 3.7e), His-SUMO-P/Q-XL is predicted at 27 kDa but ran at 36 kDa (Figure 3.7e) and His-SUMO-P/Q-N molecular mass is 18 kDa but runs above the 22 kDa marker. The expression of His-SUMO-P/Q-N was low (Figure 3.7e).

From the protein expression studies it was found that preparation of sufficient yields of GST-NCS-1 and GST-CaM could be achieved as expected and the cleaved proteins prepared. In addition, GST-P/Q-L, His-SUMO-P/Q-CBD and His-SUMO-NCS-1 were successfully expressed at levels that could be used for subsequent experiments. It was not possible to express sufficient amounts of the SUMO-P/Q-N.

3.2.2 Analysis of the Ca^{2+}-dependency of binding of GST-P/Q-L to NCS-1 using a Pull-down Assay

To initially investigate the possibility of direct Ca^{2+}-dependent binding of NCS-1 to the P/Q channel, GST-P/Q-L and NCS-1 were used in a pull-down assay. GST-P/Q-L was immobilised on GST resin, then incubated with untagged NCS-1 in a series of concentrations of free Ca^{2+}. Western blot analysis of the bound samples showed Ca^{2+}-dependent binding of NCS-1 to GST-P/Q-L (Figure 3.8a). The binding data were fitted to a hyperbolic model, which indicated that GST-P/Q-L and NCS-1 binding, occurred with a free Ca^{2+} concentration dependency of 0.85 μM (Figure 3.8b). These results indicated that NCS-1 can directly interact with C-terminal regions of the P/Q channel.

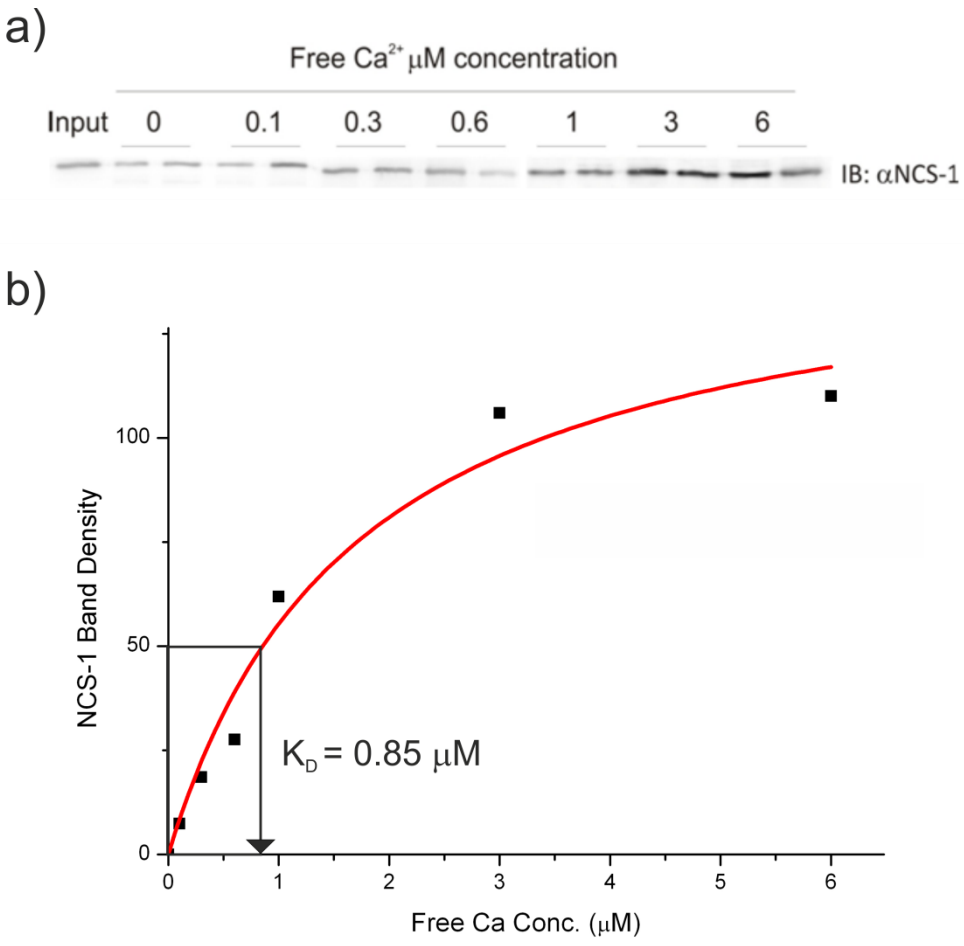

Figure 3.8. Ca^{2+}-dependent binding of GST-P/Q-L and NCS-1. Recombinant protein GST-P/Q-L (1mM) was immobilised on glutathione resin in buffer containing 0-6 μM free Ca^{2+} concentration. NCS-1 protein (1 μM) was added to the assay. a) The binding of NCS-1 to GST-P/Q-L was analysed by Western blotting using polyclonal anti-NCS-1 antibodies. b) The density of the bound NCS-1 band was determined using ImageJ software and plotted verses Ca^{2+} concentration.

3.2.3 Analysis of NCS-1 and P/Q peptide interactions by Surface Plasmon Resonance.

In an attempt to further characterise interaction of NCS-1 with P/Q peptide and to measure the binding kinetics and affinity of the NCS-1 and P/Q peptide binding, surface plasmon resonance was used. SUMO-P/Q-XL or SUMO-P/Q-CBD were immobilised on to the chip surface. NCS-1 was passed over the peptide coated chip in the presence of Ca^{2+}. NCS-1 was found to interact non-specifically with the chip surface. The nonspecific interactions did not allow specific binding between NCS-1 and the P/Q peptides to be detected using this assay. CaM has been shown to bind to the P/Q channel $C_{av}2.1$ subunit, so it was decided to use CaM as a control to determine the suitability of SPR as a method of analysis for calcium sensing protein interactions with the P/Q-IQ peptide. CaM was immobilised to the chip surface and the synthetic peptide P/Q-IQ passed across the protein coated surface in the presence of Ca^{2+}. The P/Q-IQ peptide also interacted with the chip surface non-specifically, and therefore, because of the nonspecific interactions of both P/Q-IQ and NCS-1 with the chip surface, it was decided not to pursue the use of SPR but instead to use NMR to investigate NCS-1 and P/Q peptide binding.

3.2.4 Secondary structure characterization of the P/Q-IQ peptide

Since it proved not to be possible to express recombinant proteins containing only the IQ domain a synthetic IQ peptide was prepared. To ensure the synthetic P/Q-IQ peptide contained the relevant alpha helical structure necessary for calcium sensor protein binding, it was characterised by two methods. The AGIDAR2s algorithm was used to calculate the secondary structure of the P/Q-IQ peptide. The algorithm software calculated that the P/Q-IQ peptide sequence had a total helical propensity of 8.3% (Figure 3.9a). Residues 6-14 (YAAMMIMEY) of this peptide had a helical propensity above 10% suggesting this region of the peptide forms an alpha helix. The other residues in the peptide were predicted to be below 10%. CD was used to measure the spectrum of the peptide in far UV light. TFE is thought to stabilise interactions between residue side chains and induce peptides to form native secondary structures. To measure peptide total helicity, the peptide was resuspended in a series of TFE concentrations and the spectrum was acquired.

a)

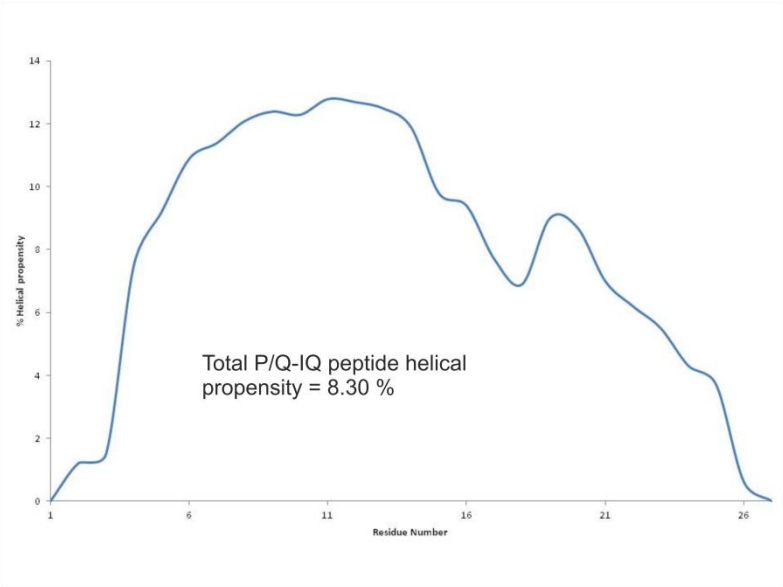

b)

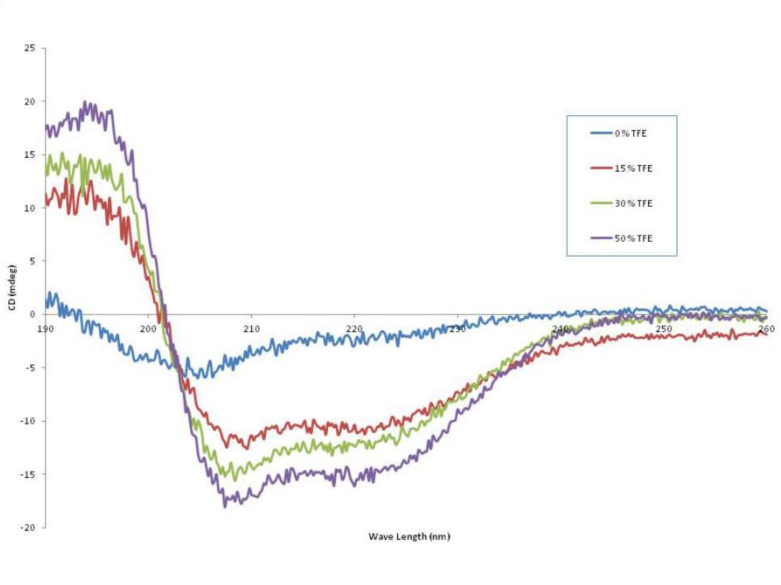

Figure 3.9. Characterisation of the synthetic IQ peptide from the P/Q channel. a) A prediction of the helical propensity was plotted for individual residues in the P/Q-IQ peptide sequence and total % helical propensity determined using AGIDAR2s algorithm software. b) A CD spectra of P/Q-IQ peptide in the absence or presence of TFE. Elipticity was plotted against wavelength for samples assayed at different TFE concentrations

When the peptide was suspended in 0% TFE: 100% water, the spectrum is characteristic of a random coiled structure (Figure 3. 9b). In the presence of TFE the CD spectra for the peptide is characteristic of an alpha helical secondary structure, showing a decrease of optical rotation at wavelength 205-222 nm. [θ_{222}] decreases from -1616 to – 2105 deg cm^2 dmol as the concentration of TFE increases from 15% to 50%. The percentage peptide helicity in 0% TFE was 0.97% suggesting a random coil structure. As the TFE concentration increased the percentage peptide helicity increased from 4.5% in 15% TFE to 5.9 % in 50 % TFE, showing that the peptide contains a helical secondary structure. Higher concentrations of TFE induce more residues in the peptide to fold into a helical conformation.

3.2.5 Gel filtration analysis of putative NCS-1 P/Q-IQ complex

To determine if NCS-1 would form higher order complexes in the presence of the P/Q-IQ peptide, analytical gel filtration was performed on the NCS-1 and P/Q-IQ mixture. The protein peak eluted at an elution volume of 12 ml (Figure 3.10). The K_{av} was 0.31 and when read from a standard curve for this analytical column indicates a molecular mass of ~20 kDa. The result suggests that NCS-1 is not forming a homodimer or higher complexes in the presence of the P/Q-IQ fragment and that the measured molecular mass is closer to that of free NCS-1 or a putative monomeric NCS-1 P/Q-IQ complex.

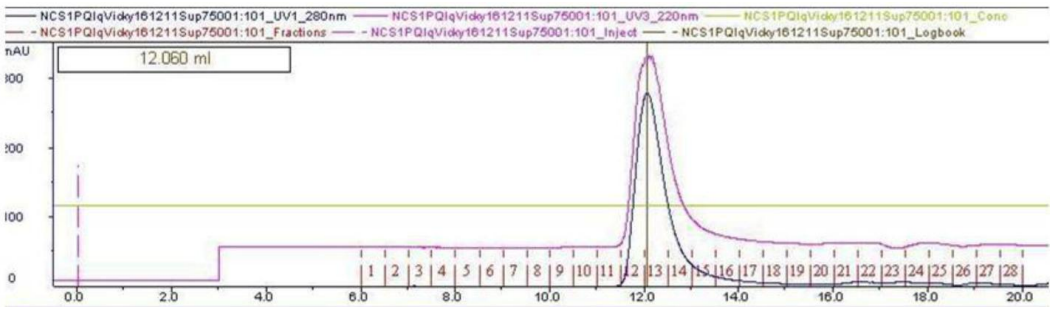

Figure 3.10 Analysis of putative NCS-1 and P/Q-IQ peptide complex formation using analytical gel filtration. The putative NCS-1 and P/Q-IQ complex (at 3.5 : 1.0 P/Q-IQ : NCS-1 ratio) was loaded on to an analytical gel filtration column in the presence of 5 mM Ca^{2+}. The chromatogram shows an elution peak volume of 12.06 ml

3.2.6 NMR Temperature Titration of NCS-1 and CaM

To determine whether high quality NMR HSQC spectra could be obtained with the cleaved and purified samples of NCS-1 and CaM experimental spectra of NCS-1 and CaM were acquired over a temperature titration for both proteins and spectra overlaid (Figure 3.11). As the temperature of acquisition increases, all the backbone and side chain peaks move to the left of the spectra for NCS-1 (Figure 3. 11a and b) and CaM (data not shown). For example NCS-1 Glu 74 and Lys 158 peaks increase in ^{1}H (ppm) on the spectra (Figure 3. 14b). The ^{15}N ^{1}H HSQC spectrum of NCS-1 (Figure 3.11) and CaM (data not shown) were acquired in the presence of Ca^{2+}, at 298K and residues were assigned by comparison to the reference spectrum (Lian et al., 2007, Handley et al., 2010) and transferred to spectra acquired 300K, 305K and 308K temperature titrations.

2.2.7 NMR analysis of CaM and P/Q-IQ peptide interaction

CaM was used as a control protein to analyse the interactions of the P/Q-IQ peptide in NMR experiments, as it has been shown previously to bind to the peptide. In the presence of Ca^{2+}, the ^{15}N ^{1}H HSQC spectrum of CaM was acquired (without P/Q-IQ peptide present) (Figure 3.12, red peaks). In a titration experiment, P/Q-IQ peptide was added incrementally until a final 4:1 ratio with CaM was achieved (Figure 3.12, black peaks). Spectra for each titration point were acquired. The spectrum for CaM alone and the spectrum of CaM bound to the P/Q-IQ peptide were overlaid (Figure 3.12). The presence of the P/Q-IQ peptide altered the chemical shift values of several residues on the $^{1}H^{15}N$ spectra (Figure 3.12a).

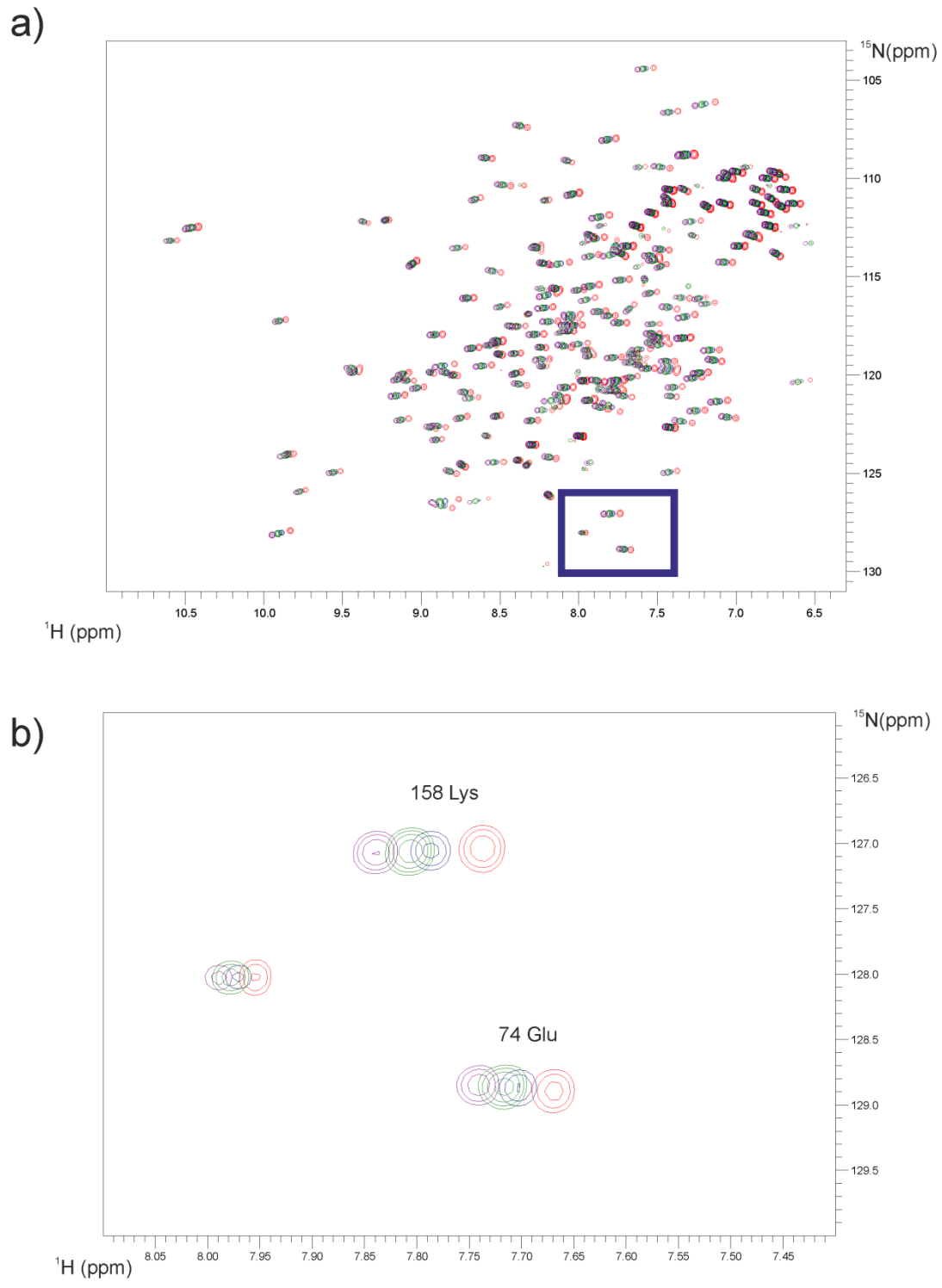

Figure 3.11. Two-dimensional NMR Analysis of NCS-1 with temperature titration. NMR was performed on an Avance Bruker 800 MHz spectrometer, in the presence of Ca^{2+}, at pH 6.5. a) The complete overlaid ^{1}H ^{15}N HSQC spectra. The blue rectangle indicates the region to be enlarged. b) The enlarged region of the overlaid spectra. The red, blue, green and magenta peaks represent residues of NCS-1 acquired at 298K, 303K, 305K and 308K respectively.

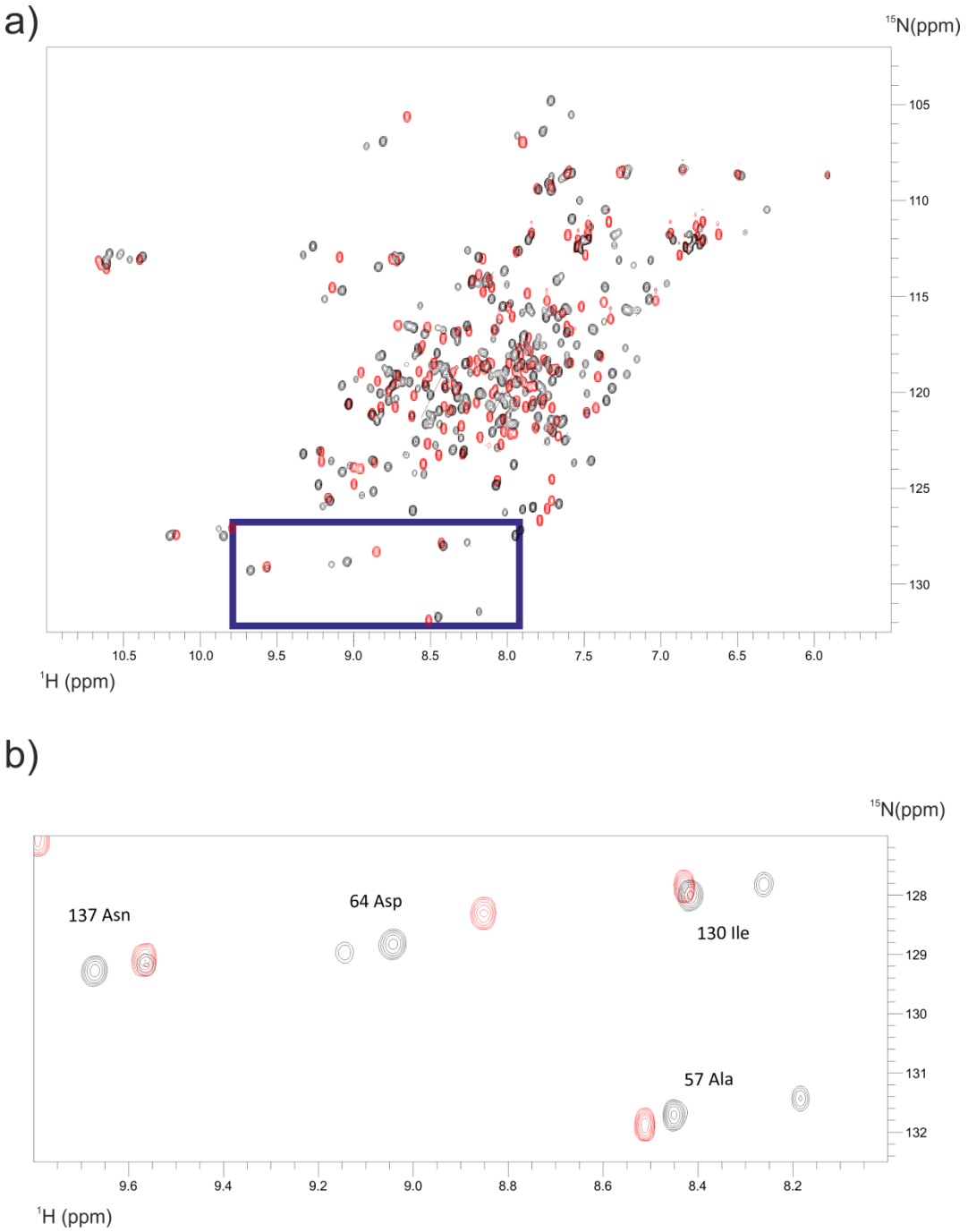

Figure 3.12 Two-dimensional NMR analysis of CaM alone and in complex with the P/Q-IQ. NMR was performed on an Avance Bruker 600 MHz spectrometer, in the presence of Ca^{2+}, at 308K, pH 6.5. a) The complete overlaid ^{1}H ^{15}N HSQC spectra. The blue rectangle indicates the region to be enlarged. b) The enlarged region of the overlaid spectra. Red peaks represent residues of CaM alone and black peaks represent residues of CaM in complex with P/Q-IQ peptide and were acquired using the final P/Q-IQ titration into the CaM sample at a 4:1 ratio.

Peaks that moved by 0.08 ppm or more on addition of the peptide suggested that the residues to which these peaks are assigned are involved in peptide binding. Eighteen N-lobe and thirteen C-lobe residues were affected (Table 1). The peaks of linker residues were not affected by the peptide. Twelve residues from both lobes have two peaks on the spectra, (Table 1, group 1), for example 57 Ala, 64 Asp, 130 Ile, 137 Asn (Figure 3.12b). The large peak represents a major conformation of the CaM and P/Q-IQ complex, while the small peak represents the minor conformation, and these double peaks show that these residues have a role in both conformations (Figure 3.12b).

The spectrum of P/Q-IQ bound CaM was compared to previously recorded spectra of CaM bound to L-Type IQ peptide and CaM residues (Table 1). Group 1 consists of the CaM residues which have double peaks on the spectrum when bound to P/Q-IQ. The minor conformation peaks have a resonance similar to CaM when bound to L-type IQ peptide and major conformation peaks have a resonance different to CaM when bound to L-type IQ peptide. Group 2 (Table 1) consists of CaM residues which have a single peak on the spectrum when bound to P/Q-IQ, and have also been shown to bind to L-type IQ peptide. Group 3 consists of CaM residues which have a single peak on the spectrum when bound to P/Q-IQ and are not shown to be involved in to be involved in L-type IQ peptide complex formation.

The data in table 1 was used to create ribbon diagram models of the minor and major conformations (Figure 3.13). Group 1 (Red) and Group 2 (blue) residues are highlighted in (Figure 3.13a) and show a predicted model of the minor conformation of the CaM and P/Q-IQ complex. Group 1 residues (Red) are also shown to be involved in the major conformation of the CaM and P/Q-IQ (Figure 3.13b) as well as the four Group 3 residues (Blue) not shown to bind to the L-type peptide. CaM residues involved in the minor and major conformations are located on both the N-lobe and the C-lobe (Figure 3.13a and b).

Table 3.1 Interpretation of NMR analysis of the CaM in complex with P/Q-IQ peptide.

CaM Location	Group 1 Perturbed Residues with two peaks in minor and major conformations	Group 2 Perturbed residues with a signal peak like L-type IQ binding	Group 3 Perturbed residues with a single peak unlike L-type IQ binding
N Lobe	Thr 26	Thr 5	Ser 17
	Ile 27	Glu 6	Leu 18
	Thr 29	Phe 16	
	Gly 33	Gly 25	
	Thr 44	Gly 40	
	Ala 57	Val 55	
	Ile 63	Gly 61	
	Asp 64	Phe 65	
C-Lobe	Thr 117	Asp 95	Leu 105
	Ile 130	Gly 96	Leu 116
	Val 136	Ile 100	
	Ala 137	Asp 102	
		Gly 132	
		Gly 134	
		Met 145	

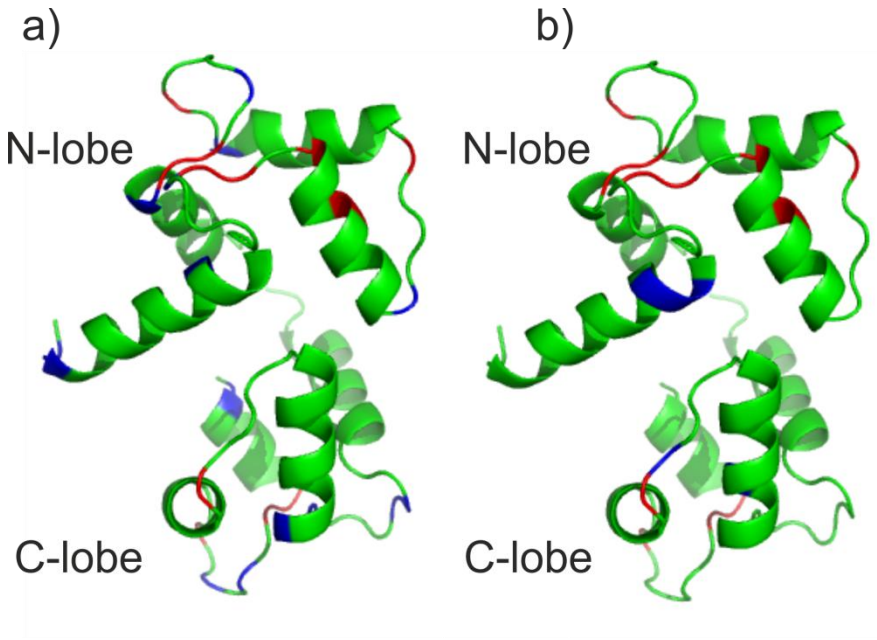

Figure 3.13 Interpretation of NMR analysis of the CaM and P/Q-IQ peptide complex. Ribbon diagrams of Ca^{2+} bound CaM showing residues perturbed by PQ-IQ peptide binding in both a) minor and b) major conformations of the complex. Residues coloured red a and b) are involved in both minor and major conformations of the complex. a) Predicted minor conformation, residues coloured blue, have previously shown to be involved in the antiparallel conformation with the L-type IQ peptide. b) Predicted major conformation, Residues coloured in blue are different to those previously shown to be involved in the antiparallel conformation with the L-type IQ peptide.

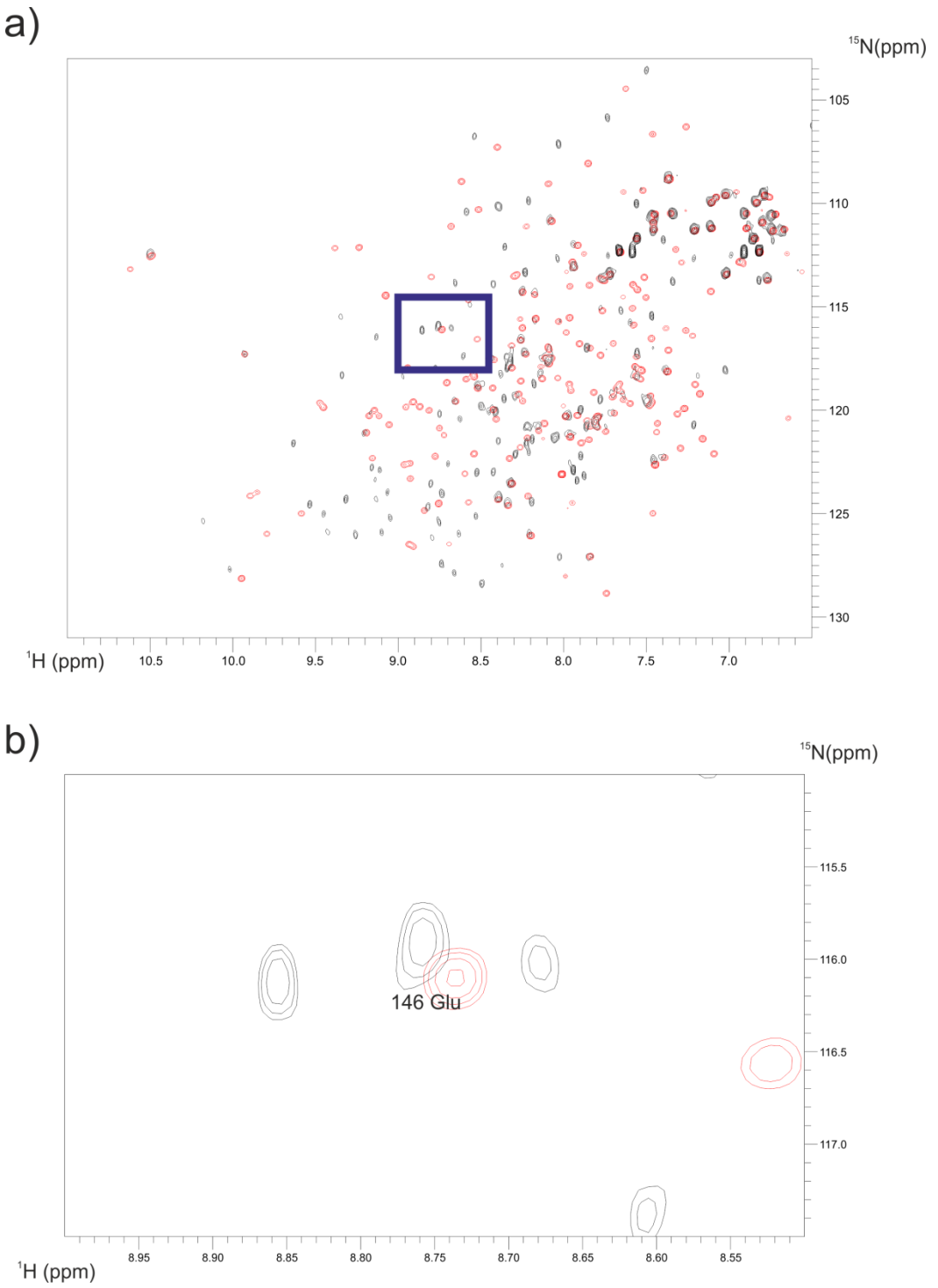

Figure 3.14 Interactions between NCS-1 and P/Q-IQ Peptide analysed using two-dimensional NMR spectroscopy. NMR was performed on an Avance Bruker 800 MHz spectrometer, in the presence of Ca^{2+}, at 308K, pH 6.5. a) Shows the complete overlaid ^{1}H ^{15}N HSQC spectra. The blue rectangle indicates the region to be enlarged. b) The enlarged region of the overlaid spectra. Red peaks represent residues of NCS-1 alone and black peaks represent residues of NCS-1 in the presence of P/Q-IQ peptide and was acquired using the final P/Q-IQ titration into the NCS-1 sample at a 3.5 : 1.0 ratio.

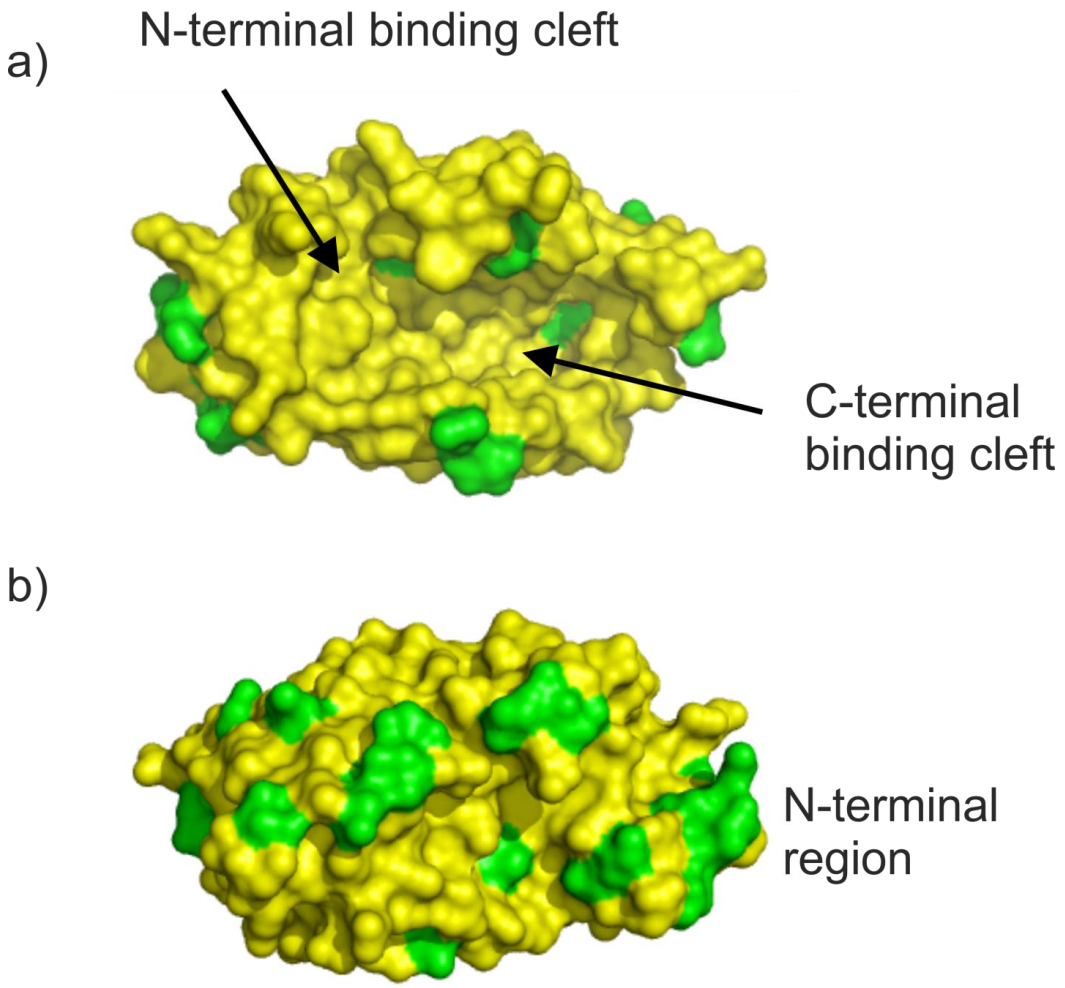

Figure 3.15 3D Interpretation of NMR analysis of NCS-1 interactions with the P/Q-IQ peptide. A protein surface model of Ca^{2+} bound NCS-1 in the presence of P/Q-IQ. a) The face of NCS-1 showing the exposed hydrophobic binding cleft and b) the opposite face of the protein rotated 180°. Residues of NCS-1 perturbed by the presence of the P/Q-IQ peptide are coloured yellow and residues unaffected by the peptide are coloured green. NCS-1 structure derived from (PBD, 1G8I).

3.2.8 NMR analysis of NCS-1 and P/Q-IQ peptide interaction

To establish if NCS-1 also binds to the IQ domain of the $C_{av}2.1$ subunit of the P/Q channel and if so what residues of NCS-1 are involved in binding, NMR was also used to investigate NCS-1 interactions with P/Q-IQ peptide. The ^{15}N ^{1}H HSQC spectrum of NCS-1 alone was acquired in the presence of Ca^{2+}. A titration of the P/Q-IQ peptide was performed until a final ratio of P/Q-IQ peptide : NCS-1 of 3.5 : 1.0 was achieved. The spectra for NCS-1 alone and in the presence of P/Q-IQ were

overlaid (Figure 3.14). Peaks, which moved by 0.08 ppm or more were identified as being perturbed by the addition of peptide to NCS-1. In the presence of the P/Q-IQ peptide, only 29 peaks remains at the same positions, whereas 151 peaks are perturbed (Figure 3.14). The peaks which change position represent backbone amide groups of residues distributed throughout the protein structure of NCS-1 (Figure 3.15a and b, yellow residues). The peaks in the spectrum which had not moved significantly (<0.08 ppm) did not represent a localised area of the structure of NCS-1. Instead residues are distributed throughout NCS-1 with the largest number within the unstructured N-terminal region (Figure 3.15a and b, green residues). The 3D interpretation of Ca^{2+} bound form NCS-1 shows the residues perturbed by the presence of the P/Q-IQ peptide.

In conclusion, the NMR data showed that CaM residues located N- and C- lobes regions previously involved in target peptide binding appear to interact with the P/Q-IQ peptide. In contrast, the results for NCS-1 interactions with the P/Q-IQ peptide were not as clear. Although the peptides presence has an effect on NCS-1 conformation, the change was global rather than to a specific region of the protein, therefore, no defined binding site or residue-specific interactions could be identified using NMR.

3.3 Discussion

It was found possible to express certain P/Q fragments in addition to NCS-1 and CaM for biochemical and biophysical analyses. The studies described here on the analysis of protein binding showed a direct Ca^{2+}-dependent interaction between NCS-1 and a long P/Q fragment (GST-P/Q-L). Further characterisation of the binding could not be achieved by use SPR because of nonspecific interactions between the SPR chip surface and the NCS-1 protein or the P/Q-IQ peptide, potentially masking NCS-1 and P/Q fragment binding. Analysis by NMR was able to show discrete regions of interaction in the control experiments with CaM in the presence of the synthetic P/Q-IQ peptide but not with NCS-1.

His-SUMO-NCS-1, His-SUMO-P/Q-N and His-SUMO-P/Q-N2 plasmids were created using cloning techniques. Tagged P/Q- peptides GST-P/Q-L, His-SUMO-P/Q-XL and His-SUMO-P/Q-CBD were successfully expressed and untagged P/Q-CBD produced after sumo cleavage. Untagged CaM and tagged NCS-1 proteins, GST-NCS-1, His-NCS-1 and His-SUMO-NCS-1 were produced and untagged versions of these proteins were created after protease cleavage. The SUMO tag and SUMO fusion proteins ran on the SDS-PAGE gels higher than expected for their molecular mass. SUMO is an globular protein with extended N-terminal and C-terminal regions (Bayer et al., 1998). The extended regions give SUMO a larger hydrodynamic radius than a compact globular protein of the same molecular mass, therefore it migrates slower on the protein gel. This may also be the reason that the untagged P/Q-CBD peptide migrated slower than expected on the gel, because peptides are often unstructured and have higher hydrodynamic radii than globular proteins of the same molecular mass.

When analysing the His-SUMO-P/Q-CBD recombinant protein after expression, a ladder of smaller molecular mass proteins, which did not increase over time, was observed. When expression was performed in Rosetta 2 (DE3) pLysS cells rather than BL21 (DE3) cells the expression of full length peptide increased significantly. The increase in expression may be due to Rosetta 2 (DE3) pLysS cells containing tRNA codons not usually found in *E. coli* and increasing expression of the full

P/Q-CBD peptide rather than smaller fragments. Another possibility is that the ladder of proteins were contaminating E. coli proteins of a small molecular mass expressed at higher levels in the BL21 cells and at a lower levels in the Rosetta 2 (DE3) pLysS. The expression of the other P/Q fragments His-SUMO-P/Q-N, His-SUMO-P/Q-XL and GST-P/Q-L could possibly be increased by expression in the Rosetta 2 (DE3) pLysS cells.

The GST-tagged recombinant proteins NCS-1, CaM and P/Q-L were successfully produced although free GST tag was the biggest component of the NCS-1 sample making this expression system less than ideal. GST cleavage from NCS-1 was not completely successful and uncleaved GST-NCS-1 was present in the untagged NCS-1 sample. GST cleavage could be made more efficient by changing the composition of the cleavage buffer (Wang and Johnson, 2001).

It was not possible to cleave the His-SUMO-tag from His-SUMO-P/Q-XL using conventional methods. A recent paper has shown it is possible to express proteins with a His-SUMO-tag which can auto-cleave by adjusting the pH of the buffer. When cleaving the His-SUMO tag from His-SUMO-P/Q-N the peptide precipitated. It may be possible to rescue this sample by pelleting the aggregated peptide and re-dissolving it in solution.

The pull-down assay carried out here showed that NCS-1 and GST-P/Q-L binding is direct and is Ca^{2+}-dependent as it showed a clear Ca^{2+}-dependent increase of untagged NCS-1 binding to the GST-P/Q-L (residues 1909-2035) fragment. Active $[Ca^{2+}]i$ in neurons varies at specific locations within the cytoplasm between 0.50-1.00 μM (Berridge, 1998). Binding of NCS-1 and GST-P/Q-L occurred half-maximally at a free Ca^{2+} concentration of 0.85 μM which falls within the active range for neuronal Ca^{2+}signaling. The NCS-1 used in this study was unmyristoylated and Mg^{2+} was present in the buffer, these conditions may have lowered the affinity of NCS-1 for Ca^{2+} as previous studies have shown (Jeromin et al., 2004, Aravind et al., 2008). The PQ-L fragment used in this assay contains both the IQ domain (residues 1909-1949) and CBD (residues 1969-2035) and also a linker region (residues 1950-1968) between the two domains as defined previously (Lee et al., 2002). It is not possible

to identify whether NCS-1 binds to one or both of the peptide domains. Two other P/Q fragments were generated with the aim of using them in further binding studies to identify which regions of the Ca_v 2.1 subunit interacted with NCS-1 but neither were used. One was an extended construct P/Q-XL (residues 1898-2035) which included the CBD domain and a larger IQ domain with an additional 11 amino acids compared to the P/Q-L fragment. The second P/Q fragment contained only the CBD.

Since it was not possible to express constructs containing the IQ domain without the CBD, a synthetic peptide, which contained an extended IQ domain, was used in binding assays. P/Q peptides containing the IQ domain used in other studies have been shown to have a helical structure. These peptides were either synthetic peptides, but of different length than that used in this study or were made as recombinant proteins. To ensure the synthetic peptide used in this study had a helical secondary structure two methods were used to characterise its structure. AGIDAR2s is a computer-based algorithm, which analyses peptide sequence. AGIDAR2s generates helical propensity for individual amino acids and the peptide as a whole. The second method, circular dichroism shows the percentage helicity for the total peptide. Both the measured and the predicted calculations of percentage showed the peptide has helical secondary structure, although helicity the values were low, ~ 5% from the CD at 50% TFE and ~8 % for the prediction. The predicted value for the individual residues showed that the region containing residues 6-14 (YAAMMIMEY) have the higher helical propensity. This region of the peptide has been shown to be involved in CaM interactions (Kim et al., 2008, Mori et al., 2008) and involved in both CDF and CDI of P/Q channel regulation. The analytical gel filtration results suggest that the NCS-1 protein in the presence of the P/Q-IQ peptide did not form higher order complexes indicating that the mixture would be suitable for use in NMR studies.

A previous NMR study has shown that the L-type IQ peptide binds to CaM in a parallel protein conformation (Lian et al., 2007). P/Q fragments containing the IQ domain have been shown to form complexes with CaM in either an antiparallel or parallel protein conformation in different crystallography studies (Kim et al., 2008,

Mori et al., 2008). The NMR spectra collected in this study suggested that the CaM interacted with the P/Q-IQ peptide in two conformations. When bound to P/Q-IQ peptide the minor conformation of the double CaM peaks were similar to how CaM behaves when bound to the L-type IQ peptide (Lian et al., 2007). CaM forms a parallel complex with the L-type IQ peptide, suggesting that the minor conformation of the CaM and P/Q-IQ peptide complex is in the parallel conformation as reported previously (Mori et al., 2008). The major conformation of the double CaM peaks were in different positions in the spectra than those involved in L-type IQ peptide interactions, suggesting that the major conformation of the CaM and P/Q-IQ complex is in an antiparallel conformation supporting the finding of the Minor group (Kim et al., 2008). Four CaM residues (Ser17, Leu18, Leu105 and Leu 116) not previously seen in L-type IQ interactions were also interpreted as being involved in the major antiparallel conformation. Whilst this is interesting, the previous L-Type CaM binding analysis was performed under different conditions than those in this study including differences in temperature and pH. To investigate this further, the spectra would need to be acquired for both L-Type and P/Q-type IQ peptides in complex with CaM under identical conditions.

The NMR spectra showed that the majority of residues in the NCS-1 protein were affected by the presence P/Q-IQ and so it was not possible to identify a specific location on NCS-1 for peptide binding. The NCS-1 amino acids affected are located in all regions of the NCS-1 protein, not just the hydrophobic binding pocket but also on the surface and all sides of the protein. This suggests a significant global change in the structure of NCS-1; this could be caused by dimerisation of NCS-1 when it interacts of the P/Q-IQ peptide (although this would not be supported by the gel filtration data) or that the P/Q-IQ peptide is able to bind non-specifically to many regions of NCS-1.

X-ray crystallography has previously been used to determine CaM binding to IQ domain peptides and to solve the NCS-1 structure (Kim et al., 2008, Mori et al., 2008, Pongs et al., 1993). To move forward with this study, X-ray crystallography may be a better method than NMR to characterise the NCS-1 and P/Q-IQ peptide complex and to identify which amino acids in the NCS-1 binding pocket are

interacting with the P/Q peptide, because crystallography ‘visualises’ the complex formation using diffracted X-rays rather than interpreting interactions indirectly using NMR.

Chapter 4: RESULTS Investigation of the Structure/Function Relationship of NCS-1 in the Model Organism *C. elegans*

4.1 INTRODUCTION

The structural features of neuronal calcium sensor (NCS) proteins, including EF hand motifs, the hydrophobic binding pocket, the C-terminal tail and N-terminal myristoylation are implicated by structural studies to be important for several functions including activation, localisation, complex formation and protein conformation.

The functional importance of the EF hand motifs has been well characterised for NCS-1 and other NCS proteins. Notably, a study using the *ncs-1* null *C. elegans* strain (qa406) used characteristics from EF structural studies and by using mutagenesis and behavioural analysis, showed a structural/functional relationship of the EF hand and Ca^{2+} binding in neuronal function (Gomez et al., 2001). Less is known of the physiological relevance of the structural characteristics of N-terminal myristoylation, the C-terminal tail and the hydrophobic binding pocket. A model organism has yet to be utilised to investigate these features for NCS-1 orthologs.

Residues in the hydrophobic pocket are conserved in many NCS proteins (Figure 4.1a). The hydrophobic pocket of NCS-1 proteins is thought to be divided up into two clefts, the N-terminal cleft and the C-terminal cleft. There have been structural studies, characterising target peptide complex formation with several NCS proteins:- yeast NCS-1 orthologs Frq1 in budding yeast (Strahl et al., 2007) and Ncs-1 in fission yeast (Lim et al., 2011), which form complexes with a peptide from the PI4 kinase orthologue Pik1 ; human KChiP1 forms complexes with $K_v4.3$ (Pioletti et al., 2006, Wang et al., 2007) and bovine recoverin forms a complex with a rhodopsin kinase peptide (Ames et al., 2006).

These studies have implicated several residues in the N- and C-terminal regions of the hydrophobic pocket in complex formation and some of these residues, are involved all NCS peptide complexes (Figure 4.1). Even though the NCS proteins have binding residues in common, there appear to be differences in modes of target peptide binding.

Figure 4.1 NCS Protein Target Peptide Sequence. Hydrophobic residues implicated in Frq1, Ncs1, KChip1 and recoverin binding to target peptides.

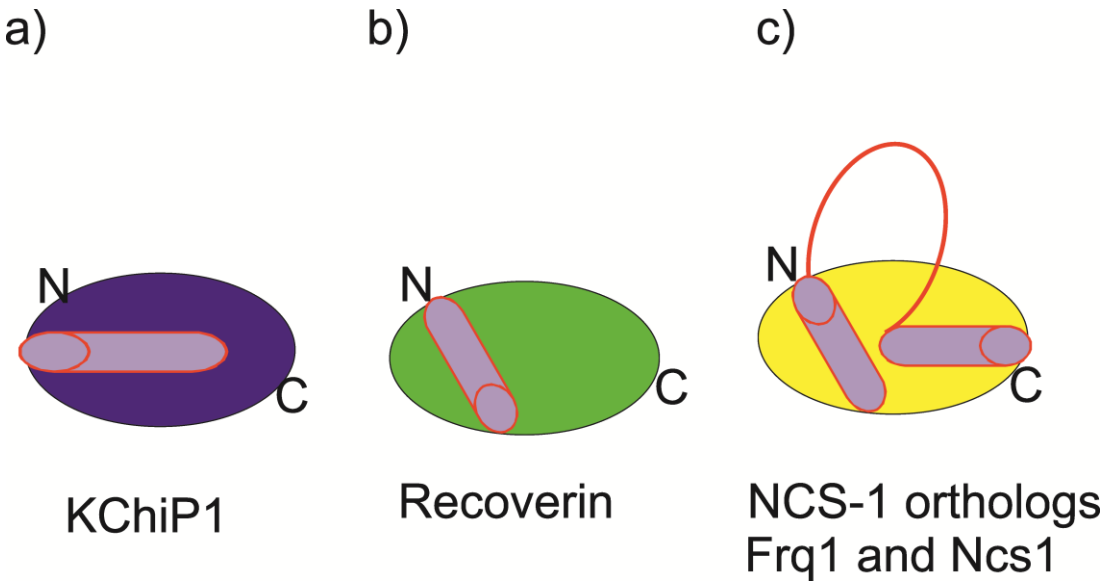

Figure 4.2 NCS Protein Target Peptide Binding to the Hydrophobic Cleft The regions of the binding cleft which are analogous to the N- and C- clefts of the NCS-1 orthologues are indicated. Cartoons of a) KChip1 protein and Kv4.3 peptide, b) recoverin protein and rhodopsin kinase peptide and c) NCS-1 orthologues and Pik1 peptide complexes. All illustrations are based on information from structural study of the complexes (Ames et al., 2006, Heidarsson et al., 2012, Lim et al., 2011, Strahl et al., 2007)

The NCS-1 yeast orthologs bind two separate alpha helixes from the target peptide of Pik1 which fully occupy the N-terminal and the C-terminal binding clefts (Lim et al., 2011, Strahl et al., 2007) (Figure 4.2a). Recoverin binds its target peptide rhodopsin kinase to the N-terminal binding cleft only. The peptide appears to occupy the whole N- terminal cleft similar to that of Pik1 with the N-terminal binding cleft of NCS-1 orthologues, except that it binds in the opposite polarity (Ames et al., 2006) (Figure 4.2b). The C-terminal cleft of recoverin appears not to be involved in target peptide complex formation as it is occupied by the C-terminal tail. During NCS-1 and target peptide binding the C-terminus is thought to move out of the binding cleft and allow protein binding. KChiP1 binds its target peptide in a different mode; it appears to have a single binding cleft which spans all of the

N-terminal and part of the C-terminal binding cleft. KChiP1 has structural differences to that of NCS-1 and recoverin, and has an extra N-terminal domain interaction with K_v4.3 which enables it to form a tetramer (Pioletti et al., 2006). These differences may be the reason the hydrophobic pocket of KChIP1 has a different 3D structure. The furthest region of the C-terminal binding cleft does not bind target protein as this region of the pocket also appear to be involved in the tetramer formation. A structure/function investigation of KChiP1 used structural information about the hydrophobic resides involved in K_v4.3 peptide binding (Pioletti et al., 2006). Mutagenesis and functional electrophysiological assays in Xenopus oocytes were used to understand the interactions of the complex (Wang et al., 2007). Myristoylation of some NCS proteins is also thought to be essential for protein function, localisation and for target protein interaction (Ames JB, 2011).

4.2 *C. elegans* RESULTS

4.2.1 Phenotyping the *ncs-1* (qa406) strain

To identify the functional role of *ncs-1* in *C. elegans* the phenotype of the *ncs-1* null strain was characterised further than had been done in previous studies.

4.2.1.1 Comparison of the Basic Reproductive and Alimentary Anatomy of *ncs-1* Null and Wild-type *C. elegans.*

It had been noted that there was a the difference in shape of the null worm to a wild-type and so the anatomy of the two strains were compared (De Castro, 1997). Day 1 hermaphrodite worms, when mounted on slides and viewed using the inverted microscope, showed no difference in the overall size and shape between the N2 wild-type and *ncs-1* null worms (qa404) at the head, mid-body or tail (Figure. 4.3). A comparison of the reproductive anatomy showed that the null strain had normal morphology, size, shape and development of each arm of the gonad. The null worms also showed wild-type anatomy of the digestive system including the pharynx, intestine and the anus (Figure. 4.3). A general observation was that the *ncs-1* null strain was wider at the mid-body when viewed using the stereomicroscope and freely moving on NGM agar or in Dent's solution (data not shown) this was not validated during this anatomy study.

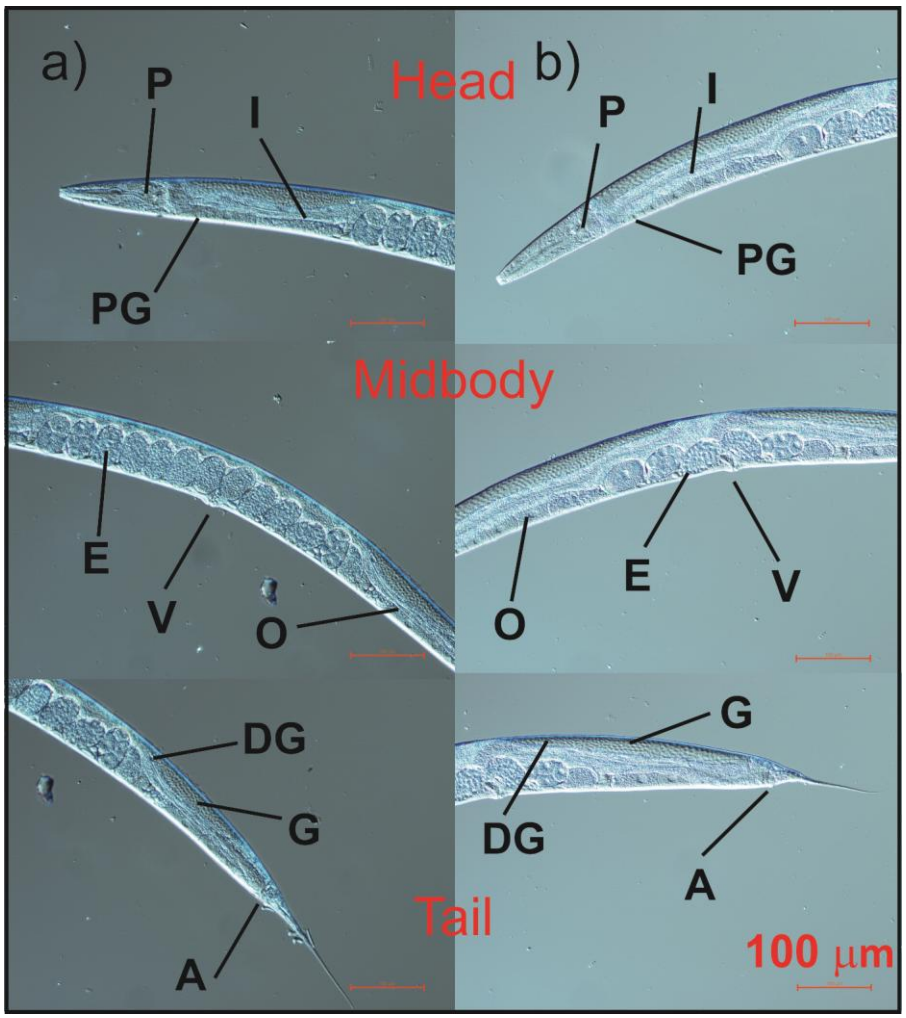

Figure 4.3 Comparison of the Basic Reproductive and Alimentary Anatomy of *ncs-1* Null and Wild-type *C. elegans.* Live imaging of (a) Wild-type and b) *ncs-1* null (qa406) strains at day one of adulthood. Reproductive anatomy: - V=Vulva, PG=Proximal gonad, DG= Distal gonad, E= Embryo O=Oocyte, G=Germline cells. Alimentary anatomy: - P=Pharynx, I=Intestine A=Anus/Rectum. Images were taken using Nikon Eclipse Ti-S inverted microscope using DIC at X200 magnification.

4.2.1.2. Comparison of the Crawling Locomotion of *ncs-1* Null and Wild-Type *C. elegans.*

NCS-1 is found in neurons and because locomotion is an indicator of neuronal function, the crawling locomotion rate of the null and wild-type strain was compared. The day 1 adult hermaphrodite *ncs-1* null strain showed no significant difference in crawling locomotion with a mean body bend rate of 17 per minute compared to that of 15 per minute for the wild-type worm (Figure 4.4).

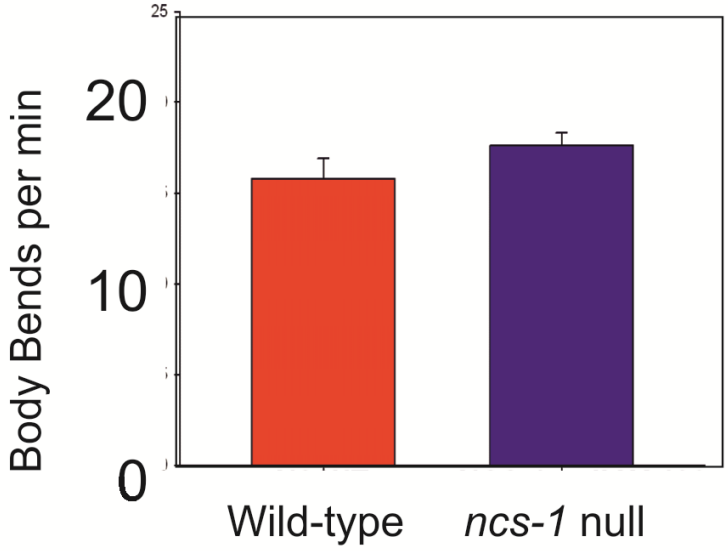

Figure 4.4 Comparison of Crawling Locomotion of *ncs-1* Null and Wild-type *C. elegans* .Crawling locomotion rate for wild-type and *ncs-1* null (qa406) worms day one adult worms was quantified by counting body bends per minute on unseeded NGM solid agar at 20^{o}C. For both strains n=20 worms. All results were expressed as means ± S.E.M.

4.2.1.3. Comparison of Cholinergic Neurotransmission of *ncs-1* Null, Wild-Type and *ric-4* Mutant Control *C. elegans.*

The rate of paralysis caused by exposure to the drug aldicarb is measured to quantify the rate of acetylcholine release at the neuromuscular junction. The day 1 adult hermaphrodite *ncs-1* null strain had a sigmoidal paralysis curve with no significant difference in rate to the N2 wild-type strain (Figure. 4.5). RIC-4 a *C. elegans* ortholog of mammalian SNARE protein snap 25 which has a role in vesicle fusion during neurotransmission (Miller et al., 1996). The *ric-4* mutant control strain show an aldicarb resistant phenotype of a delayed paralysis rate with a curve which was to the right of the wild-type and the *ncs-1* null strain (Figure. 4.5).

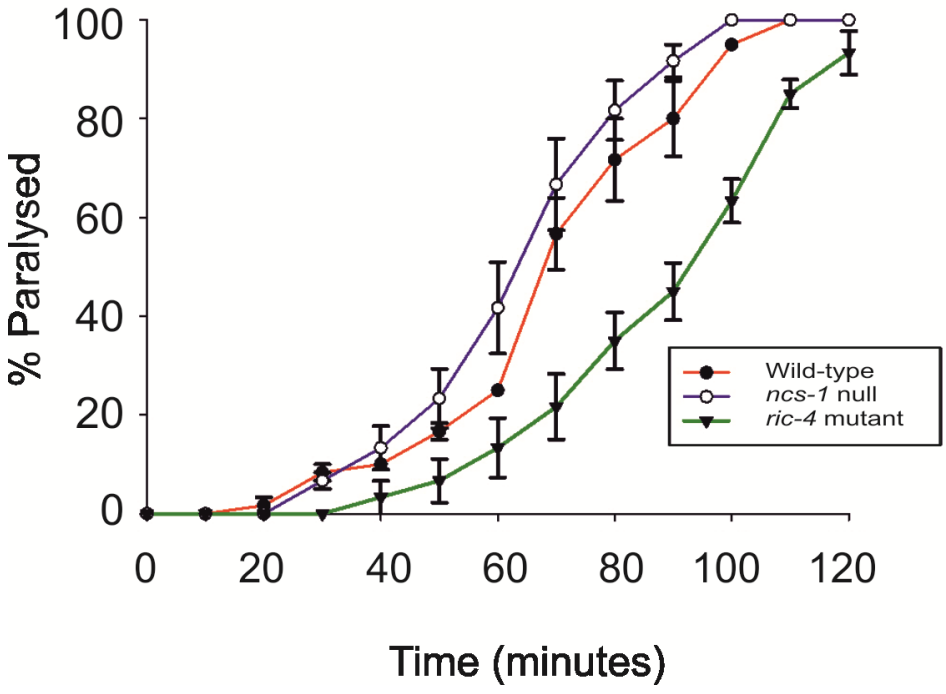

Figure 4.5 Comparison of Acetylcholine Neurotransmission of *ncs-1* Null, Wild-Type and *ric-4* Mutant Control *C. elegans.* Day one adult strains were treated with 1mM aldicarb, an acetylcholine esterase inhibitor. Onset of paralysis was measured every ten minutes by mechanical stimulation at head and tail. For all strains n=40 worms. All data were expressed as means ± S.E.M.

4.2.1.4 Comparison of Temperature-Dependent Locomotion of *ncs-1* Null and Wild-Type *C. elegans.*

NCS-1 has been previously shown to be expressed in thermosensory circuit neurons (AWC and AFD) (Gomez et al., 2001) and the AFD neuron has been shown to regulate TDL (Edwards et al., 2012). To establish whether *ncs-1* has a role in TDL, the change in locomotion of the wild-type strain between 20°C and 28°C was compared to that of the *ncs-1* null strain. At 20°C both strains had a similar coordinated locomotion rate, although the null strain was slightly slower (Figure. 4.6). After an acute rise of temperature to 28°C for 10 minutes the wild-type strain had a large and significant deceleration of locomotion. The locomotion rate of the *ncs-1* null worm at 28°C did not decrease; in contrast, it had a small but significant acceleration in locomotion rate (Figure. 4.6).

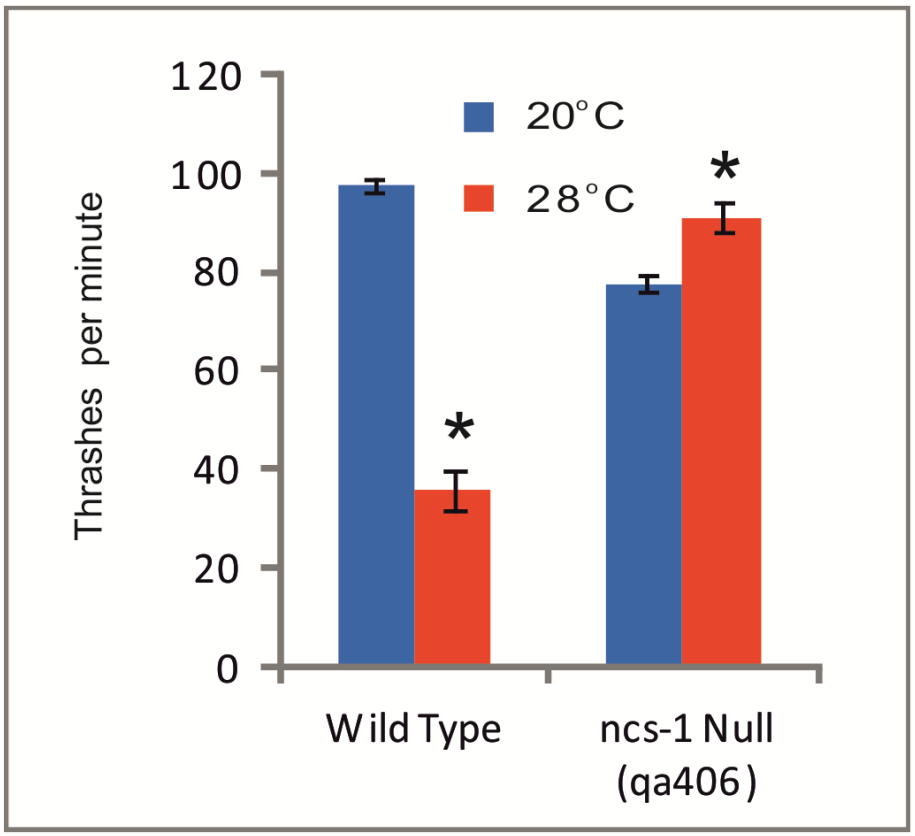

Figure 4.6 Comparison of Temperature-Dependent Locomotion of *ncs-1* Null and Wild-Type *C. elegans.* Swimming locomotion of was quantified by counting thrashes per minute of the wild-type (N2) and *ncs-1* null (qa406) animals in Dent's Buffer at 20°C and after an elevation of temperature to 28°C. For both strains n=100 worms. All data were expressed as means ± S.E.M. The statistical difference for the change in locomotion rate for each strain at 20°C and 28°C was determined using the Mann-Whitney *U* test (*=P<0.01).

4.2.2 Confirmation of Expression of Transgenic Genes by GFP Marker Expression

To validate expression of the transgenic *ncs-1* genes in the N2 and *ncs-1* null transgenic animals, expression of transgenic GFP marker genes was confirmed. All transgenic animals created in this study expressed GFP in the correct expression pattern for either pan-neuronal *rab-3a* promoter (Figure 4.7a and b) or the pan-ciliated sensory neuron *osm-6* promoter (Figure 4.7c and d)

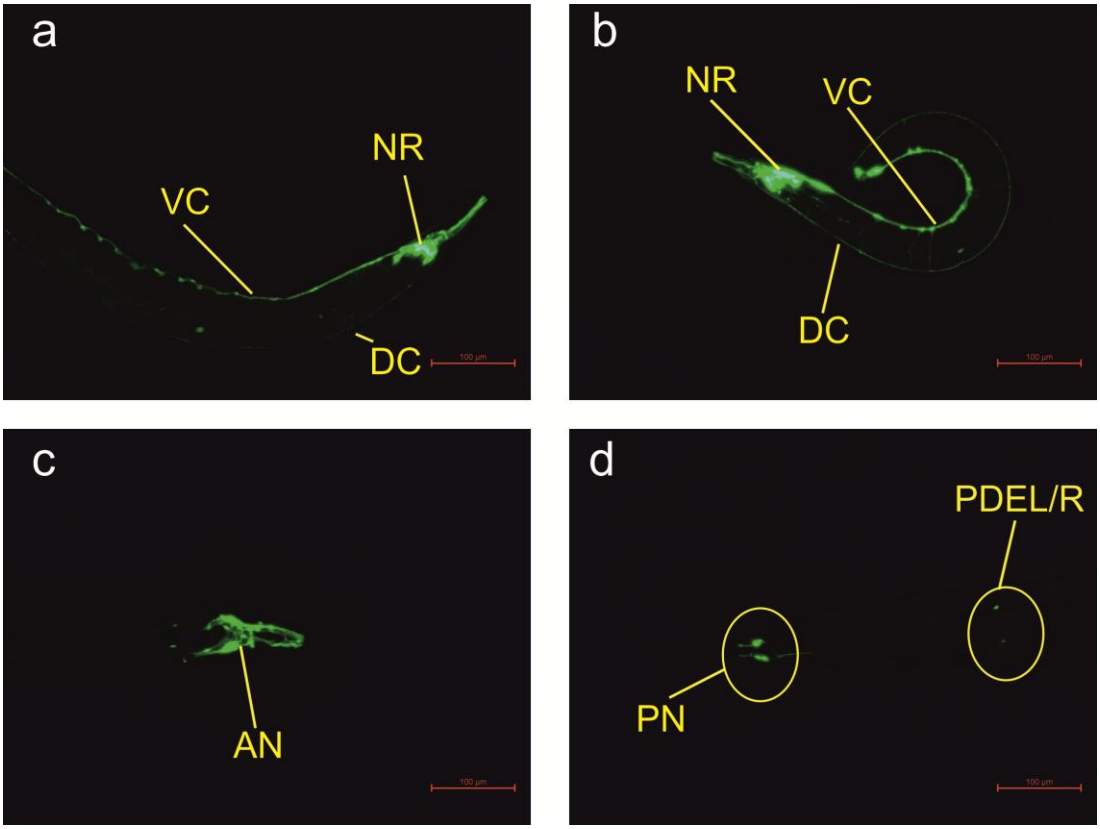

Figure 4.7 GFP Expression in NCS-1 Transgenic Animals. GFP marker gene was expressed in transgenic animals as an indicator of extra-chromosomal *ncs-1* expression. GFP expression was pan-neuronal, driven by the *rab-3a* promoter, in all neurons including NR=the nerve ring, VN=Ventral nerve cord and DN=distal nerve cord in the a) XA406 [P_{rab3a}::$_{GFP}$ $P_{ncs\text{-}1::ncs\text{-}1\ spliced}$] strain or b) XA406 [$P_{rab3a}$::$_{GFP}$ $P_{ncs\text{-}1::ncs\text{-}1}$ Δ177-191] animals. GFP was expressed in all ciliated neurons, driven by the *osm-6* promoter. It was expressed in the XA406 [$P_{osm\text{-}6}$::$_{GFP}$ $P_{ncs\text{-}1}$ Δ169-191] strain, including a) AN=amphid neurons in the head, b) PDE L/R= PDE neuron pair in mid body and PN=phasmid neurons in the tail.

Examples shown are XA406 [P_{rab3a}::$_{GFP,}$ $P_{ncs\text{-}1::ncs\text{-}1\ spliced}$] strain (Figure 4.7a) and XA406 [P_{rab3a}::$_{GFP,}$ $P_{ncs\text{-}1::ncs\text{-}1\Delta177\text{-}191}$] strain (Figure 4.7b) which both express GFP driven by the *rab3a* promoter in the nerve ring in the head of the worms, along the ventricle and dorsal nerve cords and in the tail neurons. In the XA406 [$P_{osm\text{-}6}$::$_{GFP,}$ $P_{ncs\text{-}1\ \Delta169\text{-}191]}$ strain GFP can be seen in all the ciliated sensory neurons including the amphid neurons in the head (Figure 4.7c), the PDE pair in the mid-body (Figure. 4.7d) and phasmid neurons in the tail (Figure 4.7d).

4.2.3 Temperature-Dependent Locomotion of the *ncs-1* null *C. elegans* Rescued by Transgenic Expression of Wild-Type ncs-1 Expression.

4.2.3.1 Effect of Expression of Genomic Unspliced *ncs-1* in the *ncs-1* Null Strain on Temperature-Dependent Locomotion.

To ensure that the acceleration of locomotion seen in the *ncs-1* null strain at 28°C was due to the knockout of *ncs-1* rather than other environmental or genetic factors, the null worm was transformed by injecting unspliced *ncs-1* gene which contains all the genomic uncoding regions as explained in Chapter 2 (Figure 4.8).

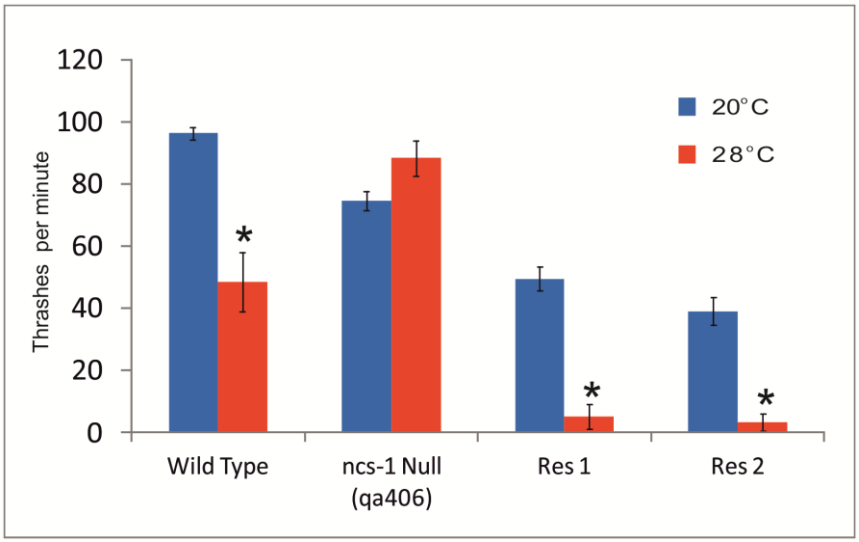

Figure 4.8 Temperature-Dependent Locomotion of the *ncs-1* null *C. elegans* Rescued by Transgenic Expression of Unspliced *ncs-1*. Two separate lines of *ncs-1* null transgenic worms expressing the genomic unspliced *ncs-1* gene under the control of its endogenous promoter (Res1 and 2) were compared to that of the N2 wild-type and *ncs-1* null (qa406). Swimming locomotion of was quantified by counting thrashes per minute of the day one adult animals in Dent's Buffer at 20°C and after an elevation of temperature to 28°C. (n=20 for all animals.) All data were expressed as means ± S.E.M. The statistical difference for the change in locomotion rate for each strain at 20°C and 28°C was determined using the Mann-Whitney *U* test (*=P<0.01).

Two transgenic rescue lines (Res 1 and Res2), each expressing identical genomic wild-type genes, whose expression was driven under its endogenous promoter showed a wild-type like rescue phenotype of deceleration of locomotion at 28^{o}C in contrast to that of the *ncs-1* null worm. (Figure 4.8).

4.2.3.2 Effect of Expression of Synthetic Spliced *ncs-1* in the *ncs-1* Null Strain on Temperature-Dependent Locomotion.

As transgenic *ncs-1* null worms were to be generated to express mutated synthetic spliced *ncs-1 genes* later in this study, the rescue was repeated in the *ncs-1* null worm but this time expressing the spliced synthetic wild-type *ncs-1* gene driven by its endogenous promoter. Again three separate lines expressing the transgenic gene were assayed for TDL and all three were shown to also have a wild-type rescue phenotype of a decrease of locomotion at 28^{o}C (Figure. 4.9a).

From the same assay, data for the multiple lines of the transgenic spliced rescue strains were pooled and all the data normalised to the mean of the N2 at 20^{o}C. The transgenic animal still showed a rescue of a deceleration of locomotion at 28^{o}C (Figure. 4.9b). All data shown in subsequent figures was normalised in the same manner and data from transgenic lines expressing the same genetic constructs were pooled, unless otherwise stated.

a)

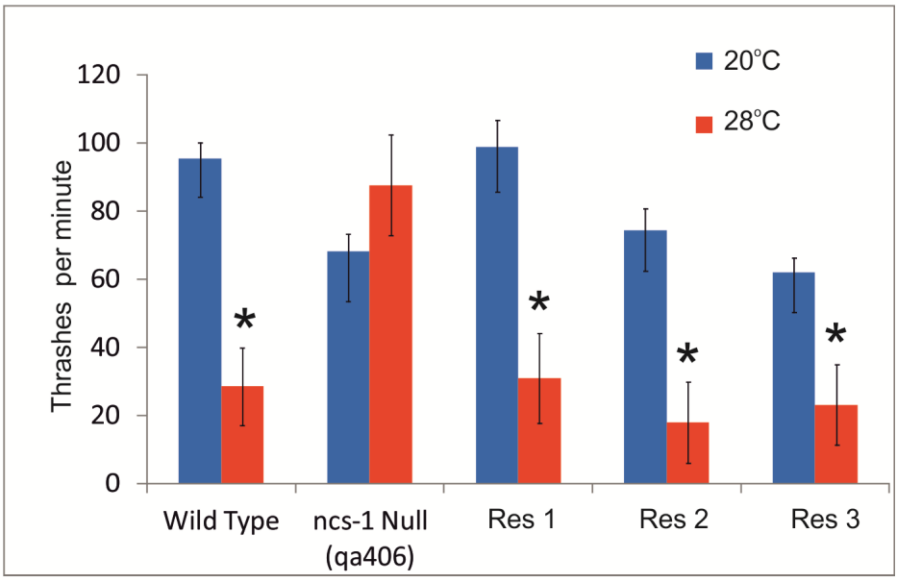

b)

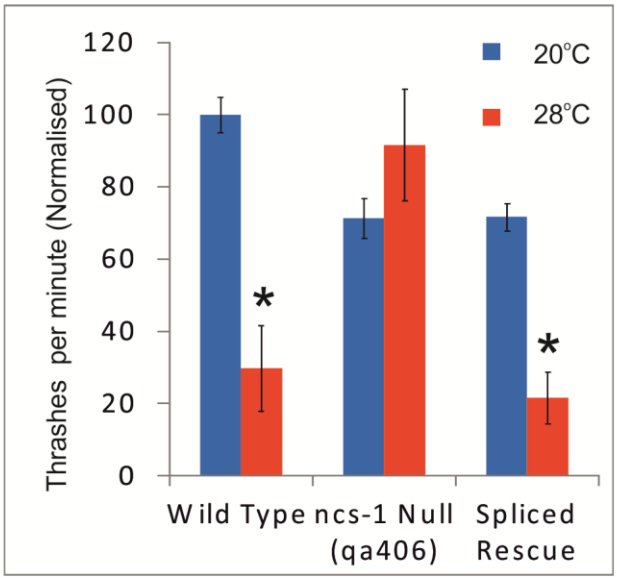

Figure 4.9 Temperature-Dependent Locomotion of the *ncs-1* Null *C. elegans* Rescued by Transgenic Expression of Spliced *ncs-1.* Swimming locomotion of was quantified by counting thrashes per minute of the day one adult animals in Dent's Buffer at 20°C and after an elevation of temperature to 28°C. (For all strains n=20 worms) a) Three separate lines of *ncs-1* null transgenic worms expressing the synthetic spliced *ncs-1* gene under the control of its endogenous promoter (Res1-3) were compared to that of the N2 wild-type and *ncs-1* null (qa406). b) The data from the separate worm line (a) Res1-3 were pooled. The data for all strains at 20°C and 28°C were normalised to the mean locomotion rate of the N2 wild-type at 20°C. All data were expressed as means ± S.E.M. The statistical difference for the change in locomotion rate for each strain at 20°C and 28°C was determined using the Mann-Whitney *U* test (*=P<0.01).

4.2.4 Anti-Human NCS-1 Antibodies in Detection of Recombinant *C. elegans* NCS-1

The monoclonal antibody used to probe the blot did not detect recombinant *C. elegans* NCS-1 protein band (Figure. 4.10a), in contrast, the polyclonal antibody did detect the band on an identical membrane (Figure. 4.10b). The polyclonal antibody was successful in detecting bands of serial dilutions of the recombinant *C. elegans* NCS-1 protein, (a gift from Dr Lee Haynes, University of Liverpool) up to a 1/10K dilution, although, the bands for *C. elegans* NCS-1 were less intense than for mammalian NCS-1 protein of an equivalent concentration (Figure. 4.10c).

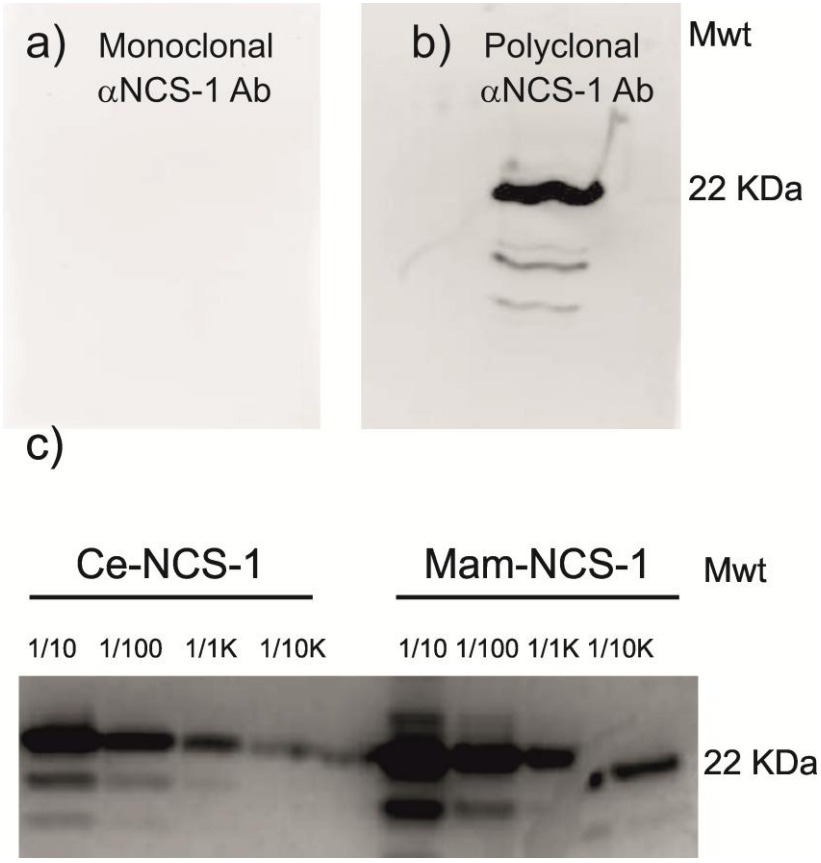

Figure 4.10 Recombinant NCS-1 protein detection by Western Blotting A comparison of NCS-1 antibodies in detecting recombinant Ce-NCS-1 protein using a) monoclonal anti-human NCS-1 antibodies or b) polyclonal anti-human NCS-1 antibodies and probed by Western blotting. c) A comparison of polyclonal anti-human NCS-1 antibody detection of recombinant Ce-NCS-1 against recombinant mammalian NCS-1 protein. Recombinant mammalian and *C. elegans* NCS-1 protein of the same concentrations were diluted in magnitudes of 10 and probed by Western blotting.

4.2.5 Effect of Expression of Unspliced *ncs-1* in the Wild-Type and *ncs-1* Null Strain on Temperature-Dependent Locomotion.

The effect of over-expression of *ncs-1* in a wild-type background was compared to the *ncs-1* null rescue. Over-expression of unspliced wild-type *ncs-1* in both the wild-type and *ncs-1* null worms decreased the locomotion rates at 20°C compared to the control N2 wild-type and *ncs-1* null (qa406) controls respectively (Figure. 4.11). Despite this, both types of transgenic animals displayed the wild-type TDL phenotype of deceleration of locomotion at 28°C compared to that of the null animal at 20°C.

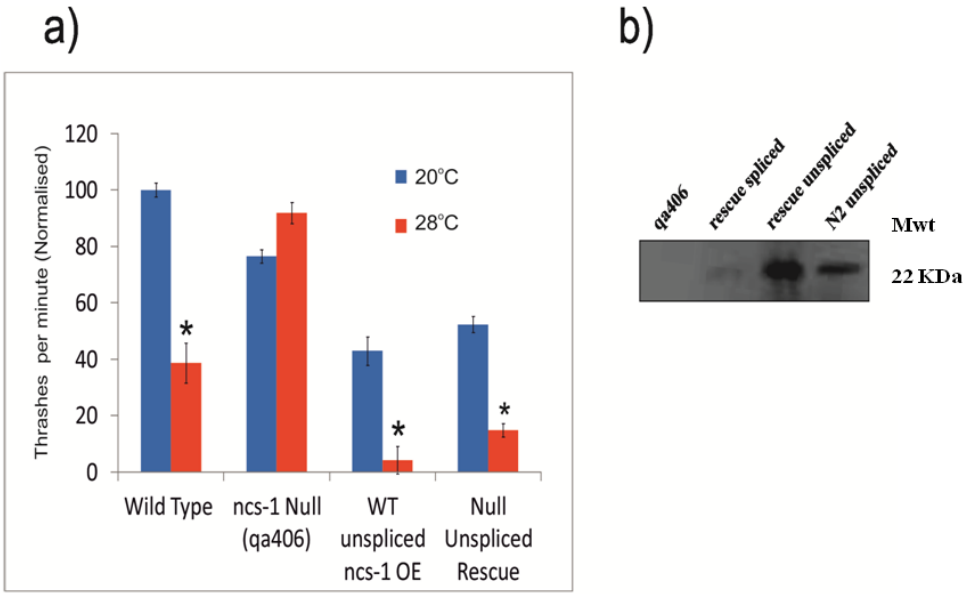

Figure 4.11 Temperature-Dependent Locomotion of the *ncs-1* null *C. elegans* Rescue *and N2 ncs-1* Over Expression and Western Blot. a) Temperature-dependent locomotion rates of *ncs-1* null and N2 wild-type worms expressing transgenic unspliced *ncs-1* under its own promoter were compared to the N2 wild-type and *ncs-1* null controls. Swimming locomotion of was quantified by counting thrashes per minute of the day one adult animals in Dent's Buffer at 20°C and after an elevation of temperature to 28°C. (For N2 and *ncs-1* null n=35 worms, for N2 *ncs-1* over expression n=40 worms and *ncs-1* rescue n=45 worms). For transgenic animals the data from three separate lines were pooled. The data for all strains at 20°C and 28°C were normalised to the mean locomotion rate of the N2 wild-type at 20°C. All data were expressed as means ± S.E.M. The statistical difference for the change in locomotion rate for each strain at 20°C and 28°C was determined using the Mann-Whitney *U* test, with the use of the Bonferonni correction for multiple comparisons (*=P<0.01). b) Western blot of *ncs-1* null, transgenic animals N2 wild-type over expressing unspliced *ncs-1*and *ncs-1* null expressing spliced or unspliced *ncs-1* all under the expression of the *ncs-1* promoter. The blot was probed using polyclonal anti-human NCS-1 antibodies.

4.2.6. Effect of Expression of *ncs-1* mutants in the *ncs-1* Null Strain

4.2.6.1 Effect of Non-Myristoylated *ncs-1* on Temperature-Dependent Locomotion

As the myristoylation of NCS proteins has been shown to be important for localisation, the function of non-myristoylated mutant was investigated by expression of *ncs-1* G2A under the control of its endogenous promoter in the *ncs-1* null worm. These also showed a wild-type rescue TDL phenotype with a decrease of locomotion at 20°C (Figure 4.12).

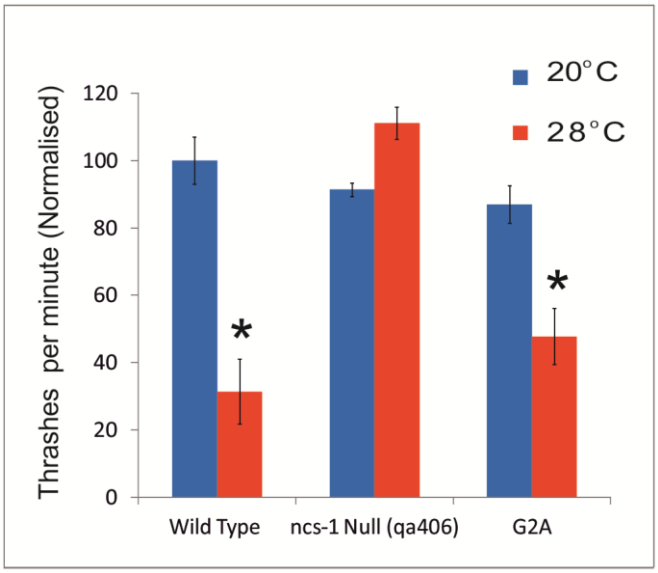

Figure 4.12 Temperature-Dependent Locomotion of the *ncs-1* Null Expressing the Non-Myristolated *ncs-1* Mutant. Temperature-dependent locomotion rate of transgenic *ncs-1* null (qa406) worm expressing non-myristolated *ncs-1* G2A mutant under its own promoter was compare to that of to the N2 wild-type and *ncs-1* null controls. Swimming locomotion of was quantified by counting thrashes per minute of the day one adult animals in Dent's Buffer at 20°C and after an elevation of temperature to 28°C. (For N2 and qa406 n=10 worms, for G2A n=30 worms and *ncs-1* rescue n=45 worms). For transgenic animal the data from three separate lines were pooled. The data for all strains at 20°C and 28°C were normalised to the mean locomotion rate of the N2 wild-type at 20°C. All data were expressed as means ± S.E.M. The statistical difference for the change in locomotion rate for each strain at 20°C and 28°C was determined using the Mann-Whitney *U* test, with the use of the Bonferonni correction for multiple comparisons (*=P<0.01).

4.2.6.2 Effect of N- and C-Terminal Binding Cleft Mutations in the Binding Pocket of *ncs-1* on Temperature-dependent Locomotion

Two N- and two C-terminal binding cleft residues of the hydrophobic pocket of *C. elegans* NCS-1 were mutated in this study. These residues have been implicated in direct target peptide interactions in structural studies in NCS-1 orthologues Frq-1 and Ncs-1 (Figure. 4.12a) (Lim et al., 2011, Strahl et al., 2007). The N-terminal binding cleft residue W30 has also been shown to be involved in binding to the NCS protein recoverin and while L89 has also been implicated both recoverin and KChiP1 binding (Pioletti et al., 2006, Wang et al., 2007). While the C-terminal binding cleft residue W103 has been implicated in KChiP1 binding and V125 residue was not implicated in recoverin or KChiP1 target peptide interactions as discussed in section 4.1. These residues are fully conserved across human NCS-1, *C. elegans* NCS-1 and *S. cerevisiae* Frq1 (Figure. 4.13a). The predicted structures of *C. elegans* NCS-1 protein based on solution NMR structure shows the C-terminal tail fills the C-terminal binding cleft (Figure. 4.13c). In contrast the X-ray crystallography structure shows an open hydrophobic pocket due to bound polyethylene glycols (Figure. 4.13b).

The N-terminal binding cleft mutant W30A showed significant wild-type rescue of TDL (Figure. 4.13a). The single N-terminal binding cleft mutation L89A failed to rescue (Figure. 4.13a), even though this mutant protein was shown to be expressed in the transgenic animals by Western blot analysis (Figure. 4.14b). Worms expressing the W30A/W103A double tryptophan mutations in both the N- terminal and C-terminal binding clefts also appeared to fail to rescue (Figure. 4.14a). The locomotion of the L89A and W30A/W103A transgenic animals at 20^{o}C was reduced to that of 40% the N2 wild-type worm but a similar decrease in locomotion rate at 20^{o}C in wild-type and ncs-*1* null transgenic strains expressing wild-type *ncs-1* was previously seen and did not mask the reduction in locomotion due to the temperature elevation (Figure. 4.11a). The double mutation W30A/L69A has a locomotion rate 20% of that of the wild-type strain and potential rescue in this strain could not be determined (Figure 4.14a).

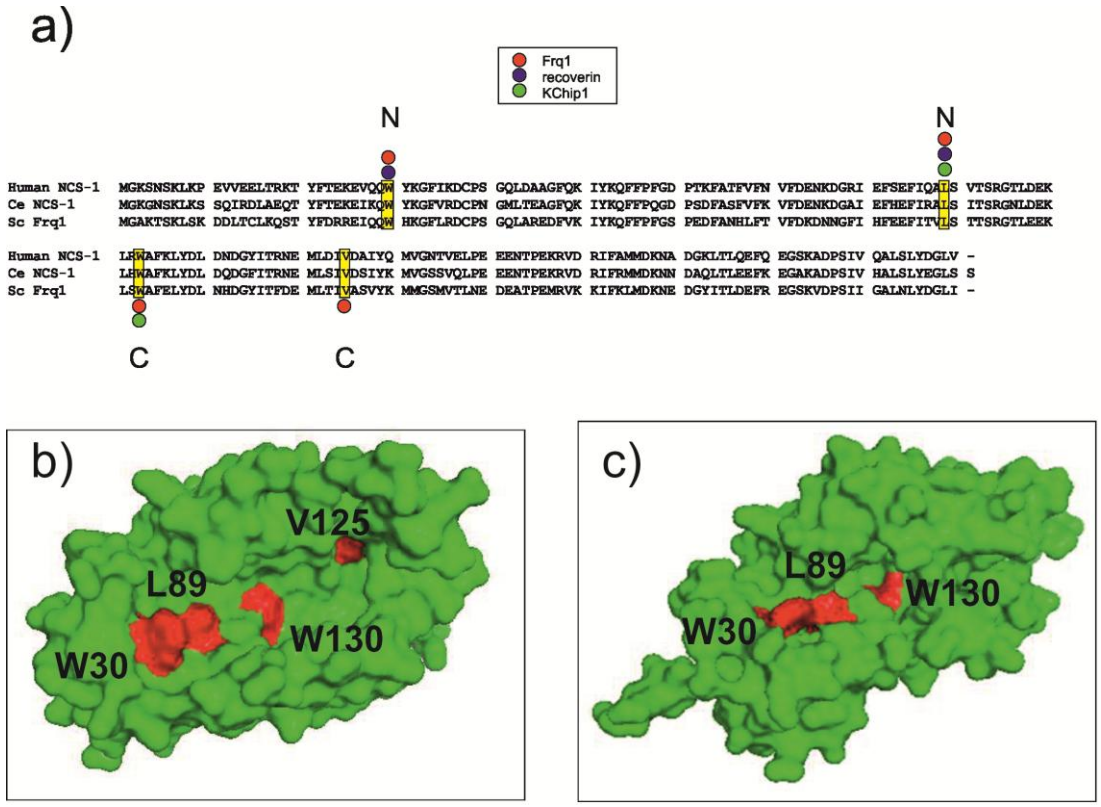

Figure 4.13 Comparison of NCS-1 orthologues and identification of N and C-terminal residues for targeted mutation. a) Alignment of human, *C elegans* and *S. cerevisiae* NCS-1 sequences. Conserved N- and C-terminal binding residues W30, L89, W103 and V125, highlighted in yellow were selected for mutation. Residues shown to interact target peptide in NCS complex structural studies are implicated by red circle=Frq1, green circle=KChiP1 or blue circle=recovern. Predicted *C. elegans* structures acquired using Swiss Model Software. Mutated residues shown in red b) Structure based on the human crystal structure (PDB 1G8I) showing that the hydrophobic groove is open. c) Structure based on the human NCS-1 NMR structure (PBD 2LCP). Residue V125 is inaccessible due to the C-terminal tail residues 177-191 occupying the C-terminal binding cleft of the hydrophobic pocket.

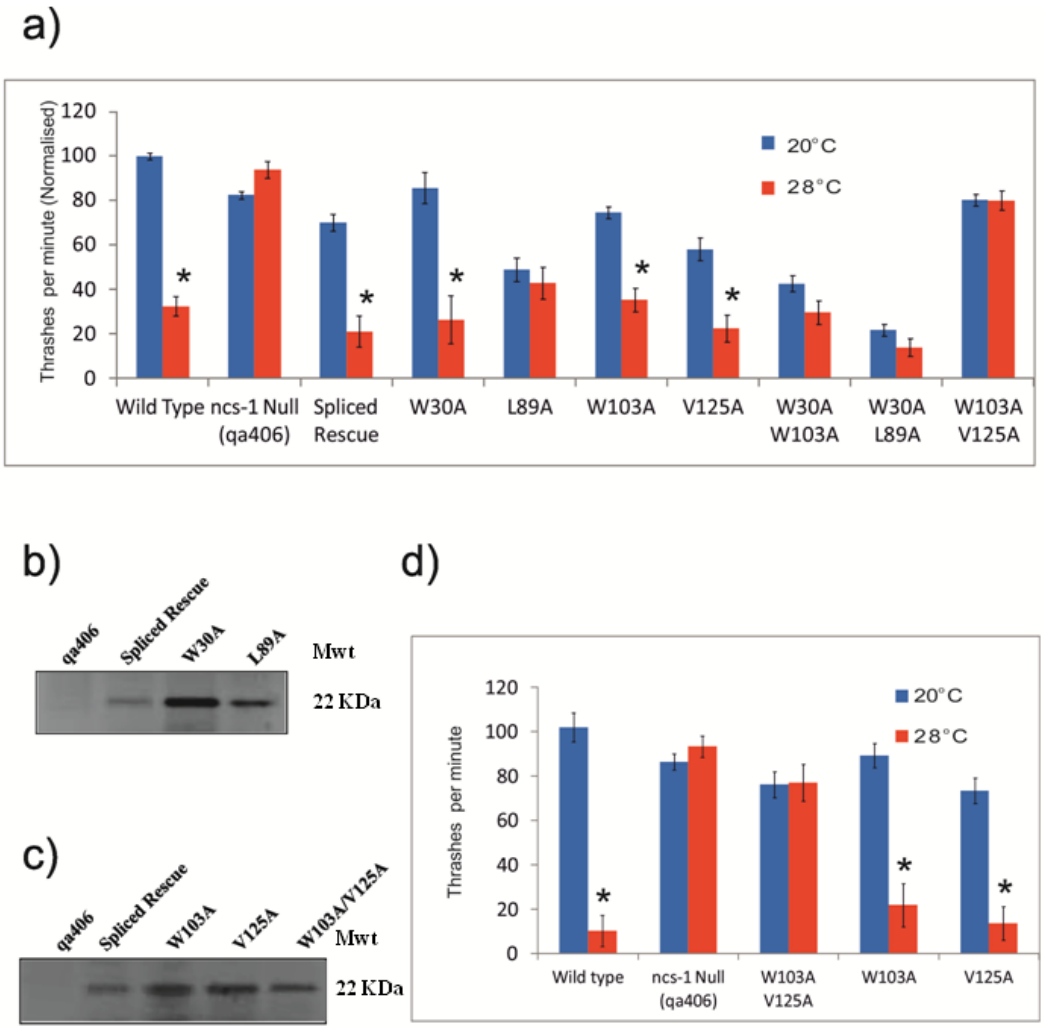

Figure 4.14 Temperature-dependent Locomotion and Western Blots of Transgenic *ncs-1* Null Animals, Expressing Mutant *ncs-1* Single and Double Binding Cleft Mutations in the Hydrophobic Pocket a) Temperature-dependent locomotion rate of transgenic *ncs-1* null worm expressing wild-type or mutant spliced *ncs-1* under its own promoter were determined and all were compared to that of to the N2 wild-type and *ncs-1* null (qa406) controls. Swimming locomotion was quantified by counting thrashes per minute of the day one adult animals in Dent's Buffer at 20°C and after an elevation of temperature to 28°C. (n=28-84 worms). For transgenic animal the data from three separate lines were pooled. The data for all strains at 20°C and 28°C were normalised to the mean locomotion rate of the N2 wild-type at 20°C. All data were expressed as means ± S.E.M. The statistical difference for the change in locomotion rate for each strain at 20°C and 28°C was determined using the Mann-Whitney *U* test, with the use of the Bonferonni correction for multiple comparisons (*=P<0.01). Western blot analysis of *ncs-1* null (qa406) transgenic worms with expressing either wild-type *ncs-1* or *ncs-1* with b) single N terminal binding cleft mutations or c) single or double C-terminal binding cleft mutations, all driven by the *ncs-1* promoter. The blot was probed using polyclonal anti-human NCS-1 antibodies. d) Temperature-dependent locomotion of transgenic *ncs-1* null worms expressing *ncs-1* with single and double mutations of the C terminal binding cleft of the hydrophobic pocket. Swimming locomotion of was quantified by counting thrashes per minute of the animals in Dent's Buffer at 20°C and after an elevation of temperature to 28°C. (For all strains n=15 worms). For transgenic animal the data from three separate lines were pooled. The data was not normalised but shown as raw data as all strains were assayed together on the same days. All data were expressed as means ± S.E.M. The statistical difference for the change in locomotion rate for each strain at 20°C and 28°C was determined using the Mann-Whitney *U* test, with the use of the Bonferonni correction for multiple comparisons (*=P<0.01).

The double C-terminal binding cleft *ncs-1* mutation W103A/V125A did not show a decline in locomotion while also found to be expressed in the worm (Figure. 4.14c). Interestingly, the C-terminal binding cleft single mutants W103A and V125A did show a wild-type rescue TDL phenotype. Similar results were obtained when direct comparison of TDL the single and double C-terminal binding cleft assayed together, at the same time, verifying the single mutations rescued the phenotype in the *ncs-1* null background while the double C- terminal binding cleft mutation did not rescue (Figure. 4.14d).

4.2.6.3 Effect C-Terminal Tail Truncations of NCS-1 Protein on Temperature-dependent Locomotionin *C. elegans*

A series of truncated *C. elegans* NCS-1 proteins were expressed the *ncs-1* null worm to establish the role of the C-terminus in NCS-1 function. The NCS-1 Δ177-191 truncated protein contained a deletion of 14 amino acids of C-terminal loop up to the final α helix in the protein, which according to the predicted model, would have exposed part of the C-terminal binding cleft (Figure. 4.15a), including V125 residue, shown earlier to be involved in C-terminal binding cleft function. The two larger truncations Δ174-191 and Δ169-191 contained deletions of 17 and 24 amino acids, respectively, and not only contained a deletion of the C terminal loop but also 3 or 10 amino acid residues from the proceeding α helix loop.

Expression of *ncs-1* Δ177-191 and Δ174-191 under the control of its endogenous promoter in the *ncs-1* null worm also showed a significant wild-type rescue TDL phenotype of a decrease of locomotion at 20^{o}C (Figure 4.15b). Expression of *ncs-1* Δ169-191 not only rescued the wild-type phenotype but also showed a gain of function as locomotion at the elevated temperature was more reduced than in the wild-type worms (Figure 4.15b).

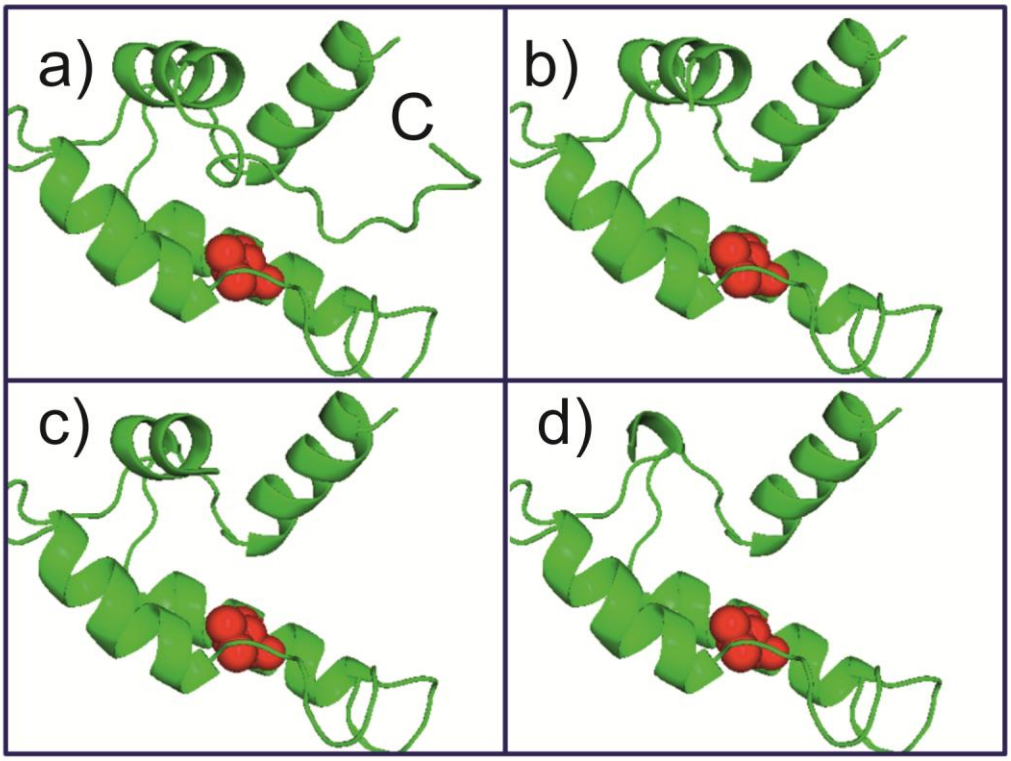

e)

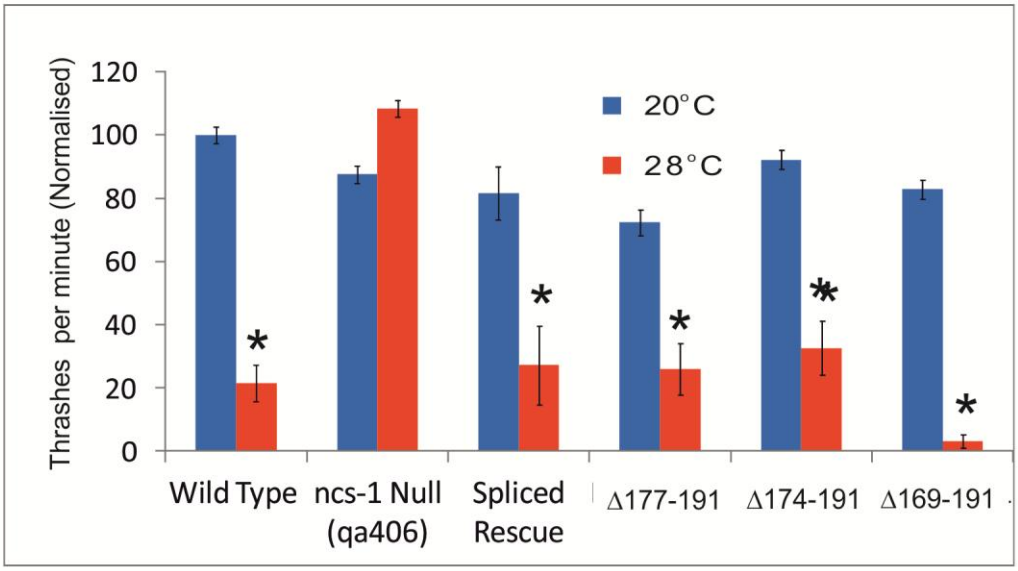

Figure 4.16 Temperature-dependent Locomotion and Western Blots of Transgenic *ncs-1* Null Animals Expressing Mutant *ncs-1* with Deletions of its C-terminal Tail. (Full legend overleaf)

Figure 4.16 Temperature-dependent Locomotion and Western Blots of Transgenic *ncs-1* Null Animals Expressing Mutant *ncs-1* with Deletions of its C-terminal Tail. (Figure on previous page) a-d) Model prediction of *C. elegans* NCS-1 protein structure (residues 95-189), using the human NCS-1 structure which was derived using solution NMR (PBD 2LCP). The models show the NCS-1 wild-type and C-terminal deletions used for transgenic expression in this study. a) The wild-type figure shows NCS-1 C-terminal binding cleft of the hydrophobic pocket occupied by the C-terminal tail and is in close proximity to V125 shown in red. b-d) The amount of C-terminal tail occupying the C-terminal binding cleft is reduced as the length of the tail is reduced sequentially in *ncs-1* b) Δ-177-191, c) Δ-174-191 and d) Δ-169-191 mutants. e) Temperature-dependent locomotion rate of transgenic *ncs-1* null worm expressing spliced wild-type or C-terminal truncations of *ncs-1* under its own and all were compared to that of to the N2 wild-type and *ncs-1* null (qa406) controls. Swimming locomotion of was quantified by counting thrashes per minute of the day one adult animals in Dent's Buffer at 20^{o}C and after an elevation of temperature to 28^{o}C. (n=15-30 worms). For transgenic animal the data from three separate lines were pooled. The data for all strains at 20^{o}C and 28^{o}C were normalised to the mean locomotion rate of the N2 wild-type at 20^{o}C. All data were expressed as means ± S.E.M. The statistical difference for the change in locomotion rate for each strain at 20^{o}C and 28^{o}C was determined using the Mann-Whitney *U* test, with the use of the Bonferonni correction for multiple comparisons (*=P<0.01).

4.2.7 Effect *ncs-1* expression in Sensory and AIY Neurons on Temperature-dependent Locomotion

NCS-1 has been shown to be expressed in three types of thermosensory circuit neurons, the AFD, AWC and AIY neuronal pairs (Figure 4.16a). To establish in which neurons NCS-1 protein is regulating the temperature-dependent locomotion unspliced wild-type *ncs-1* was expressed in the *ncs-1* null strain driven by three promoters. It was driven under its endogenous promoter and as seen previously (Figure 4.11), this strain displayed a ~40% lower locomotion rate than the N2 wild-type strain at 20^{o}C but still showed a wild-type rescue of a decrease of locomotion at 28^{o}C. Expression of wild-type *ncs-1* driven by the *osm-6* promoter would express the protein in all ciliated sensory neurons including the AFD and AWC neurons and in a third thermosensory neuron, ASI, not shown to express *ncs-1* endogenously (Figure 4.16a). This strain showed no rescue of the wild-type TDL phenotype in the null background at 28^{o}C even though the protein was shown to be expressed in the transgenic strain (Figure 4.16c). In contrast, expression of the wild-type protein in the pair of AIY interneurons did rescue the wild-type TDL phenotype with a significant decrease in locomotion at the elevated temperature.

Interesting, over expression of the unspliced wild-type NCS-1 protein by the *osm-6* or the AIY neuron promoter did not cause a reduction in locomotion at 20^{o}C (Figure 4.14b) which was seen previously in the over expression driven by the endogenous promoter (Figure 4.11a).

The *ttx-3* null *C. elegans* strain (*ot22*) contains genetically ablated AIY neurons as the transcription factor TTX-3 is essential in the maturation of functioning AIY neurons (Hobert et al., 1997). The AIY ablated strain showed a gain of function of TDL at 28^{o}C, as it was affected more severely than the wild-strain, with a complete inhibition of locomotion contrary to the increase in locomotion of the *ncs-1* null strain (Figure 4.16d).

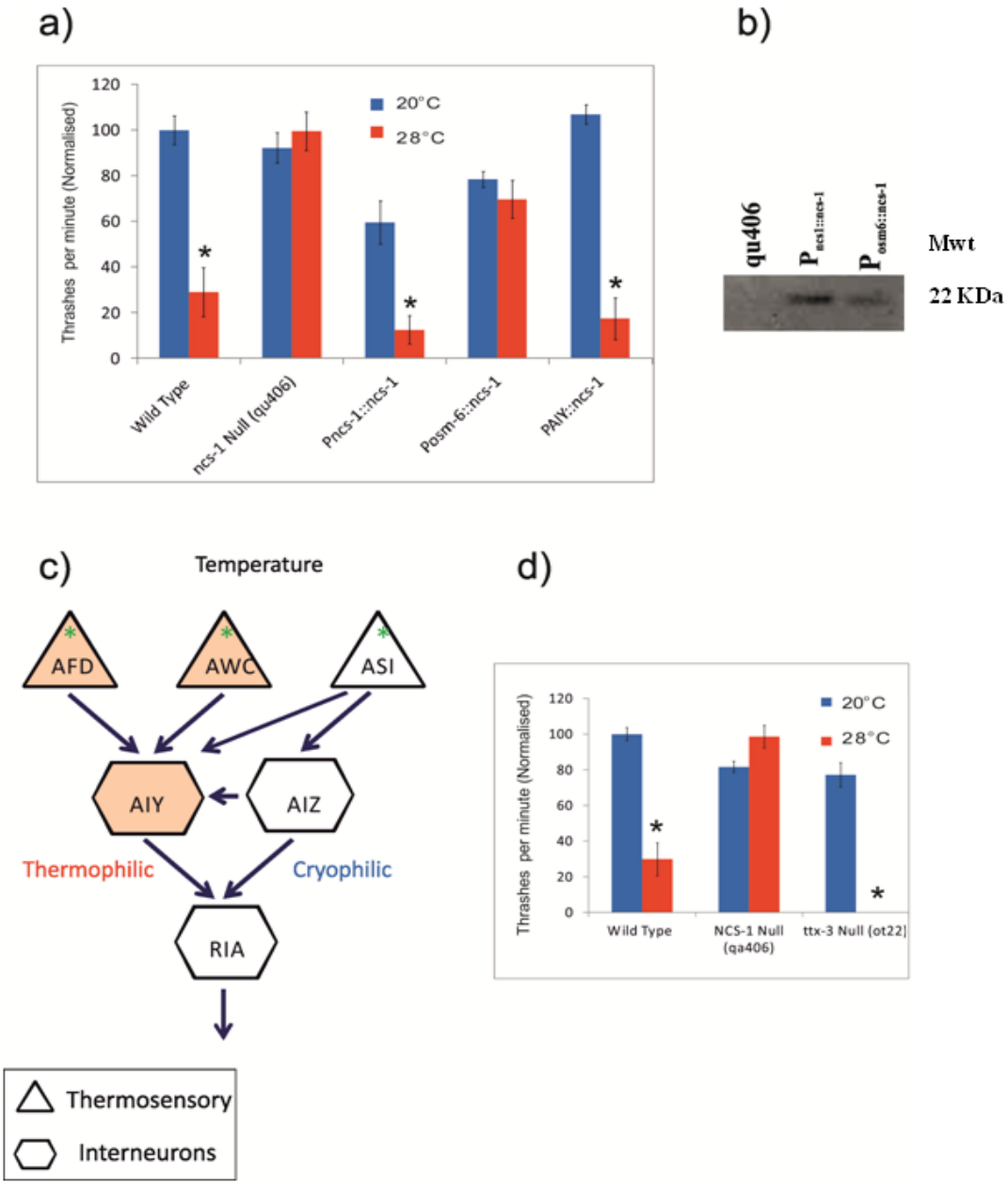

Figure 4.16 Identification of Neurons In Which the Temperature-dependent Locomotion Function of NCS-1 Occurs.(Full legend overleaf)

Figure 4.16 Identification of Neurons In Which the Temperature-dependent Locomotion Function of NCS-1 Occurs. (Figure on previous page) a) Temperature-dependent locomotion rate of transgenic *ncs-1* null worm expressing unspliced *ncs-1* under its own promoter for endogenous expression, under the osm-6 promoter for expression in all ciliated sensory neurons and under the AIY specific promoter for expression in the left and right AIY neurons and all were compared to that of to the N2 wild-type and *ncs-1* null (qa406) controls. Swimming locomotion of was quantified by counting thrashes per minute of the day one adult animals in Dent's Buffer at 20^{o}C and after an elevation of temperature to 28^{o}C. (For all animals, n=15 worms except PAIY where n=45 worms) For transgenic animal the data from three separate lines were pooled. The data for all strains at 20^{o}C and 28^{o}C were normalised to the mean locomotion rate of the N2 wild-type at 20^{o}C. All data were expressed as means ± S.E.M. The statistical difference for the change in locomotion rate for each strain at 20^{o}C and 28^{o}C was determined using the Mann-Whitney *U* test, with the use of the Bonferonni correction for multiple comparisons (*=P<0.01). b) Western blot of *ncs-1* null, transgenic animals expressing unspliced *ncs-1* all under the expression of the *ncs-1* promoter and the *osm-6* promoter. The blot was probed using polyclonal anti-human NCS-1 antibodies c) Diagram of the thermosensory neuronal network which are involved in thermotaxis adapted from Nishida *et al*, 2011 (Nishida et al., 2011) with additional neurons added to this pathway(Beverly et al., 2011).The neurons shaded in pink have been show to express NCS-1 (Gomez et al., 2001). The asterisk indicates the ciliated thermosensory neurons in this pathways in which genes can be expressed driven by the osm-6 promoter. d) Temperature-dependent locomotion rate of the AIY neuron ablated *ttx-3* null strain (ott22) and was compared to N2 wild-type and *ncs-1* null (qa406) controls. Swimming locomotion of was quantified by counting thrashes per minute of the day one adult animals in Dent's Buffer at 20^{o}C and after an elevation of temperature to 28^{o}C. (For all animals n=20 worms). The data for all strains at 20^{o}C and 28^{o}C were normalised to the mean locomotion rate of the N2 wild-type at 20^{o}C. All data were then expressed as means ± S.E.M. The statistical difference for the change in locomotion rate for each strain at 20^{o}C and 28^{o}C was determined using the Mann-Whitney *U* test, with the use of the Bonferonni correction for multiple comparisons (*=P<0.01).

4.2.8 Effect of Knockdown of PIFK-1 on temperature-dependent locomotion

In order to begin to indentify the potential target for NCS-1 in the regulation of the TDL behaviour worm orthologues of known mammalian interacting proteins were investigated. One of these (pifk-1) is the worm orthologue of PI4kIIIβ. The *pifk-1* null strain (tm2348) showed a TDL phenotype (Figure 4.17). There was a significant decrease in locomotion at 28°C, unlike the *ncs-1* null strain but the reduction in the rate of locomotion was not as severe as with the wild-type worms. The locomotion rate at 28°C of the *pifk-1* null strain was 73% of the locomotion rate at 20°C but the wild-type locomotion rate at 28°C was reduced to only 7%.

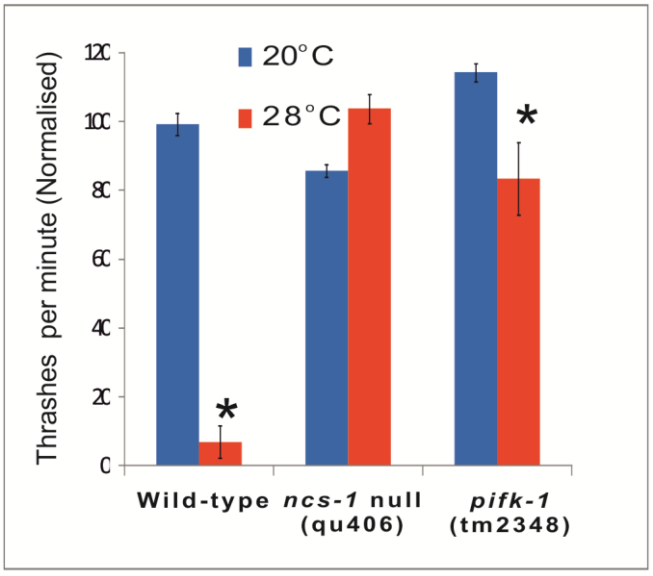

Figure 4.17 Temperature-dependent Locomotion of *pifk-1* null *C. elegans* Temperature-dependent locomotion rate of *ncs-1* null worms (tm2348) was compared to that of to the N2 wild-type and *ncs-1* null controls. Swimming locomotion was quantified by counting thrashes per minute of the day one adult animals in Dent's Buffer at 20°C and after an elevation of temperature to 28°C. (For N2 and qa406 n=10 worms, for G2A n=30 worms and *ncs-1* rescue n=45 worms). The data for all strains at 20°C and 28°C were normalised to the mean locomotion rate of the N2 wild-type at 20°C. All data were expressed as means ± S.E.M. The statistical difference for the change in locomotion rate for each strain at 20°C and 28°C was determined using the Mann-Whitney *U* test, with the use of the Bonferonni correction for multiple comparisons (*=P<0.01).

4.3 DISCUSSION

The *C. elegans ncs-1* null worm was found to be a good model for investigation of structure/function relationships of NCS-1 using the TDL assay. The key residues in the hydrophobic pocket, identified in structural studies, were shown to be important for the function of NCS-1 in the regulation of temperature-dependent locomotion in the single pair of AIY interneurons in the *C. elegans* model. The C-terminal tail domain and myristoylation of NCS-1 were shown not to be involved functionally (or at last to be essential) in regulation of temperature-dependent locomotion in this study.

NCS-1 has been shown to be essential in the regulation of temperature-dependent locomotion in *C. elegans*. The *ncs-1* null mutant (qa406) was shown to be defective in this behaviour, displaying a novel phenotype of an acceleration of locomotion rate after acute exposure to high temperature. This has not been seen previously. Phenotypes seen previously are a reduction in locomotion rate of to ~40% in the wild-type at 28^{o}C compared to that at 20^{o}C. DAG signalling pathway mutants showed other defective phenotypes, with locomotion rates of between 0-100% at 28^{o}C when compared to the rate at 20^{o}C (Edwards et al., 2012). The increase in locomotion behaviour at 28^{o}C was confirmed to be caused by the absence of NCS-1 expression in the null worm after expression of wild-type NCS-1 protein, under its own promoter, using an extra-chromosomal rescued this behaviour giving a significant slowing of locomotion at the higher temperature.

The physiological relevance of four residues in the N- and C- terminal clefts of hydrophobic pocket of NCS-1, were tested using the TDL assay. The hydrophobic residues were mutated to alanine as done previously in a NCS structure/function studies of hydrophobic resides and shown to effect the properties of the hydrophobic pocket and function (Wang et al., 2007). The L89 residue situated in the N-terminal binding cleft was shown to be important for the function of NCS-1 in the regulation of TDL. In the NCS structural studies this residue has been shown to be involved in complex formation with target peptides i*n vitro* (Ames et al., 2006, Pioletti et al., 2006, Lim et al., 2011, Strahl et al., 2007).

The residue W30, also situated in the N-terminal binding cleft, has also been implicated to be important in complex formation in structural studies. This investigation could not identify if this residue was functionally significant in TDL regulation. Its function may have been masked in the W30A/L89A double mutation N-terminal binding cleft mutations due to an extensively reduced locomotion rate at 20^{o}C. This reduction may have been cause by toxic effects of the mutated protein possible due to aggregation or off target signalling but this was not investigated during this project.

It appears the whole C-terminal binding cleft must be involved in target interaction because mutations of the individual residues W103 and V125 are not sufficient to prevent rescue of TDL regulation by NCS-1 but when mutations of both residues are introduced into the protein it failed to rescue. Residue V125 has been implicated in Pik1 peptide complex formation in the Frq1 and Ncs-1 complex (Ames et al., 2006). This residue was not shown to be involved in KChiP1 and recoverin target complex structures as the C-terminal tails of these proteins makes the valine residue inaccessible to the target peptides for interaction (Strahl et al., 2007, Ames et al., 2006). Biochemical and structural studies of these binding cleft mutations could be used to validate and further investigate the functions of these binding cleft resides. Cellular studies could be used to investigate further the functions of these residues in mammalian systems.

In NCS-1 the C-terminal tail has been shown to occupy the C-terminal part of the hydrophobic pocket and on binding to target peptide the tail has been shown to move, fully exposing the binding groove, including the W103 and V125 residues (Strahl et al., 2007, Heidarsson et al., 2012). This suggests that the C-terminal tail is not required for target peptide binding modulation and supports the functional data found in this study where truncations of the C-terminal tail did not have a negative effect on NCS-1 function. In human NCS-1, a point mutation of R102Q, has been implicated to have a role in Autism (Piton et al., 2008). This residue is next to W103 and structural studies have shown that in the wild-type protein, R102

interacts with the C-terminal tail in a stable form. The Autism R102Q mutant protein has structural changes, leading to the 169-190 residues of the C-terminal tail being more dynamic and the protein having an increased affinity to target protein. To test the function of the R102 residue it may be possible to use the worm. Previous studies have shown it is possible to express human orthologues of *C. elegans* proteins in a null background and fully rescue function, for example expression of mammalian Munc-18 gene rescues the *unc-18* null strain for wild-type locomotion and neuronal function (Gengyo-Ando et al., 1996). Human NCS-1 could be expressed in the *C. elegans ncs-1* null strain to test if it rescues the TDL function. If this is the case, it would be interesting to repeat this with the human NCS-1 R102Q mutated protein and establish if it affects the TDL pathway. It would also be interesting to compare biochemically and structurally the interactions of the wild-type, Δ169-190, R102A and W103A/V125 mutations to further characterise the C-terminal binding cleft and C-terminal tail modulation of target peptide binding.

The G2 residue is essential for myristolation of NCS-1 (O'Callaghan et al., 2002). The N-terminal myristoyl tail of NCS-1 is not essential for TDL regulation in the worm as expression of the non-myristlolated protein showed wild-type rescue. This result may be because the mutated protein is over expressed. Either way this result also suggests that NCS-1 may not have a role in recruitment of bound target proteins to membranes in *C. elegans* TDL as suggested in other studies (de Barry et al., 2006). In fission yeast non-myristoylated Ncs1 appears to also be functionally active (Hendricks et al., 1999), although, the myristoyl tail does appear to function in repositioning Ncs1 from the cytoplasm to the plasma membrane via a the myristoyl switch mechanism. It is possible that NCS-1 in *C. elegans* has two distinct sites of function, one bound to the membrane and one free in the cytoplasm.

In an earlier study, NCS-1 was shown to be expressed in three pairs of thermosensory neurons, the AFD neurons, the AWC neurons and the AIY interneurons. Temperature-dependent locomotion was found to be regulated by the AFD sensory neuron (Edwards et al., 2012). This study has shown that NCS-1 regulates TDL through the AIY interneuron and not the AFD thermosensory neuron

as expected. Western blotting confirmed the expression NCS-1 driven by the *osm-6* promoter, but did not confirm expression levels in individual neurons. It could be that in the AFD and AWC neurons that the protein is not expressed sufficient levels to regulate TDL in a wild-type manner, however this is unlikely because the Western blot did show that the overall levels of protein were much higher than endogenously expressed NCS-1.

The absence of locomotion at 28^{o}C of the AIY neuron ablated *ttx-3* mutant strain is the opposite of what was expected considering that NCS-1 regulates TDL though the AIY neuron. These results suggest that regulation of temperature-dependent locomotion is driven by a TDL stimulatory pathway in the AIY neurons in the wild-type worm, which is dampened, but not completely inhibited by NCS-1 (Figure 4.17).

It is likely that this pathway is activated by a signal from the pre-synaptic AFD neurons (Figure 4.17), as it was shown to be involved in the TDL neuronal circuit previously (Edwards et al., 2012) and the AFD has also been shown to regulate the AIY in other temperature sensory pathways. In the *ncs-1* null worm it appears that the TDL stimulatory pathway is unregulated leading to a increase in TDL and in the AIY ablated strain here is no stimulatory mechanism due to the absence of the AIY neuron leading to an absence of locomotion (Figure 4.17). NCS-1 may directly bind to and inhibit a target protein in the TDL stimulation pathway at the time of the acute rise in temperature. The benefit to the wild-type worm of the dampened/stimulation mechanism between NCS-1 and the TDL stimulatory pathway has not been investigated in this study, but it may be necessary for physiological thermophilic behaviours as the AIY ablation strain is thermophilic (Hobert et al., 1997). Other unidentified pathways, possibly in the AFD and cryophilic AIZ neurons (Hobert et al., 1997), stops all locomotion at high temperatures.

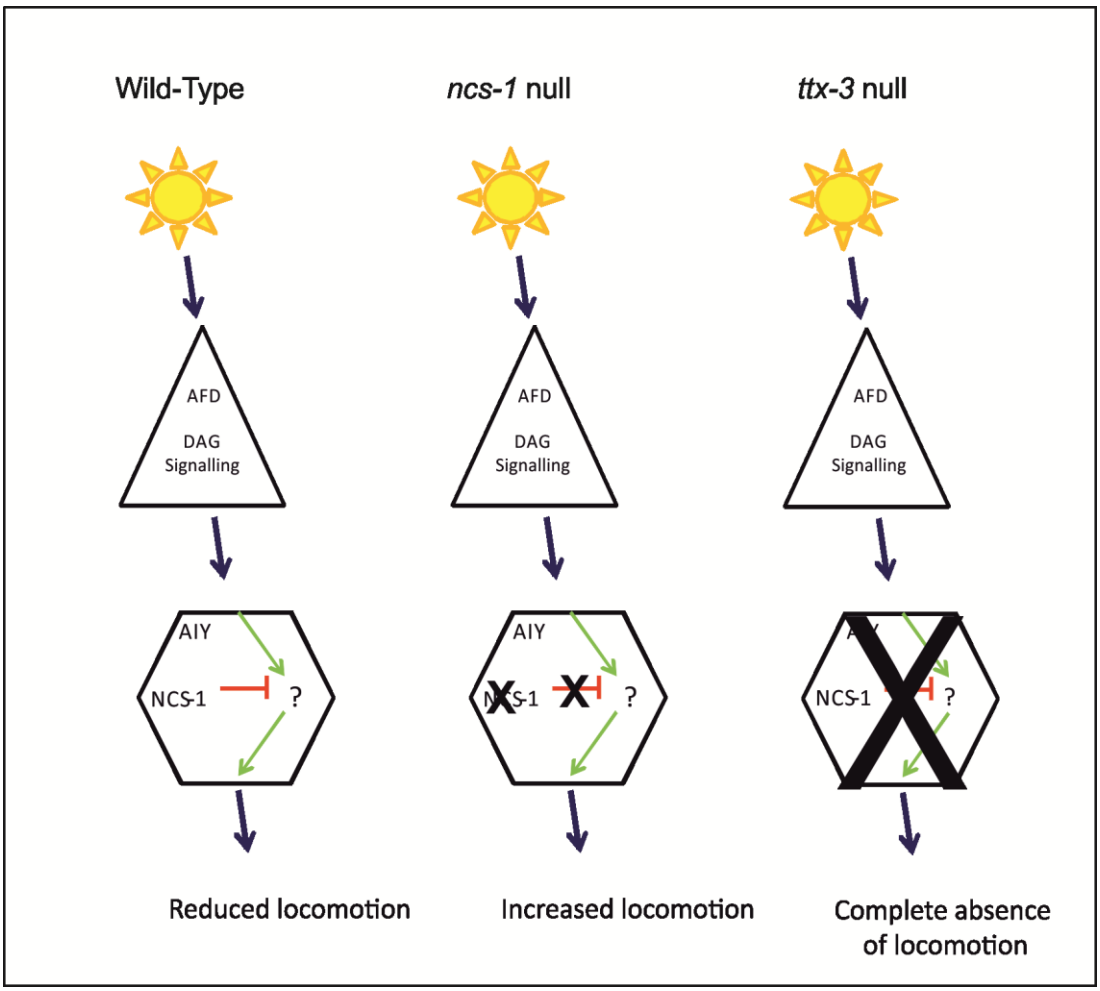

Figure 4.18 The Predicted Neuronal Circuit and Molecular pathway of the Temperature-dependent Locomotion in *C. elegans*. Illustration of a potential mechanism of TDL in *C. elegans* based on the finding of this study and Edwards et al, 2012 (Edwards et al., 2012). After exposure to acute heat, a) NCS-1 dampens the TDL stimulatory pathway in AIY neuron in the wild-type worm. b) A lack of NCS-1 in the AIY neuron in the *ncs-1* null strain (qa406) shows an increase of TDL. c) There is no TDL stimulatory pathway because there is a loss of a functioning AIY neuron in the *ttx-3* null worm (ot22) and the worms

The *ncs-1* null (qa406) has previously been shown to display a defect in the thermotaxis behaviour, isothermal tracking, where the wild-type worm learns to associate food with a specific temperature (Gomez et al., 2001), this behaviour was also found to be regulated by NCS-1 through AIY interneurons. The *ncs-1* null strain has not been assessed for the other thermotaxis behaviour, the biased random walk; it would be interesting to see if the mutant strain had a defective phenotype for this behaviour. The *ncs-1* null animal has been assed for thermoavoidance phenotypes and no defect was found (Ghosh et al., 2012, Gomez et al., 2001). This is not surprising because as discussed in Chapter 1 thermoavoidance is controlled

by a different neuronal circuit network going through the AIB rather than the AIY interneurons compared with thermotaxis behaviours (Wittenburg and Baumeister, 1999, Liu et al., 2012). As the regulation exerted by NCS-1 on both isothermal tracking and TDL pathways involves the AIY neuron it would be interesting to see if TDL was also regulated by other isothermal tracking regulatory proteins and pathways.

As we have established that the AIY neuron is the site of NCS-1 TDL regulation, it would be interesting to express the NCS-1 mutants studied here in the AIY neurons only to validate that the mechanism is regulate by key elements of NCS-1 structure in this neuronal pair. The function of calcium binding was not investigated in this study. Calcium binding was shown to be involved in the function isothermal tracking of NCS-1 in *C. elegans* using EF hand mutants (Gomez et al., 2001). It has yet to be established if isothermal tracking and TDL are phenotypes related to the same or different temperature sensitive neuronal mechanisms within the worm. To establish this, the TDL assay could be performed on other mutant worms shown previously to be defective in isothermal tracking regulation. It is possible to detect changes in calcium signalling inside specific neurons by expression of fluorescent cameleon Ca^{2+} indicator proteins (Chung et al., 2013). This system has already been developed and used to measure calcium signalling changes in temperature sensing pathways in the AFD and the AIY neurons (Kuhara et al., 2011). It would be interesting to compare changes in calcium signalling in the these neurons in the wild-type, *ncs-1* null, *ncs-1* mutants and also any subsequent mutant strains found to interact with *ncs-1* in the TDL pathway.

The target protein for NCS-1 regulation of the TDL pathway was not identified in this study. The *C. elegans* PI4K orthologue, PIFK-1 is a potential target of NCS-1 as it displayed a TDL phenotype and structural studies of yeast orthologues have shown complex formation via the N- and C-terminal binding clefts. More work is required to establish if it is a target protein. This would include expression of PIFK-1 in the *pifk-1* null worm in the AIY neurons to see if it rescues the phenotype, and to also to

cross the *ncs-1* and *pifk-1* null strains to establish if they regulate TDL via the same or different pathways.

This study has shown that the assay for temperature-dependent locomotion is robust, reproducible and is easy and quick to perform, taking approximately 30 minutes to assay an individual animal at both temperatures. In the case of the *ncs-1* null worm this shows a distinct phenotype. To increase the numbers of animals assessed for this behaviour or to screen many strains at the same time it may be beneficial in the future to develop the technique, so a greater number of worms could be assayed at the 20^{o}C or 28^{o}C at the same time and/or record and use computer analysis to define the behaviour. This could be useful for screening strains containing mutants of potential target proteins for *ncs-1*.

In conclusion, Inhibition of the TDL stimulatory pathway is a function of NCS-1 in *C. elegans*. NCS-1 inhibits a TDL stimulatory pathway specifically in the AIY neuron. NCS-1 expressed in other cell types including the thermosensory neurons AFD and AWC appears not to be involved in this behaviour. NCS-1 interacts with target proteins in the TDL stimulatory pathway via both the N-terminal and C-terminal binding clefts of the hydrophobic pocket. Neither the C-terminal tail nor myristoylation appear to have a role in the inhibition of the TDL stimulatory pathway.

Chapter 5: DISSCUSION

5.1 Discussion

The understanding of Ca^{2+} signalling has moved forward rapidly in recent years with its role in normal physiology and in disease becoming clearer. There are many aspects, though, which are still not understood. Therefore, characterising the function of NCS proteins in more detail will give insight into the molecular basis of neuronal Ca^{2+} signalling and neuronal disorders and may provide targets for future drug discovery. By combining two very different disciplines, *in vitro* biochemical/biophysical analysis and physiological studies using *C. elegans*, the work described in this thesis aimed to characterise NCS-1 binding, structure and function and contribute towards an understanding of neuronal Ca^{2+} signalling.

NCS-1 has been implicated to bind to multiple target proteins including PI4KIIIβ (Hendricks et al., 1999), IP_3R (Zhang et al., 2010, Boehmerle et al., 2006), D2R (Lian et al., 2011) and IL1RAPL1 (Handley et al., 2010). The $Ca_v2.1$, a subunit of the P/Q Ca^{2+} channel, has also been revealed through reverse genetics as major target protein of NCS-1 (frequenin) in *Drosophila* (Dason et al., 2009). Physiological functions have been attributed to interactions between NCS-1 and $Ca_v2.1$ but no direct binding between the proteins has been demonstrated (Weiss and Burgoyne, 2001, Tsujimoto et al., 2002). In contrast, CaM, CaBP-1 and VILIP-2 Ca^{2+} sensor proteins have been shown to bind to the IQ and/or the CBD domains on the C-terminal tail of the channel (Lee et al., 2002, Lee et al., 1999, Lautermilch et al., 2005, Findeisen and Minor Jr, 2010, Kim et al., 2008, Mori et al., 2008, Demaria et al., 2001).

The first aim of this project was to establish direct NCS-1 and $Ca_v2.1$ binding. Using biochemical and biophysical methods, identify the region of the Ca^{2+} channel that binds to NCS-1, characterise the binding in detail and to identity of residues involved of the NCS-1 binding pocket. Using pull-down assays, it was established that a long peptide fragment of $Ca_v2.1$ containing both the IQ and CBD domains, interacted directly with NCS-1 in a Ca^{2+}-dependent manner. Use of NMR showed an interaction of the NCS-1 protein with a peptide fragment of $Ca_v2.1$, which contained only the IQ domain, in the presence of Ca^{2+}. Further work characterising the

binding of NCS-1 and the peptide fragment of $Ca_v2.1$ containing the CBD domain, was put aside so that this study could then focus on the IQ domain.

Protein binding analysis using SPR was unable to provide NCS-1 and IQ peptide binding kinetics or stoichiometry data due to the properties of NCS-1 in the assay. Isothermal titration calorimetry (ITC) is an alternative protein binding analysis technique which may be suitable to measure the characteristics of the NCS-1/IQ peptide complex. Once a system has been established to measure protein binding constants it may be possible to measure other features of NCS-1/IQ peptide association, for example, to establish the optimum Ca^{2+} concentration for complex formation and competition binding analysis with NCS-1 and CaM or CaBP-1 which also bind to the IQ peptide.

It was not possible to identify a specific region of NCS-1 that the IQ peptide binds to using NMR, although, it would be logical to assume it binds to the hydrophobic pocket as this is the region of yeast NCS-1 that the peptide binds (Strahl et al., 2007). It has also been shown that the IQ peptide binds to in the hydrophobic binding sites of CaM (Kim et al., 2008). A major aim of this part of the study was to use NMR to identify which amino acids in the hydrophobic pocket of NCS-1 were responsible for the interaction with the IQ peptide. It was not possible to achieve this aim because the interaction caused an apparent massive conformational change in NCS-1. The majority of NCS-1 amino acids protein were effected making it impossible to distinguish binding sites using this technique. X-ray crystallography is an alternative technique to analyse the structure of protein complexes at high resolution and may be suitable to generate a structure of the NCS-1/IQ peptide complex and identify which residues of the NCS-1 hydrophobic pocket interact with the peptide.

The second part of this thesis validated NCS-1 structural features in a whole organism. The *C. elegans* worm has been used extensively as a neuronal model and previously has been used to characterise the function of NCS-1. NCS-1 was shown to be expressed predominantly in sensory neurons in the worm (Gomez et al.,

2001). Its function in a single pair of AIY interneurons was linked to the thermosensory behaviour of isothermal tracking and memory (Gomez et al., 2001). The *ncs-1* null strain was used to characterise the function of the EF-hand motif and it was established that NCS-1 regulates isothermal tracking and memory in a Ca^{2+} dependant manner (Gomez et al., 2001). In the current study the *ncs-1* null strain was used as a physiological system to assess NCS-1 structural aspects implicated by other biophysical studies. It was established that NCS-1 is not essential for wild-type growth, anatomy, locomotion and neuronal transmission. It was, however, linked to TDL, which had previously been shown to be regulated in the AFD sensory neuron pair which play a major role in thermotaxis. NCS-1 was previously shown to play no role in isothermal tracking or memory regulation in the AFD sensory neurons (Gomez et al., 2001). In contrast, TDL was shown to be regulated by the AFD sensory neuron pair (Edwards et al., 2012). By expressing NCS-1 in a series of neurons, it was found during this study that NCS-1 did not regulate TDL in the AFD neurons but exerted its function in the AIY neurons.

By expressing a series of mutated NCS-1 proteins in the *ncs-1* null worm, the relevance of structural features to protein function were assessed. Expression of NCS-1 with the G2A mutation, which is unable to be myristoylated (O'Callaghan et al., 2002), was able to rescue wild-type TDL. Other studies have suggested that non-myristoylated NCS-1 is functional but has a less efficient for physiological activity than the wild-type protein (Hendricks et al., 1999). It is possible that NCS-1 is involved in membrane targeting and aids the relocation of target protein with which it forms complexes. The current study showed that non-myristoylated NCS-1 still functions in a wild-type manner and suggests that NCS-1 is not involved in target protein localisation or membrane translocation. It may be that myristoylation of NCS-1 is required in other physiological pathways but is not required for TDL - this would need further investigation.

Structural studies have suggested that the C-terminal tail of NCS-1 occupies the C-terminal binding cleft and moves out of the cleft so that this is free for target binding. The work done in the current study supported this mechanism since the

C-terminal tail was not required for the rescue of physiological function in TDL. As to why the C-terminal tail occupies the C-terminal binding cleft in the non-target bound form was not investigated in this study. It has been suggested that the C-terminal tail self regulates NCS-1 function by preventing off target binding when NCS-1 is in its active Ca^{2+} bound state. When appropriate, the C-terminal tail vacates the C-terminal cleft, fully exposing the hydrophobic groove for target protein interactions. (Heidarsson et al., 2012, Strahl et al., 2007).

Several previous structural studies have identified amino acids in binding pocket of NCS proteins that interact with target proteins (Lim et al., 2011, Strahl et al., 2007, Pioletti et al., 2006, Wang et al., 2007, Ames et al., 2006) In these studies, the targets used were short peptides derived from the full-length target proteins. There was a possibility that these interactions identified in *in vitro* studies did not occur in physiological systems. The current study showed that a common residue in the N-terminal binding cleft of the hydrophobic pocket involved target peptide binding with recoverin, KChIP-1 or NCS-1 have a physiological role in TDL suggesting that NCS proteins have a conserved binding mechanism. The study also showed that the whole C-terminal binding cleft of NCS-1 is involved in its TDL regulatory function. The *C. elegan*s TDL assay will provide a system to allow validation of future NCS-1 structural findings, including those of the complex of NCS-1 with the C-terminus of Cav2.1 if its structure can be solved.

Mammalian proteins can be expressed in *C. elegans*. It would be interesting to see if human NCS-1 expression in the AIY neuron of the null strain would rescue the wild-type phenotype. This would be a useful tool to evaluate the role of human NCS-1 in neuronal Ca^{2+} signalling and could be use to establish what characteristics of human NCS-1 have a functional role. For example, human NCS-1 R102A mutation has been linked to Autism (Piton et al., 2008), it may be possible using the *C. elegans* assay TDL to investigate the effect the mutation has on the worm behaviour when compared to the human wild-type protein.

The next direction to take this study would be the identification of the target protein NCS-1 responsible for NCS-1 function in TDL. The obvious candidate is the *C. elegans* PI4kinase IIIβ orthologue PIFK-1. During this study it has been shown that NCS-1 residues implicated in the interaction of yeast NCS-1 and PI4 kinase IIIβ are important physiologically in the worm. The *pifk-1*mutant showed a defective TDL phenotype, although not as severe as the *ncs-1* null. Creating an *ncs-1* and *pifk-1* double mutant strain would provide information using the TDL assay as to whether these two proteins are involved in the same pathway. It would also be interesting to see if the phenotype of the *pifk-1* mutant could be rescued by expression of *pifk-1* in AIY neurons that are the site of NCS-1 function.

5.2 Conclusion

In conclusion, work in this thesis has investigated the physiological significance of key structural elements of NCS-1. It has shown that both the N- and the C-terminal binding clefts of NCS-1 are important for function and thus involved in target protein binding. NCS-1 may not be involved in the membrane translocation of target proteins as it still functions in the absence of the N-myristoyl group. The C-terminal tail appears to have no physiological role in TDL, supporting previous suggestions that it is not likely to interact directly with target proteins but instead may have a self-inhibitory role. This study has established that the TDL assay is able to be used to evaluate NCS-1 function in a neuronal system and has provided insights into the physiologically relevant target-binding mechanisms used by NCS-1.

References

ADAMS, P. J., RUNGTA, R. L., GARCIA, E., VAN DEN MAAGDENBERG, A. M. J. M., MACVICAR, B. A. & SNUTCH, T. P. 2010. Contribution of calcium-dependent facilitation to synaptic plasticity revealed by migraine mutations in the P/Q-type calcium channel. *Proceedings of the National Academy of Sciences of the United States of America,* 107**,** 18694-18699.

ALTUN, Z. F., HERNDON, L. A., CROCKER, C., LINTS, R. & HALL, D. H. E. S. 2002-2012. *WormAtlas* [Online]. Available: http://www.wormatlas.org.

AMES, J. B., HENDRICKS, K. B., STRAHL, T., HUTTNER, I. G., HAMASAKI, N. & THORNER, J. 2000. Structure and calcium-binding properties of Frq1, a novel calcium sensor in the yeast *Saccharomyces cerevisiae*. *Biochemistry,* 39**,** 12149-12161.

AMES, J. B., LEVAY, K., WINGARD, J. N., LUSIN, J. D. & SLEPAK, V. Z. 2006. Structural basis for calcium-induced inhibition of rhodopsin kinase by recoverin. *J Biol Chem,* 281**,** 37237-45.

AMES JB, L. S. 2011. Molecular structure and target recognition of neuronal calcium sensor proteins. *Biochim Biophys Acta,* 13**,** 13.

ARAVIND, P., CHANDRA, K., REDDY, P. P., JEROMIN, A., CHARY, K. V. R. & SHARMA, Y. 2008. Regulatory and Structural EF-Hand Motifs of Neuronal Calcium Sensor-1: Mg^{2+} Modulates Ca^{2+} Binding, Ca^{2+}-Induced Conformational Changes, and Equilibrium Unfolding Transitions. *Journal of Molecular Biology,* 376**,** 1100-1115.

AUGUSTINE, G. J., SANTAMARIA, F. & TANAKA, K. 2003. Local calcium signaling in neurons. *Neuron,* 40**,** 331-346.

BAHI, N., FRIOCOURT, G., CARRIÉ, A., GRAHAM, M. E., WEISS, J. L., CHAFEY, P., FAUCHEREAU, F., BURGOYNE, R. D. & CHELLY, J. 2003. IL1 receptor accessory protein like, a protein involved in X-linked mental retardation, interacts with Neuronal Calcium Sensor-1 and regulates exocytosis. *Human Molecular Genetics,* 12**,** 1415-1425.

BARCLAY, J. W., MORGAN, A. & BURGOYNE, R. D. 2005. Calcium-dependent regulation of exocytosis. *Cell Calcium,* 38**,** 343-353.

BARCLAY, J. W., MORGAN, A. & BURGOYNE, R. D. 2012. Neurotransmitter release mechanisms studied in *Caenorhabditis elegans*. *Cell Calcium,* 52**,** 289-295.

BARGMANN, C. I. & HORVITZ, H. R. 1991. Chemosensory neurons with overlapping functions direct chemotaxis to multiple chemicals in *C. elegans*. *Neuron,* 7**,** 729-42.

BARR, M. M. 2005. *Caenorhabditis elegans* as a model to study renal development and disease: sexy cilia. *J Am Soc Nephrol,* 16**,** 305-12.

BARR, M. M. & STERNBERG, P. W. 1999. A polycystic kidney-disease gene homologue required for male mating behaviour in *C. elegans*. *Nature,* 401**,** 386-9.

BAYER, P., ARNDT, A., METZGER, S., MAHAJAN, R., MELCHIOR, F., JAENICKE, R. & BECKER, J. 1998. Structure determination of the small ubiquitin-related modifier SUMO-1. *J Mol Biol,* 280**,** 275-86.

BERRIDGE, M. J. 1998. Neuronal calcium signaling. *Neuron,* 21**,** 13-26.

BERRIDGE, M. J. 2010. Calcium hypothesis of Alzheimer's disease. *Pflugers Archiv European Journal of Physiology,* 459**,** 441-449.

BERRIDGE, M. J., LIPP, P. & BOOTMAN, M. D. 2000. The versatility and universality of calcium signalling. *Nature Reviews Molecular Cell Biology,* 1**,** 11-21.

BEVERLY, M., ANBIL, S. & SENGUPTA, P. 2011. Degeneracy and neuromodulation among thermosensory neurons contribute to robust thermosensory behaviors in *Caenorhabditis elegans*. *J Neurosci,* 31**,** 11718-27.

BIRON, D., WASSERMAN, S., THOMAS, J. H., SAMUEL, A. D. & SENGUPTA, P. 2008. An olfactory neuron responds stochastically to temperature and modulates *Caenorhabditis elegans* thermotactic behavior. *Proc Natl Acad Sci U S A,* 105**,** 11002-7.

BITO, H., DEISSEROTH, K. & TSIEN, R. W. 1997. Ca^{2+}-dependent regulation in neuronal gene expression. *Current Opinion in Neurobiology,* 7**,** 419-429.

BOEHMERLE, W., SPLITTGERBER, U., LAZARUS, M. B., MCKENZIE, K. M., JOHNSTON, D. G., AUSTIN, D. J. & EHRLICH, B. E. 2006. Paclitaxel induces calcium oscillations via an inositol 1,4,5-trisphosphate receptor and neuronal calcium sensor 1-dependent mechanism. *Proc Natl Acad Sci U S A,* 103**,** 18356-61.

BRENNER, S. 1974. The genetics of *Caenorhabditis elegans*. *Genetics,* 77**,** 71-94.

BURGOYNE, R. D. 2007. Neuronal calcium sensor proteins: Generating diversity in neuronal Ca^{2+} signalling. *Nature Reviews Neuroscience,* 8**,** 182-193.

BURGOYNE, R. D. & HAYNES, L. P. 2012. Understanding the physiological roles of the neuronal calcium sensor proteins. *Mol Brain,* 5**,** 1756-6606.

CATTERALL, W. A. 2000. Structure and regulation of voltage-gated Ca^{2+} channels. *Annual Review of Cell and Developmental Biology.*

CATTERALL, W. A. & FEW, A. P. 2008. Calcium Channel Regulation and Presynaptic Plasticity. *Neuron,* 59**,** 882-901.

CHALFIE, M., SULSTON, J. E., WHITE, J. G., SOUTHGATE, E., THOMSON, J. N. & BRENNER, S. 1985. The neural circuit for touch sensitivity in *Caenorhabditis elegans*. *J Neurosci,* 5**,** 956-64.

CHALFIE, M., TU, Y., EUSKIRCHEN, G., WARD, W. W. & PRASHER, D. C. 1994. Green fluorescent protein as a marker for gene expression. *Science,* 263**,** 802-5.

CHEN, X. & BURGOYNE, R. D. 2012. Identification of common genetic modifiers of neurodegenerative diseases from an integrative analysis of diverse genetic screens in model organisms. *BMC Genomics,* 13**,** 1471-2164.

CHUNG, S. H., SUN, L. & GABEL, C. V. 2013. In vivo neuronal calcium imaging in *C. elegans*. *J Vis Exp,* 10**,** 50357.

CSC, *C. E.* S. C. 1998. Genome sequence of the nematode *C. elegans*: A platform for investigating biology. *Science,* 282**,** 2012-2018.

DASON, J. S., ROMERO-POZUELO, J., MARIN, L., IYENGAR, B. G., KLOSE, M. K., FERRUS, A. & ATWOOD, H. L. 2009. Frequenin/NCS-1 and the Ca^{2+}-channel α1-subunit co-regulate synaptic transmission and nerve-terminal growth. *Journal of Cell Science,* 122**,** 4109-4121.

DE BARRY, J., JANOSHAZI, A., DUPONT, J. L., PROCKSCH, O., CHASSEROT-GOLAZ, S., JEROMIN, A. & VITALE, N. 2006. Functional implication of neuronal calcium sensor-1 and phosphoinositol 4-kinase-beta interaction in regulated exocytosis of PC12 cells. *J Biol Chem,* 281**,** 18098-111.

DE CASTRO, E. 1997. *Caenorhabditis elegans Neuronal Calcium Sensor-1: From Gene to Behavior.* PhD, Université de Genève

DECASTRO, E., NEF, S., FIUMELLI, H., LENZ, S. E., KAWAMURA, S. & NEF, P. 1995. Regulation of Rhodopsin Phosphorylation by a Family of Neuronal Calcium Sensors. *Biochem Biophys Res Commun,* 216**,** 133-140.

DEMARIA, C. D., SOONG, T. W., ALSEIKHAN, B. A., ALVANIA, R. S. & YUE, D. T. 2001. Calmodulin bifurcates the local Ca^{2+} signal that modulates P/Q-type Ca^{2+} channels. *Nature,* 411**,** 484-489.

DIVERSÉ-PIERLUISSI, M., REMMERS, A. E., NEUBIG, R. R. & DUNLAP, K. 1997. Novel form of crosstalk between G protein and tyrosine kinase pathways. *Proceedings of the National Academy of Sciences of the United States of America,* 94**,** 5417-5421.

DOWNES, C. P., GRAY, A. & LUCOCQ, J. M. 2005. Probing phosphoinositide functions in signaling and membrane trafficking. *Trends in Cell Biology,* 15**,** 259-268.

EDWARDS, M. R., JOHNSON, J. R., RANKIN, K., JENKINS, R. E., MAGUIRE, C., MORGAN, A., BURGOYNE, R. D. & BARCLAY, J. W. 2012. PKC-2 Phosphorylation of UNC-18 Ser322 in AFD Neurons Regulates Temperature Dependency of Locomotion. *The Journal of Neuroscience,* 32**,** 7042-7051.

ELLIS, H. M. & HORVITZ, H. R. 1986. Genetic control of programmed cell death in the nematode *C. elegans*. *Cell,* 44**,** 817-29.

FINDEISEN, F. & MINOR JR, D. L. 2010. Progress in the structural understanding of voltage-gated calcium channel (CaV) function and modulation. *Channels,* 4.

FIRE, A., XU, S., MONTGOMERY, M. K., KOSTAS, S. A., DRIVER, S. E. & MELLO, C. C. 1998. Potent and specific genetic interference by double-stranded RNA in *Caenorhabditis elegans*. *Nature,* 391**,** 806-11.

GENGYO-ANDO, K., KITAYAMA, H., MUKAIDA, M. & IKAWA, Y. 1996. A murine neural-specific homolog corrects cholinergic defects in *Caenorhabditis elegans unc-18* mutants. *J Neurosci,* 16**,** 6695-702.

GÉNIN, A., DAVIS, S., MEZIANE, H., DOYÈRE, V., JEROMIN, A., RODER, J., MALLET, J. & LAROCHE, S. 2001. Regulated expression of the neuronal calcium sensor-1 gene during long-term potentiation in the dentate gyrus in vivo. *Neuroscience,* 106**,** 571-577.

GHOSH, R., MOHAMMADI, A., KRUGLYAK, L. & RYU, W. S. 2012. Multiparameter behavioral profiling reveals distinct thermal response regimes in *Caenorhabditis elegans*. *BMC Biol,* 10**,** 1741-7007.

GOMEZ, M., DE CASTRO, E., GUARIN, E., SASAKURA, H., KUHARA, A., MORI, I., BARTFAI, T., BARGMANN, C. I. & NEF, P. 2001. Ca^{2+} Signaling via the Neuronal Calcium Sensor-1 Regulates Associative Learning and Memory in *C. elegans*. *Neuron,* 30**,** 241-248.

HANDLEY, M. T. W., LIAN, L., P., H. L. & D., B. R. 2010. Structural and Functional Deficits in a Neuronal Calcium Sensor-1 Mutant Identified in a Case of Autistic Spectrum Disorder. *PLoS ONE,* 5**,** e10534.

HAYNES, L. P., FITZGERALD, D. J., WAREING, B., O'CALLAGHAN, D. W., MORGAN, A. & BURGOYNE, R. D. 2006. Analysis of the interacting partners of the neuronal calcium-binding proteins L-CaBP1, hippocalcin, NCS-1 and neurocalcin δ. *Proteomics,* 6**,** 1822-1832.

HAYNES, L. P., SHERWOOD, M. W., DOLMAN, N. J. & BURGOYNE, R. D. 2007. Specificity, promiscuity and localization of ARF protein interactions with NCS-1 and phosphatidylinositol-4 kinase-IIIβ. *Traffic,* 8**,** 1080-1092.

HAYNES, L. P., TEPIKIN, A. V. & BURGOYNE, R. D. 2004. Calcium-binding Protein 1 Is an Inhibitor of Agonist-evoked, Inositol 1,4,5-Trisphosphate-mediated Calcium Signaling. *Journal of Biological Chemistry,* 279**,** 547-555.

HAYNES, L. P., THOMAS, G. M. H. & BURGOYNE, R. D. 2005. Interaction of neuronal calcium sensor-1 and ADP-ribosylation factor 1 allows bidirectional control of phosphatidylinositol 4-kinase β and trans-golgi network-plasma membrane traffic. *Journal of Biological Chemistry,* 280**,** 6047-6054.

HEDGECOCK, E. M. & RUSSELL, R. L. 1975. Normal and mutant thermotaxis in the nematode *Caenorhabditis elegans*. *Proceedings of the National Academy of Sciences,* 72**,** 4061-4065.

HEIDARSSON, P. O., BJERRUM-BOHR, I. J., JENSEN, G. A., PONGS, O., FINN, B. E., POULSEN, F. M. & KRAGELUND, B. B. 2012. The C-Terminal Tail of Human Neuronal Calcium Sensor 1 Regulates the Conformational Stability of the Ca^{2+}-Activated State. *Journal of Molecular Biology,* 417**,** 51-64.

HENDRICKS, K. B., WANG, B. Q., SCHNIEDERS, E. A. & THORNER, J. 1999. Yeast homologue of neuronal frequenin is a regulator of phosphatidylinosrtol-4-OH kinase. *Nature Cell Biology,* 1**,** 234-241.

HOBERT, O. 2013. *The neuronal genome of Caenorhabditis elegans* [Online]. Available: http://www.wormbook.org/chapters/www_neuronalgenome/neuronalgenome.html [Accessed August 13, 2013.

HOBERT, O., MORI, I., YAMASHITA, Y., HONDA, H., OHSHIMA, Y., LIU, Y. & RUVKUN, G. 1997. Regulation of interneuron function in the *C. elegans* thermoregulatory pathway by the ttx-3 LIM homeobox gene. *Neuron,* 19**,** 345-57.

HOPE, I. A. 1999. *C. elegans A Practical Approach,* Oxford, OUP. p 144-147.

JENKINS, P. M., MCEWEN, D. P. & MARTENS, J. R. 2009. Olfactory cilia: linking sensory cilia function and human disease. *Chem Senses,* 34**,** 451-64.

JEROMIN, A., MURALIDHAR, D., PARAMESWARAN, M. N., RODER, J., FAIRWELL, T., SCARLATA, S., DOWAL, L., MUSTAFI, S. M., CHARY, K. V. R. & SHARMA, Y. 2004. N-terminal myristoylation regulates calcium-induced conformational changes in neuronal calcium sensor-1. *Journal of Biological Chemistry,* 279**,** 27158-27167.

JINNO, S., JEROMIN, A., RODER, J. & KOSAKA, T. 2002. Immunocytochemical localization of neuronal calcium sensor-1 in the hippocampus and cerebellum of the mouse, with special reference to presynaptic terminals. *Neuroscience,* 113**,** 449-461.

JOHNSON, J. R., JENN, R. C., BARCLAY, J. W., BURGOYNE, R. D. & MORGAN, A. 2010. *Caenorhabditis elegans*: a useful tool to decipher neurodegenerative pathways. *Biochem Soc Trans,* 38**,** 559-63.

JOUVENCEAU, A., EUNSON, L. H., SPAUSCHUS, A., RAMESH, V., ZUBERI, S. M., KULLMANN, D. M. & HANNA, M. G. 2001. Human epilepsy associated with dysfunction of the brain P/Q-type calcium channel. *Lancet,* 358**,** 801-807.

KABBANI, N., NEGYESSY, L., LIN, R., GOLDMAN-RAKIC, P. & LEVENSON, R. 2002. Interaction with neuronal calcium sensor NCS-1 mediates desensitization of the D2 dopamine receptor. *Journal of Neuroscience,* 22**,** 8476-8486.

KALETTA, T. & HENGARTNER, M. O. 2006. Finding function in novel targets: *C. elegans* as a model organism. *Nat Rev Drug Discov,* 5**,** 387-98.

KIM, E. Y., RUMPF, C. H., FUJIWARA, Y., COOLEY, E. S., VAN PETEGEM, F. & MINOR JR, D. L. 2008. Structures of Ca_V2 Ca^{2+}/CaM-IQ Domain Complexes Reveal Binding Modes that Underlie Calcium-Dependent Inactivation and Facilitation. *Structure,* 16**,** 1455-1467.

KIMATA, T., SASAKURA, H., OHNISHI, N., NISHIO, N. & MORI, I. 2012. Thermotaxis of *C. elegans* as a model for temperature perception, neural information processing and neural plasticity. *Worm,* 1**,** 31-41.

KIMURA, K. D., MIYAWAKI, A., MATSUMOTO, K. & MORI, I. 2004. The *C. elegans* thermosensory neuron AFD responds to warming. *Curr Biol,* 14**,** 1291-5.

KIONTKE, K. & SUDHAUS, W. 2006. *Ecology of Caenorhabditis species* [Online]. WormBook. Available: http://www.wormbook.org [Accessed 24th Feburary 2014.

KNIERIM, E., LEISLE, L., WAGNER, C., WESCHKE, B., LUCKE, B., BOHNER, G., DREIER, J. P. & SCHUELKE, M. 2011. Recurrent stroke due to a novel voltage sensor mutation in cav2.1 responds to verapamil. *Stroke,* 42**,** e14-e17.

KRETSINGER, R. H. & NOCKOLDS, C. E. 1973. Carp muscle calcium-binding protein. II. Structure determination and general description. *Journal of Biological Chemistry,* 248**,** 3313-3326.

KUHARA, A., OHNISHI, N., SHIMOWADA, T. & MORI, I. 2011. Neural coding in a single sensory neuron controlling opposite seeking behaviours in *Caenorhabditis elegans*. *Nat Commun,* 2.

KUHARA, A., OKUMURA, M., KIMATA, T., TANIZAWA, Y., TAKANO, R., KIMURA, K. D., INADA, H., MATSUMOTO, K. & MORI, I. 2008. Temperature Sensing by an Olfactory Neuron in a Circuit Controlling Behavior of *C. elegans*. *Science,* 320**,** 803-807.

KUMAR, M., AHMAD, S., AHMAD, E., SAIFI, M. A. & KHAN, R. H. 2012. In silico prediction and analysis of caenorhabditis EF-hand containing proteins. *PLoS One,* 7.

LAUDE, A. J. & SIMPSON, A. W. M. 2009. Compartmentalized signalling: Ca^{2+} compartments, microdomains and the many facets of Ca^{2+} signalling. *FEBS Journal,* 276**,** 1800-1816.

LAUTERMILCH, N. J., FEW, A. P., SCHEUER, T. & CATTERALL, W. A. 2005. Modulation of CaV2.1 channels by the neuronal calcium-binding protein visinin-like protein-2. *Journal of Neuroscience,* 25**,** 7062-7070.

LEE, A., SCHEUER, T. & CATTERALL, W. A. 2000. Ca^{2+}/calmodulin-dependent facilitation and inactivation of P/Q-type Ca^{2+} channels. *Journal of Neuroscience,* 20**,** 6830-6838.

LEE, A., WESTENBROEK, R. E., HAESELEER, F., PALCZEWSKI, K., SCHEUER, T. & CATTERALL, W. A. 2002. Differential modulation of Cav2.1 channels by calmodulin and Ca^{2+}-binding protein 1. *Nature Neuroscience,* 5**,** 210-217.

LEE, A., WONG, S. T., GALLAGHER, D., LI, B., STORM, D. R., SCHEUER, T. & CATTERALL, W. A. 1999. Ca^{2+}/calmodulin binds to and modulates P/Q-type calcium channels. *Nature,* 399**,** 155-159.

LEE, A., ZHOU, H., SCHEUER, T. & CATTERALL, W. A. 2003. Molecular determinants of Ca^{2+}/calmodulin-dependent regulation of Cav2.1 channels. *Proceedings of the National Academy of Sciences of the United States of America,* 100**,** 16059-16064.

LEE, J. H. & GLEESON, J. G. 2010. The role of primary cilia in neuronal function. *Neurobiol Dis,* 38**,** 167-72.

LEUNG, M. C., WILLIAMS, P. L., BENEDETTO, A., AU, C., HELMCKE, K. J., ASCHNER, M. & MEYER, J. N. 2008. *Caenorhabditis elegans*: an emerging model in biomedical and environmental toxicology. *Toxicol Sci,* 106**,** 5-28.

LIAN, L.-Y., PANDALANENI, S. R., PATEL, P., MCCUE, H. V., HAYNES, L. P. & BURGOYNE, R. D. 2011. Characterisation of the Interaction of the C-Terminus of the Dopamine D2 Receptor with Neuronal Calcium Sensor-1. *PLoS ONE,* 6**,** e27779.

LIAN, L. Y., MYATT, D. & KITMITTO, A. 2007. Apo calmodulin binding to the L-type voltage-gated calcium channel Cav1.2 IQ peptide. *Biochem Biophys Res Commun,* 353**,** 565-70.

LIM, S., STRAHL, T., THORNER, J. & AMES, J. B. 2011. Structure of a Ca^{2+}-myristoyl switch protein that controls activation of a phosphatidylinositol 4-kinase in fission yeast. *Journal of Biological Chemistry,* 286**,** 12565-12577.

LIU, S., SCHULZE, E. & BAUMEISTER, R. 2012. Temperature- and touch-sensitive neurons couple CNG and TRPV channel activities to control heat avoidance in *Caenorhabditis elegans*. *PLoS One,* 7**,** 20.

LOPEZ, Y. 2010. *UDP-GLUCOSE:GLYCOPROTEIN GLUCOSYLTRANSFERASE (UGGT-1) AND UPR GENES MODULATE C. elegans NECROTIC CELL DEATH.* PhD Thesis, The State University of New Jersey and University of Medicine and Dentistry of New Jersey.

MA, X. & SHEN, Y. 2012. Structural Basis for Degeneracy among Thermosensory Neurons in *Caenorhabditis elegans*. *The Journal of Neuroscience,* 32**,** 1-3.

MATTSON, M. P. & MAGNUS, T. 2006. Ageing and neuronal vulnerability. *Nature Reviews Neuroscience,* 7**,** 278-294.

MCCUE, H. V., HAYNES, L. P. & BURGOYNE, R. D. 2010. The diversity of calcium sensor proteins in the regulation of neuronal function. *Cold Spring Harbor perspectives in biology,* 2.

MCFERRAN, B. W., GRAHAM, M. E. & BURGOYNE, R. D. 1998. Neuronal Ca^{2+} Sensor 1, the Mammalian Homologue of Frequenin, Is Expressed in Chromaffin and PC12 Cells

and Regulates Neurosecretion from Dense-core Granules. *Journal of Biological Chemistry,* 273**,** 22768-22772.

MCINTIRE, S. L., JORGENSEN, E., KAPLAN, J. & HORVITZ, H. R. 1993. The GABAergic nervous system of *Caenorhabditis elegans*. *Nature,* 364**,** 337-41.

MILLER, K. G., ALFONSO, A., NGUYEN, M., CROWELL, J. A., JOHNSON, C. D. & RAND, J. B. 1996. A genetic selection for *Caenorhabditis elegans* synaptic transmission mutants. *Proceedings of the National Academy of Sciences,* 93**,** 12593-12598.

MOCHIDA, S., FEW, A. P., SCHEUER, T. & CATTERALL, W. A. 2008. Regulation of Presynaptic CaV2.1 Channels by Ca^{2+} Sensor Proteins Mediates Short-Term Synaptic Plasticity. *Neuron,* 57**,** 210-216.

MORI, I. & OHSHIMA, Y. 1995. Neural regulation of thermotaxis in *Caenorhabditis elegans*. *Nature,* 376**,** 344-8.

MORI, I., SASAKURA, H. & KUHARA, A. 2007. Worm thermotaxis: a model system for analyzing thermosensation and neural plasticity. *Curr Opin Neurobiol,* 17**,** 712-9.

MORI, M. X., VANDER KOOI, C. W., LEAHY, D. J. & YUE, D. T. 2008. Crystal Structure of the CaV2 IQ Domain in Complex with Ca^{2+}/Calmodulin: High-Resolution Mechanistic Implications for Channel Regulation by Ca^{2+}. *Structure,* 16**,** 607-620.

MURAYAMA, T., TAKAYAMA, J., FUJIWARA, M. & MARUYAMA, I. N. 2013. Environmental alkalinity sensing mediated by the transmembrane guanylyl cyclase GCY-14 in *C. elegans*. *Curr Biol,* 23**,** 1007-12.

NAKAMURA, T. Y., JEROMIN, A., MIKOSHIBA, K. & WAKABAYASHI, S. 2011. Neuronal calcium sensor-1 promotes immature heart function and hypertrophy by enhancing Ca^{2+} signals. *Circ Res,* 109**,** 512-23.

NEJATBAKHSH, N. & FENG, Z. P. 2011. Calcium binding protein-mediated regulation of voltage-gated calcium channels linked to human diseases. *Acta Pharmacologica Sinica,* 32**,** 741-748.

NISHIDA, Y., SUGI, T., NONOMURA, M. & MORI, I. 2011. Identification of the AFD neuron as the site of action of the CREB protein in *Caenorhabditis elegans* thermotaxis. *EMBO Rep,* 12**,** 855-62.

NOBELPRIZE.ORG. 2002. *The Nobel Prize in Physiology or Medicine 2002* [Online]. Nobel Media AB 2013. Available: http://www.nobelprize.org/nobel_prizes/medicine/laureates/2002/ [Accessed 6 Aug 2013.

NOBELPRIZE.ORG. 2006. *The Nobel Prize in Physiology or Medicine 2006* [Online]. Nobel Media AB 2013. Available: <http://www.nobelprize.org/nobel_prizes/medicine/laureates/2006/> [Accessed Web. 7 Aug 2013.

NOBELPRIZE.ORG. 2008. *"The Nobel Prize in Chemistry 2008"* [Online]. Nobel Media AB 2013. Available: <http://www.nobelprize.org/nobel_prizes/chemistry/laureates/2008/> [Accessed 6 Aug 2013.

O'CALLAGHAN, D. W., IVINGS, L., WEISS, J. L., ASHBY, M. C., TEPIKIN, A. V. & BURGOYNE, R. D. 2002. Differential Use of Myristoyl Groups on Neuronal Calcium Sensor Proteins as a Determinant of Spatio-temporal Aspects of Ca^{2+} Signal Transduction. *Journal of Biological Chemistry,* 277**,** 14227-14237.

OLSEN, A., VANTIPALLI, M. C. & LITHGOW, G. J. 2006. Using *Caenorhabditis elegans* as a model for aging and age-related diseases. *Ann N Y Acad Sci***,** 120-8.

OPHOFF, R. A., TERWINDT, G. M., VERGOUWE, M. N., VAN EIJK, R., OEFNER, P. J., HOFFMAN, S. M. G., LAMERDIN, J. E., MOHRENWEISER, H. W., BULMAN, D. E., FERRARI, M., HAAN, J., LINDHOUT, D., VAN OMMEN, G. J. B., HOFKER, M. H., FERRARI, M. D. & FRANTS, R. R. 1996. Familial hemiplegic migraine and episodic

ataxia type-2 are caused by mutations in the Ca^{2+} channel gene CACNL1A4. *Cell,* 87**,** 543-552.

PERKINS, L. A., HEDGECOCK, E. M., THOMSON, J. N. & CULOTTI, J. G. 1986. Mutant sensory cilia in the nematode *Caenorhabditis elegans*. *Dev Biol,* 117**,** 456-87.

PIOLETTI, M., FINDEISEN, F., HURA, G. L. & MINOR, D. L., JR. 2006. Three-dimensional structure of the KChIP1-Kv4.3 T1 complex reveals a cross-shaped octamer. *Nat Struct Mol Biol,* 13**,** 987-95.

PITON, A., MICHAUD, J. L., PENG, H., ARADHYA, S., GAUTHIER, J., MOTTRON, L., CHAMPAGNE, N., LAFRENIÈRE, R. G., HAMDAN, F. F., JOOBER, R., FOMBONNE, E., MARINEAU, C., COSSETTE, P., DUBÉ, M. P., HAGHIGHI, P., DRAPEAU, P., BARKER, P. A., CARBONETTO, S. & ROULEAU, G. A. 2008. Mutations in the calcium-related gene IL1RAPL1 are associated with autism. *Human Molecular Genetics,* 17**,** 3965-3974.

PONGS, O., LINDEMEIER, J., ZHU, X. R., THEIL, T., ENGELKAMP, D., KRAH-JENTGENS, I., LAMBRECHT, H. G., KOCH, K. W., SCHWEMER, J., RIVOSECCHI, R., MALLART, A., GALCERAN, J., CANAL, I., BARBAS, J. A. & FERRUS, A. 1993. Frequenin - A novel calcium-binding protein that modulates synaptic efficacy in the Drosophila nervous system. *Neuron,* 11**,** 15-28.

PRAGNELL, M., DE WAARD, M., MORI, Y., TANABE, T., SNUTCH, T. P. & CAMPBELL, K. P. 1994. Calcium channel β-subunit binds to a conserved motif in the I-II cytoplasmic linker of the α1-subunit. *Nature,* 368**,** 67-70.

RAJARAM, S., SEDENSKY, M. M. & MORGAN, P. G. 2000. *The sequence and associated null phenotype of a C. elegans neurocalcin-like gene*, Genesis. 2000 Apr;26(4):234-9.

RYU, W. S. & SAMUEL, A. D. T. 2002. Thermotaxis in *Caenorhabditis elegans* analyzed by measuring responses to defined thermal stimuli. *Journal of Neuroscience,* 22**,** 5727-5733.

SAAB, B. J., GEORGIOU, J., NATH, A., LEE, F. J. S., WANG, M., MICHALON, A., LIU, F., MANSUY, I. M. & RODER, J. C. 2009. NCS-1 in the Dentate Gyrus Promotes Exploration, Synaptic Plasticity, and Rapid Acquisition of Spatial Memory. *Neuron,* 63**,** 643-656.

SASAKURA, H. & MORI, I. 2012. Behavioral plasticity, learning, and memory in *C. elegans*. *Current Opinion in Neurobiology,* 23**,** 92-99.

SCHAFER, W. R. 2012. *Tackling thermosensation with multidimensional phenotyping*, BMC Biol. 2012 Nov 19;10:91. doi: 10.1186/1741-7007-10-91.

SCHLECKER, C., BOEHMERLE, W., JEROMIN, A., DEGRAY, B., VARSHNEY, A., SHARMA, Y., SZIGETI-BUCK, K. & EHRLICH, B. E. 2006. Neuronal calcium sensor-1 enhancement of InsP3 receptor activity is inhibited by therapeutic levels of lithium. *J Clin Invest,* 116**,** 1668-74.

SENGUPTA, P. & SAMUEL, A. D. 2009. *Caenorhabditis elegans*: a model system for systems neuroscience. *Curr Opin Neurobiol,* 19**,** 637-43.

STRAHL, T., HUTTNER, I. G., LUSIN, J. D., OSAWA, M., KING, D., THORNER, J. & AMES, J. B. 2007. Structural insights into activation of phosphatidylinositol 4-kinase (Pik1) by yeast frequenin (Frq1). *Journal of Biological Chemistry,* 282**,** 30949-30959.

SUDHAKAR BABU, Y., BUGG, C. E. & COOK, W. J. 1988. Structure of calmodulin refined at 2.2 Ã… resolution. *Journal of Molecular Biology,* 204**,** 191-204.

SULSTON, J. E. & HORVITZ, H. R. 1977. Post-embryonic cell lineages of the nematode, *Caenorhabditis elegans*. *Dev Biol,* 56**,** 110-56.

SULSTON, J. E., SCHIERENBERG, E., WHITE, J. G. & THOMSON, J. N. 1983. The embryonic cell lineage of the nematode *Caenorhabditis elegans*. *Dev Biol,* 100**,** 64-119.

TAVERNA, E., SABA, E., LINETTI, A., LONGHI, R., JEROMIN, A., RIGHI, M., CLEMENTI, F. & ROSA, P. 2007. Localization of synaptic proteins involved in neurosecretion in different membrane microdomains. *Journal of Neurochemistry,* 100**,** 664-677.

TAVERNA, E., SABA, E., ROWE, J., FRANCOLINI, M., CLEMENTI, F. & ROSA, P. 2004. Role of Lipid Microdomains in P/Q-type Calcium Channel (Cav2.1) Clustering and Function in Presynaptic Membranes. *Journal of Biological Chemistry,* 279**,** 5127-5134.

TSALIK, E. L. & HOBERT, O. 2003. Functional mapping of neurons that control locomotory behavior in *Caenorhabditis elegans*. *J Neurobiol,* 56**,** 178-97.

TSUJIMOTO, T., JEROMIN, A., SAITOH, N., RODER, J. C. & TAKAHASHI, T. 2002. Neuronal calcium sensor 1 and activity-dependent facilitation of P/Q-type calcium currents at presynaptic nerve terminals. *Science,* 295**,** 2276-2279.

VARSHNEY, L. R., CHEN, B. L., PANIAGUA, E., HALL, D. H. & CHKLOVSKII, D. B. 2011. Structural properties of the *Caenorhabditis elegans* neuronal network. *PLoS Comput Biol,* 7**,** 1001066.

VON STETINA, S. E., WATSON, J. D., FOX, R. M., OLSZEWSKI, K. L., SPENCER, W. C., ROY, P. J. & MILLER, D. M., 3RD 2007. Cell-specific microarray profiling experiments reveal a comprehensive picture of gene expression in the *C. elegans* nervous system. *Genome Biol,* 8.

VRANKEN, W. F., BOUCHER, W., STEVENS, T. J., FOGH, R. H., PAJON, A., LLINAS, M., ULRICH, E. L., MARKLEY, J. L., IONIDES, J. & LAUE, E. D. 2005. The CCPN data model for NMR spectroscopy: Development of a software pipeline. *Proteins: Structure, Function, and Bioinformatics,* 59**,** 687-696.

WANG, H., YAN, Y., LIU, Q., HUANG, Y., SHEN, Y., CHEN, L., CHEN, Y., YANG, Q., HAO, Q., WANG, K. & CHAI, J. 2007. Structural basis for modulation of Kv4 K+ channels by auxiliary KChIP subunits. *Nat Neurosci,* 10**,** 32-9.

WANG, Q. M. & JOHNSON, R. B. 2001. Activation of Human Rhinovirus-14 3C Protease. *Virology,* 280**,** 80-86.

WEISS, J. L. & BURGOYNE, R. D. 2001. Voltage-independent Inhibition of P/Q-type Ca^{2+} Channels in Adrenal Chromaffin Cells via a Neuronal Ca^{2+} Sensor-1-dependent Pathway Involves Src Family Tyrosine Kinase. *Journal of Biological Chemistry,* 276**,** 44804-44811.

WESTENBROEK, R. E., SAKURAI, T., ELLIOTT, E. M., HELL, J. W., STARR, T. V. B., SNUTCH, T. P. & CATTERALL, W. A. 1995. Immunochemical identification and subcellular distribution of the α1A subunits of brain calcium channels. *Journal of Neuroscience,* 15**,** 6403-6418.

WHITE, J. G., SOUTHGATE, E., THOMSON, J. N. & BRENNER, S. 1986. The structure of the nervous system of the nematode *Caenorhabditis elegans*. *Philos Trans R Soc Lond B Biol Sci,* 314**,** 1-340.

WHITE, J. Q. & JORGENSEN, E. M. 2012. Sensation in a single neuron pair represses male behavior in hermaphrodites. *Neuron,* 75**,** 593-600.

WITTENBURG, N. & BAUMEISTER, R. 1999. Thermal avoidance in *Caenorhabditis elegans*: an approach to the study of nociception. *Proc Natl Acad Sci U S A,* 96**,** 10477-82.

WOLL MP, D. C. D., BEWLEY MC, TACELOSKY DM, LEVENSON R, FLANAGAN JM. 2011. Interaction between the D2 Dopamine Receptor and Neuronal Calcium Sensor-1 Analyzed by Fluorescence Anisotropy. *Biochemistry.,* 50**,** 8780-91. Epub 2011 Sep 25.

ZHANG, K., HEIDRICH, F. M., DEGRAY, B., BOEHMERLE, W. & EHRLICH, B. E. 2010. Paclitaxel accelerates spontaneous calcium oscillations in cardiomyocytes by interacting with NCS-1 and the $InsP_3R$. *J Mol Cell Cardiol,* 49**,** 829-35.

ZHANG, M., TANAKA, T. & IKURA, M. 1995. Calcium-induced conformational transition revealed by the solution structure of apo calmodulin. *Nature Structural Biology,* 2**,** 758-767.

ZHAO, X., VÁRNAI, P., TUYMETOVA, G., BALLA, A., TÓTH, Z. E., OKER-BLOM, C., RODER, J., JEROMIN, A. & BALLA, T. 2001. Interaction of Neuronal Calcium Sensor-1 (NCS-1)

with Phosphatidylinositol 4-Kinase β Stimulates Lipid Kinase Activity and Affects Membrane Trafficking in COS-7 Cells. *Journal of Biological Chemistry,* 276**,** 40183-40189.

ZHUCHENKO, O., BAILEY, J., BONNEN, P., ASHIZAWA, T., STOCKTON, D. W., AMOS, C., DOBYNS, W. B., SUBRAMONY, S. H., ZOGHBI, H. Y. & LEE, C. C. 1997. Autosomal dominant cerebellar ataxia (SCA6) associated with small polyglutamine expansions in the α1A-voltage-dependent calcium channel. *Nature Genetics,* 15**,** 62-69.